



UNIVERSITÀ  
DEGLI STUDI  
DI PADOVA



Dipartimento di ingegneria industriale (DII)

Sports Tech Research Center, Sports Tech Research Centre, Department of  
Quality Technology and Management, Mechanical Engineering and Mathematics,  
Mid Sweden University (SWE)

MASTER DEGREE IN MECHANICAL ENGINEERING

## **Development of a sustainable alpine sitski for the dissemination of inclusive paralympic skiing**

Home University Supervisor:

**Prof. Nicola Petrone**

Host University Supervisor:

**Prof. Andrey Koptug**

Student:

**Gianmarco Rocco**

**2055073**



*Non è nelle stelle  
che è conservato il nostro destino,  
ma in noi stessi*



## Ringraziamenti

A mia mamma e mio papà, che da lunghi anni sostengono e supportano tutte le mie decisioni e le mie iniziative. Senza di voi niente di tutto questo si sarebbe realizzato. Spero di avervi reso fieri ed orgogliosi di questo traguardo quanto lo sono io.

Un grande ringraziamento va al professor Petrone, per avermi seguito e consigliato durante tutti questi mesi, con grande pazienza e con spirito paterno.

I would say thanks to professor Koptuyg for helping me in every possible way to have a comfortable stay in Sweden and for providing me with an educational experience from both an academic and personal perspective.

Ringrazio l'ing. Zanardi per il preziosissimo aiuto nella costruzione di un prototipo e nella stesura e revisione di questa tesi.

Ringraziamento speciale a tutti i Chinotti per aver reso la mia esperienza universitaria indimenticabile. Tutto ciò che abbiamo passato insieme resterà sempre scolpito nella mia mente. Bisogna ammettere che alcune cose sono difficili da scordare, ma questa è un'altra storia.

Un grande abbraccio a tutte le persone che ho conosciuto in Svezia, in particolare a Giorgia, Luca e Simone per aver reso la fredda Svezia un Paese capace di scaldarmi il cuore. Non più alla 212, ma sarò lieto di cucinare per voi ancora e ancora!

Anche se dovrete ringraziarmi voi per essere stato il miglior Dinamico della storia, a tutti gli amici del team QuartodiLitro e, in particolare, Eugenio, Filippo e Gabriele dico che mi avete fatto davvero godere questi tre anni di fatica, gioia e dolori. Grazie. Camilla e Maia saranno per sempre *roba nostra*.

Infine, ultimi ma non ultimi, ringrazio tutti le persone che mi sono state vicine, mi hanno aiutato, ascoltato e sopportato in questi anni. Scusate se non metto tutti i vostri nomi, ma vi assicuro che vi ho pensati tutti.



# Content

<b>Abstract</b> .....	<b>1</b>
<b>Riassunto esteso</b> .....	<b>3</b>
<b>1. Introduction</b> .....	<b>5</b>
1.1. History .....	5
1.2. Aim of the thesis .....	6
<b>2. Monoski Projects</b> .....	<b>7</b>
2.1. Matteo Ferrari .....	7
2.2. Davide Piccinin.....	9
2.3. Dario Vanzetto .....	13
2.4. Giovanni Colla.....	16
<b>3. Product Innovation</b> .....	<b>19</b>
<b>4. Competitive Benchmarking</b> .....	<b>21</b>
4.1. Kinematic Analysis.....	22
Pixel Analysis Procedure.....	22
Position Analysis of a planar mechanism.....	23
4.2. Models Implementation in MSC Adams .....	25
Scarver by Tessier .....	25
Tempo by Tessier .....	27
Impact Evolution.....	29
Monoski Racer by Alois Praschberger.....	31
Results and Comparison .....	32
4.3. 2x2 Comparison Matrices .....	35
<b>5. Technology Scouting</b> .....	<b>39</b>

5.1.	Monoshock Absorber.....	40
5.2.	Release System.....	42
<b>6.</b>	<b>Definition of the kinematic scheme of the monoski.....</b>	<b>45</b>
6.1.	Constraints and Target .....	45
6.2.	Final Design Scheme .....	46
6.3.	Results and comparison .....	48
<b>7.</b>	<b>Mechanical design.....</b>	<b>51</b>
7.1.	Introduction .....	51
7.2.	Production System .....	52
7.3.	Design Concept.....	55
7.4.	Foot.....	59
7.5.	Lower Triangle.....	61
7.6.	Lift up System.....	63
7.7.	Quick Release System.....	66
7.8.	Beams.....	69
7.9.	Upper Triangle.....	71
7.10.	Frame .....	73
7.11.	Assembly .....	76
<b>8.</b>	<b>Structural calculations .....</b>	<b>81</b>
8.1.	FEA Analysis .....	81
8.2.	Load Calculations.....	83
	Static Load Size .....	84
8.3.	Stress on main structural parts .....	84
	FEM Results .....	86



8.4. Bearings verification.....	91
SKF 608 – 2Z.....	93
SKF 61901 2Z.....	93
SKF HK 1612 .....	94
8.5. Verification of bolted joints – CNR-UNI 10011 - 1988 .....	95
Lower Triangle – Foot.....	95
Upper Beam – Frame.....	99
<b>Conclusions and future development .....</b>	<b>103</b>
<b>Bibliography .....</b>	<b>105</b>
<b>List of figures.....</b>	<b>107</b>
<b>List of Tables.....</b>	<b>111</b>
<b>Appendix A – Drawings .....</b>	<b>113</b>



## **Abstract**

In this thesis, we address the design of an innovatively designed sitski with the aim of making Paralympic skiing a more economically inclusive sport for anyone who wishes to participate. The initial design constraints we tackled are of a kinematic nature, as, in order to be usable and make a sitski perform optimally, it must necessarily adhere to certain characteristics that will be further described in the discussion.

Once the operational characteristics were identified, starting from a basic framework that adhered to them, we proceeded to design and evaluate various design and material alternatives, always keeping in mind that the primary objective of this discussion is to create an economically sustainable object.

After selecting the design that best aligns with the initial design requirements, while considering individual components in light of the available technologies for the actual prototype production, finite element analyses were conducted with the goal of refining the model in terms of dimensions and thicknesses, as well as ensuring the reliability of the vehicle.



## Riassunto esteso

Nella presente tesi, viene affrontata la progettazione di uno sitski progettato in modo innovativo con l'obiettivo di rendere lo sci paralimpico uno sport economicamente più accessibile per chiunque desideri partecipare.

Nei capitoli 1 e 2 sono state approfondite la storia dei sitski e i precedenti lavori sulla tematica svolti presso il dipartimento di ingegneria industriale di Padova.

Nel capitolo 4 sono state svolte le analisi cinematiche di alcuni monosci commerciali al fine di individuare i vincoli di progettazione iniziali. Per essere utilizzabile e ottenere prestazioni ottimali, uno sitski deve necessariamente aderire, infatti, a determinate caratteristiche.

All'interno del capitolo 5 sono state presentate alcune fonti di ispirazioni provenienti da un mondo esterno a quello dei sitski, che sono poi state utili alla realizzazione di alcune parti del modello.

Nel capitolo 6 è stato definito lo schema cinematico di base per il monosci con le sue caratteristiche di movimento. Da questo è poi stato presentato, all'interno del capitolo 7, in ogni sua parte, il monosci realizzato a partire da quello schema di base indicato nel capitolo 6. In particolare, sono state descritte le scelte progettuali a livello di metodo di produzione e di concept design.

Infine, il capitolo 8 è stato dedicato alle verifiche strutturali, condotte tramite l'analisi del modello agli elementi finiti, la verifica dei cuscinetti e la verifica delle giunzioni bullonate.

Nella pagina dedicata agli sviluppi futuri sono stati indicati i futuri step di sviluppo e analisi del modello secondo il redattore della tesi, comprendenti in particolare il testing del modello sul campo e la verifica dell'attuale sostenibilità del progetto.



# 1. Introduction

## 1.1. History

Para-alpine skiing is a winter sport, an adaptation of alpine skiing for individuals with disabilities. Its origins can be traced back to the post-World War II era, which saw a significant number of soldiers left with disabilities.

Among them, Franz Wendel, a German soldier who lost a leg, can be considered one of the earliest examples of para-alpine skiing. He attached crutches to a pair of short skis, making a pivotal moment in the sport's development.

During the same period, in Austria, Sepp Zwicknagel, a veteran who had lost both legs due to a grenade, displayed remarkable resilience and self-taught himself to ski, using a primordial version of a sitski. Later he became a ski instructor at Kitzbühel, one of the most famous and exclusive ski resorts in the world. Zwicknagel's efforts helped establish a division within the Austrian Ski Association specifically for disabled skiers.

Ludwig Guttman, a prominent figure in the history of Paralympic sports, played a key role in organizing ski events for individuals with disabilities, further popularizing adaptive skiing, including sit-skiing.

Over time, the concept of sit-skiing and adaptive skiing began to spread internationally, with various organizations and individuals contributing to its development and popularity. Sit-ski technology continued to evolve to meet the specific needs of different disabilities. Today, sit-skis come in various designs and configurations, catering to a wide range of disabilities. They provide individuals with lower limb impairments the opportunity to enjoy the thrill of skiing and compete in adaptive skiing events, including the Paralympic Games.

At the first Paralympic Winter Games in Örnsköldsvik, Sweden, in 1976, athletes competed in Slalom and Giant Slalom and three distances in Nordic Skiing. Downhill was added to Paralympic program in 1984 in Innsbruck, Austria, and Super-G was added in 1994 in Lillehammer, Norway. Sit-skiing, or mono-skiing, was introduced as a demonstration sport at

the Innsbruck 1984 Paralympic Games and became a medal event in Nagano 1998 Paralympic Games.

Paralympic Alpine Skiing is subdivided into three competition classes, according to “IPC (International Paralympic Committee) Classification Rules and Regulations”: Standing class (e.g. upper or lower body limb loss, skiing with or without prosthetic or cerebral palsy), Visually Impaired class, and Sitting class (IPC, 2015).

The present work is focused on the last class, sitting athletes having acquired or congenital paralysis or lower limb loss, because of the interesting (from a mechanical point of view) equipment used.

## **1.2. Aim of the thesis**

In the world of adaptive sports, the term "inclusivity" has emerged as a guiding principle, emphasizing the need to ensure that individuals with disabilities have equitable access to sports and recreation.

While the Paralympic Games and other adaptive skiing events have played a pivotal role in increasing awareness and participation in alpine skiing among individuals with disabilities, the accessibility of the sport remains limited due to the high cost and technical challenges associated with specialized equipment. Sitskis are adaptive devices that allow skiers to sit while descending steep mountain terrains, utilizing their upper body strength and core stability to control their movements. However, despite the immense potential of sitskiing in promoting inclusivity within the alpine skiing community, several barriers persist. The limited availability of affordable and sustainable sitski designs have restricted the dissemination of this extraordinary sport.

This master thesis seeks to address this critical issue by focusing on the development of a sustainable alpine sitski.

This thesis will explore the design, materials, and manufacturing processes necessary to create a sustainable sitski that overcomes the barriers to access. In doing so, it seeks to empower individuals with lower limb impairments to experience the joy and excitement of alpine skiing, facilitating the broader dissemination of inclusive Paralympic skiing and furthering the objectives of the adaptive sports community.



## 2. Monoski Projects

The project started from the foundations previously laid down by Davide Piccinin [1], Matteo Ferrari [2], Dario Vanzetto [3] and Giovanni Colla [4] in their thesis called respectively “*Kinematic and kinetic analysis of a Paralympic skier during slalom - 2016*”, “*Design and validation of a dynamometric load cell for the measurement of loads acting on a Paralympic monoski – 2016*”, “*Acquisition and analysis of kinematic and kinetic data on a top Paralympic skier during giant slalom – 2017*” and “*Development and validation of an Instrumented Monoski for kinematic and kinetic data collection – 2022*”.

Ferrari developed and created the load cell (called Dynafoot) during his thesis work; Piccinin conducted validation tests comparing it with the force plates (called Dynaplate) created by Paride Gardin [6] during his thesis “*Analisi del comportamento strutturale del Sistema complesso sci-attacco scarpone – 2007*”. Vanzetto successfully tested the force plates with a Paralympic athlete with interesting findings from which an article was later published [5].

### 2.1. Matteo Ferrari

In his thesis project, Ferrari conceptualized the Dynafoot, a dynamometric multicomponent load cell designed to gauge the external forces and moments generated by a Paralympic monoski during downhill maneuvers.

The aluminum foot structure from Tessier's Scarver was selected for conversion into a dynamometric load cell. This transformation involved seamlessly integrating it into the monoski without altering its original geometry. By maintaining the foot's geometry, four apertures were strategically crafted—two on the left and two on the right. This configuration facilitated the creation of four vertical channels and two lateral channels, employing a system of strain gauges. The dimensions of these openings were precisely chosen to induce localized stress, ensuring optimal sensitivity of the cell without surpassing the material's yield stress.

Regrettably, the finite elements simulations were conducted solely on half of the structure, neglecting the fact that the pitch moment exhibits antisymmetric characteristics. Nevertheless, the conducted tests indicate that the load cell, configured with this geometry, demonstrates commendable sensitivity.

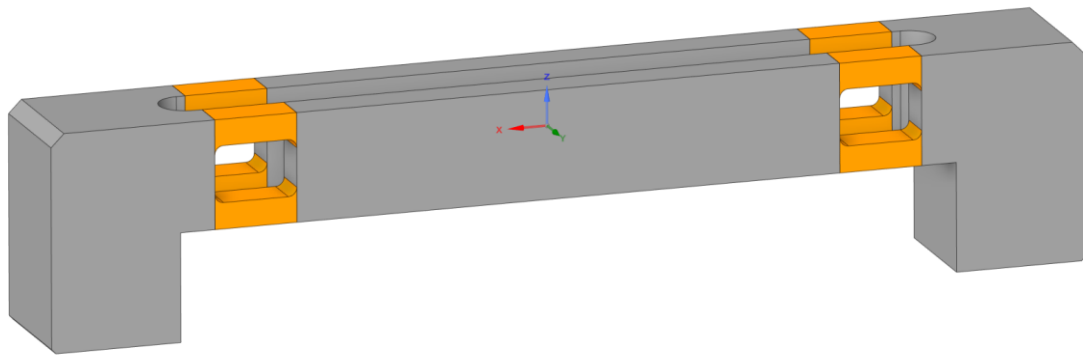


Figure 2.1 - Dynafoot

The load cell underwent testing in Folgaria during the winter of 2016, employing a lightweight and portable BTS pocket system for data acquisition. Out of the four runs conducted, only two yielded reliable results.

To gain a deeper understanding of the forces affecting the ski, force values were normalized to the Total Weight of the skier + Scarver + clothes + devices, denoted as  $TW = 885\text{ N}$ . It is evident that the dynamometric load cell exhibited satisfactory mechanical behavior in terms of vertical force, roll, and pitch. However, the lateral signal intensity was notably lower, attributed to its lower sensitivity compared to other channels and the inherent low lateral loads during downhill runs.

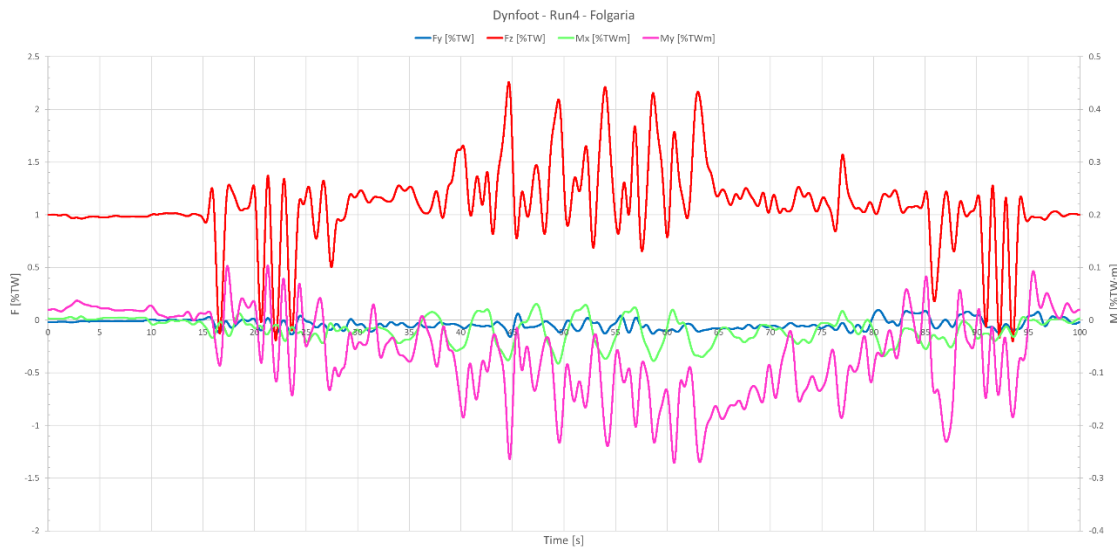


Figure 2.2 – Results of Ferrari’s test

## 2.2. Davide Piccinin

Davide Piccinin's research commenced with the validation of the Dynaplate (Fig. 2.3) as an instrumental tool for scrutinizing various skiing techniques. This involved orchestrating two distinct trials on the slopes—one to draw comparisons between athletes of divergent skill levels (amateur and professional) and another to assess the disparities between different dynamometric systems (Dynaplate and Dynafoot). Notably, the chosen monoski for these experiments was the Scarver by Tessier.



*Figure 2.3 – Dynaplate*

The initial phase of testing unfolded during the ISEA WinterCamp 2016 in San Martino di Castrozza, Italy, spanning from February 28th to March 4th, 2016. Over the course of two days, Andrea Stella, an amateur Paralympic skier, executed a total of six runs. Subsequently, Alessandro Varotto, a seasoned professional in Paralympic monoskiing, underwent a comparable regimen, completing five runs.

For these experiments, a comprehensive array of sophisticated devices was employed, including:

- Xsens suit: MVN motion capturing system (provided courtesy of Aalborg University)
- Leica GNSS: a high-precision Global Navigation Satellite System (provided by Ljubljana University)
- Dynamometric Force Plates: a load cell measuring  $F_z$ ,  $M_x$ ,  $M_y$  (supplied by Padova University)

Results derived from these tests were meticulously normalized based on the Total Weight of the skier + equipment. The weights of Stella and Varotto were 65 kg and 77 kg, respectively, while the monoski itself weighed 17.09 kg. Piccinin delved into an intricate comparison of various parameters vis-à-vis the skiers' styles. This involved a detailed analysis of key metrics such as Z-axis peak force, maximum  $\Delta X$  of COP (Center of Pressure), mean value of COP, and time. The observed trend revealed an elevation in the force applied to the ski during the transition from a wide slalom to a narrow slalom, a phenomenon observed in both athletes. While Stella experienced a noteworthy increase of +13.11%, Varotto's surge was relatively inconspicuous at +0.42%. An intriguing finding emerged when scrutinizing the forces exerted by Varotto, showcasing his prowess as a professional skier—15.55% more force in wide slalom and 2.58% more in narrow slalom compared to Stella.

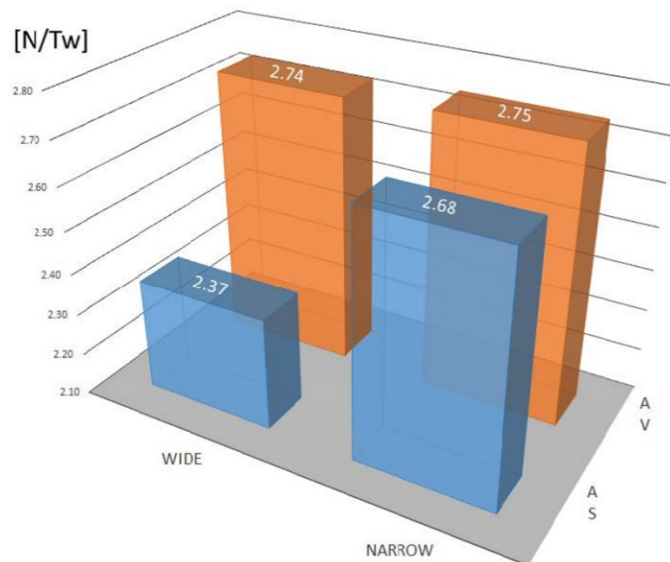


Figure 2.4 – Mean values of force peaks

Furthermore, the comparative analysis of skiing techniques, primarily based on force dynamics, underscored Varotto's superior control over the Scarver. He consistently produced more force, maintaining a commendable level of uniformity compared to Stella. Intriguingly, both athletes exhibited similar force application patterns in specific curves, hinting at potential variations influenced by slope contours and snow conditions.

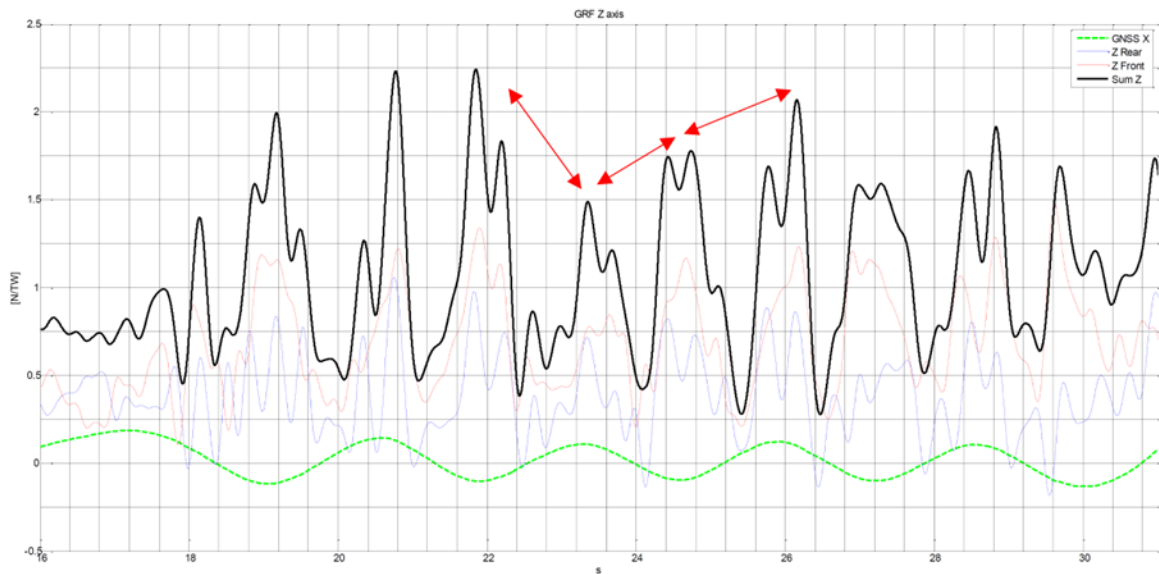


Figure 2.5 - Stella's 3rd wide run

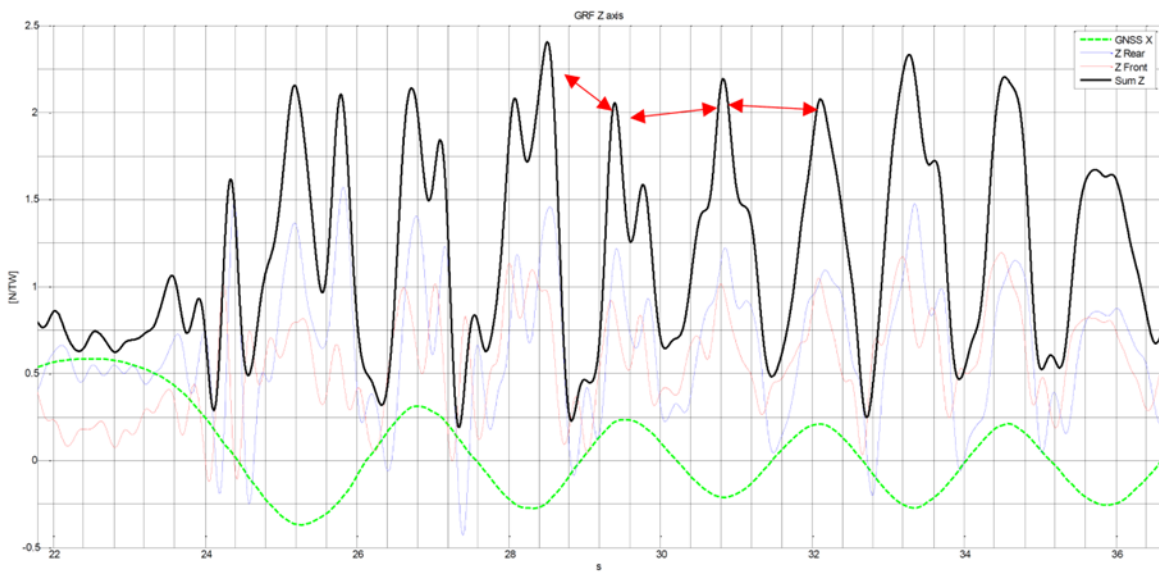


Figure 2.6 - Varotto's 2nd wide run

Upon delving into the COP data, a discernible tendency surfaced—an increase in  $\Delta X$  from wide to narrow slalom, indicative of a propensity for skiers to lean forward. Stella's mean COP position witnessed a notable surge of 40.59%, while Varotto's exhibited a remarkable increase of 1000.86%. The distinct balance disparities between Stella and Varotto were evidently manifested, with Stella favoring a more forward-leaning posture in both wide and narrow slalom scenarios.

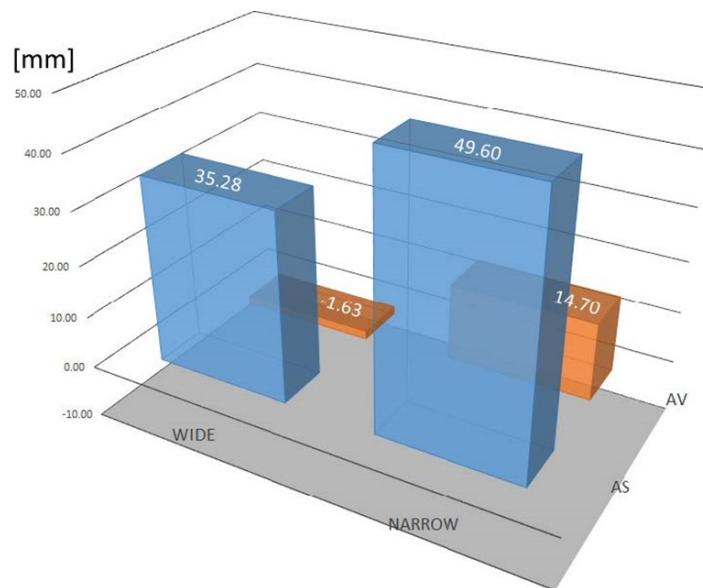


Figure 2.7 - Mean values of XCOP

This divergence in skiing techniques was further illuminated through an analysis of the COP charts, accentuating the forward shift of the average COP position during the transition from wide to narrow slalom. Varotto's skiing technique exhibited a consistent correlation with COP movements, following a discernible pattern throughout the run, whereas Stella's technique appeared less structured, lacking a recognizable pattern.

In a parallel exploration within the same season, another intriguing test unfolded on March 24th in Folgaria, Italy. This particular experiment aimed to draw a comparison between two dynamometric systems: Dynaplate, curated by Paride Gardin, and Dynafoot, developed by Matteo Ferrari. Originally, the plan was to synchronize data collection using both systems simultaneously, offering divergent perspectives on the same run. However, technical constraints led to sequential tests, potentially overlooking nuanced variations between different runs.

Remarkably, both load cell systems showcased consistent results, even though a direct side-by-side comparison proved unattainable. Regrettably, Dynaplate encountered operational issues during the tests, resulting in data spoilage, with only one out of three runs being salvaged due to water infiltration, compromising the strain gauge signals.

### **2.3. Dario Vanzetto**

In his thesis research, Vanzetto conducted a series of tests with the renowned alpine skier and World/Olympic champion, Christoph Kunz. This experimentation transpired in Adelboden, Switzerland, during March 2017. Notably, for this particular set of tests, Kunz utilized the Impulse Boost monoski manufactured by Unicent GmbH.

Vanzetto opted to employ the Dynaplate system, conceptualized and actualized by Paride Gardin in 2006 for the measurement of Ground Reaction Forces. Additionally, he incorporated a magnetostrictive potentiometer from Athena to gauge the damper stroke and speed.

Unfortunately, complications arose when attempting to connect all 10 channels, resulting in a discernible reduction in the voltage supplied by the amplifiers. Consequently, Vanzetto had to limit the usage to only three channels, focusing exclusively on the measurement of Vertical forces, Pitch, and Roll moments.

The vulnerability of this load acquisition system stemmed from the instability of the amplifier used to connect the load cells to the data logger. This introduced reliability issues in terms of signal stability, as temperature variations led to signal drift during the runs. To address this challenge, a test protocol was implemented: the athlete was elevated from the ground for 10 seconds to establish a precise "zero" point, both before and after each run, mitigating signal drift.

A total of 6 runs were recorded, during which the monoski setup, specifically variations in the Center of Pressure (COP) position, was altered every two runs. Unfortunately, during the 7th run, some cables of the Dynaplate were punctured by the suspension mechanism of the monoski.

Few considerations were made, in particular, the following were chosen as key parameters: Z-axis peak force, variation of  $X_{COP}$ , mean value of COP and damper stroke and speed peaks and the purpose is to study them in relation to the different phases of the turn.

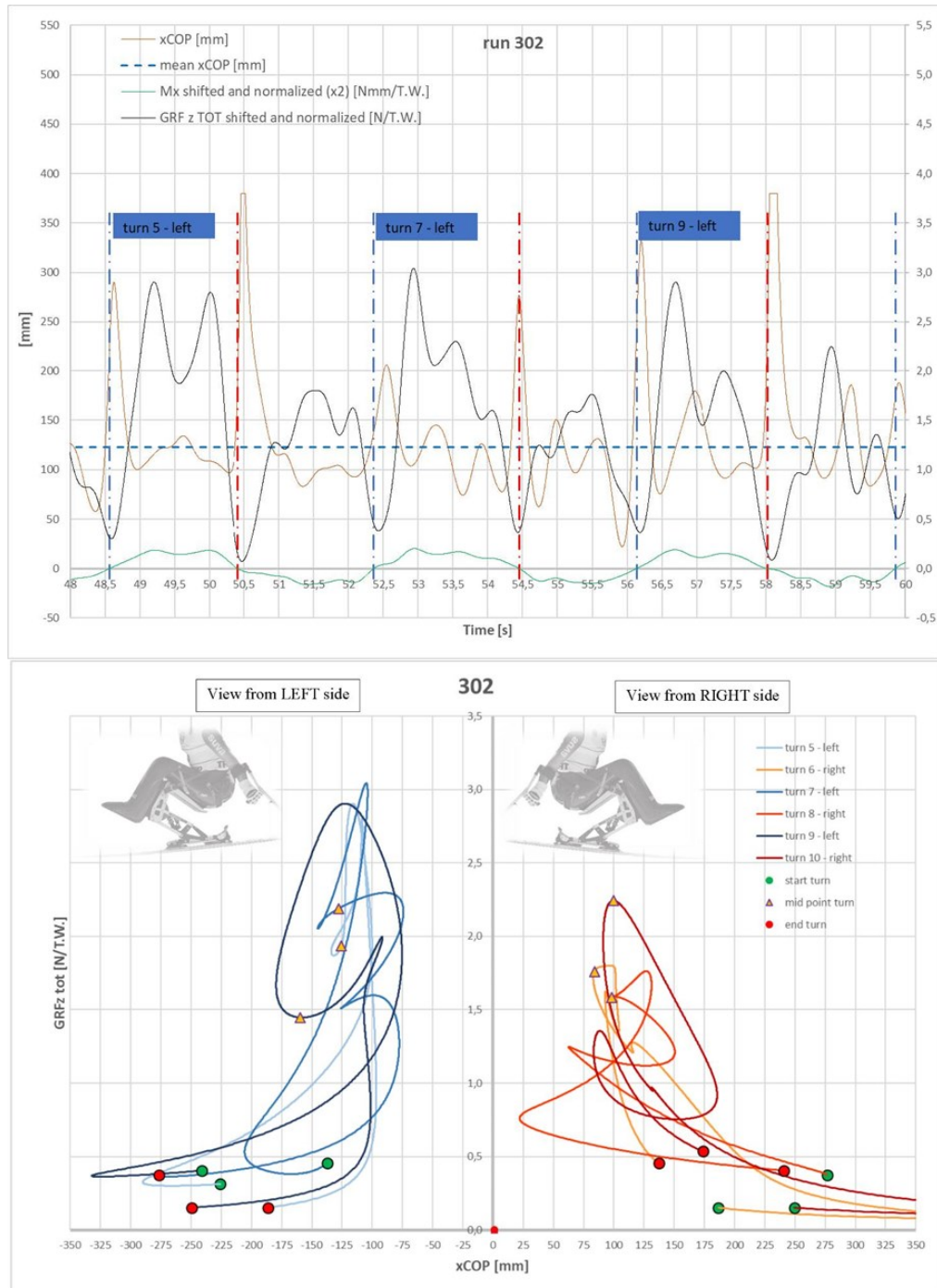


Figure 2.8 – Results from run 302



The observed pattern indicates that when the Center of Pressure (COP) is shifted backward, the peaks of the total Ground Reaction Force in the vertical direction (GRF-z) decrease. This implies that as the COP of the monoski is set further back, the athlete's ability to exert force on the ski diminishes. This initial observation aligns with Kunz's subjective evaluations and is corroborated by the lap time analysis. Notably, run 302, which exhibits the highest subjective rating, also happens to be the fastest run.

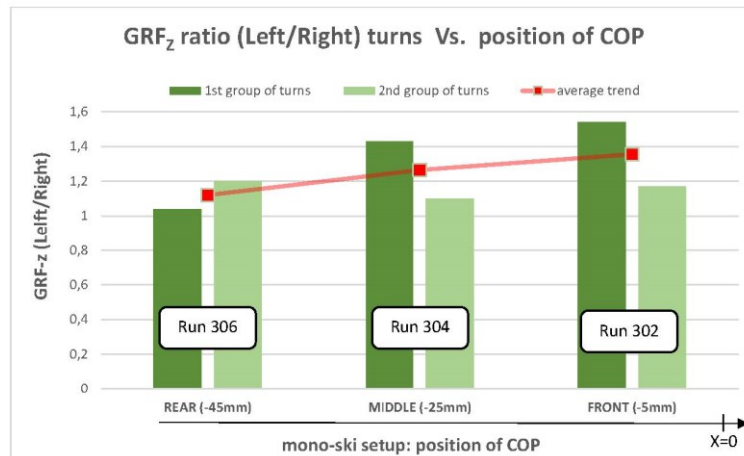


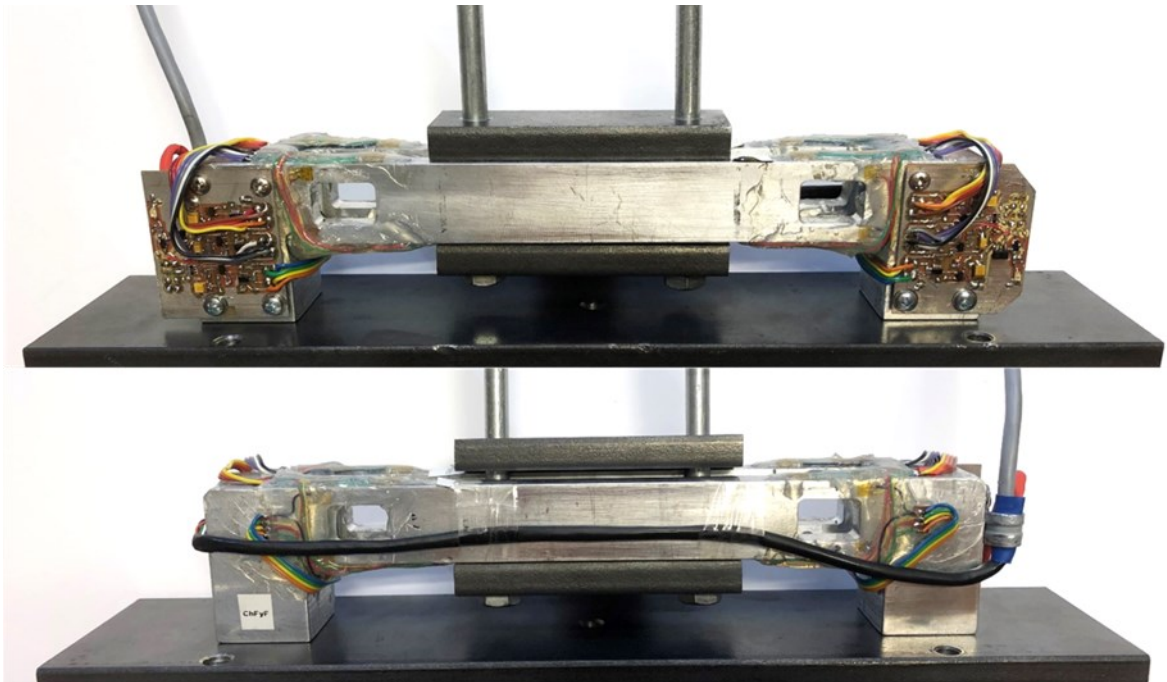
Figure 2.9 - GRF (left/right) - position of COP

The mentioned phenomenon becomes more conspicuous when the loads (total Ground Reaction Force in the vertical direction, GRF-z) are elevated, as exemplified by the set of turns in Figure 8. This suggests that the athlete successfully anticipated the left turns.

The positioning of the Center of Pressure (COP) along the longitudinal X axis plays a crucial role. Notably, as the COP is positioned forward, there is a corresponding increase in the attained vertical forces. It is evident, both from the lap time analysis and the athlete's subjective ratings, that optimal performance is achieved when the base of the monoski is situated in the most anterior position relative to the foot (boot of the monoski).

## 2.4. Giovanni Colla

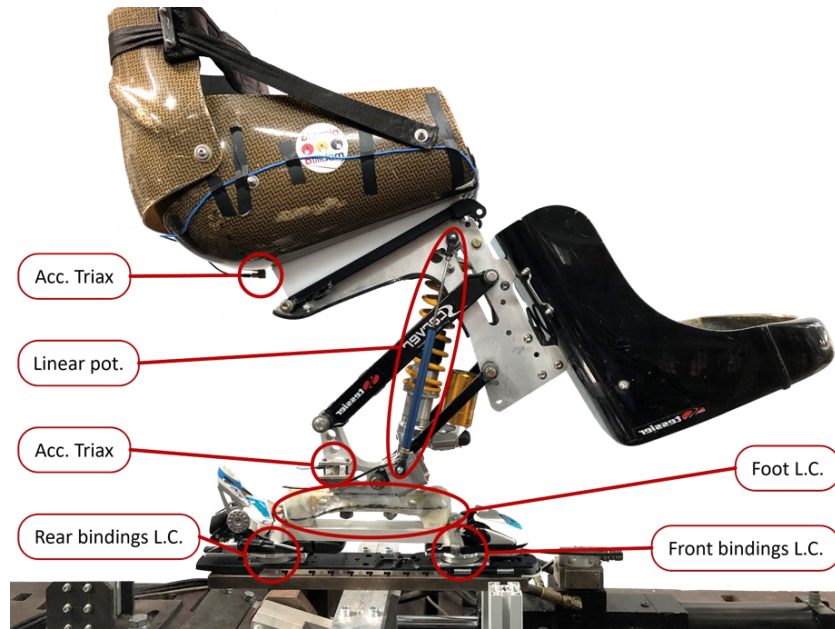
The primary goal of this thesis was to develop mechanical and electronic tools for studying the complex monoski system in both indoor and outdoor environments. The key objectives included the creation of an Instrumented Monoski capable of collecting kinematic and kinetic data, focusing on ground reaction forces, damper stroke and speed variations, seat and body vibrations, and inclination. Additionally, the research aimed to enhance the Multicomponent Load Cell by integrating an amplification stage and calibrating it using an innovative method called Neural Networks.



*Figure 2.10 – Amplified Load Cell*

The research began with an extensive literature review to identify relevant articles and dissertations related to monoskis. Calibration methods for load cells were explored, with a particular emphasis on employing Neural Networks from the Deep Learning Toolbox of MATLAB. The selection of optimal sensors for acquiring the kinematics of the monoski frame and skier was a crucial aspect. Ground reaction forces were measured using the developed Multicomponent load cell, while damper stroke and speed were monitored through a linear potentiometer parallel to the shock absorber. Triaxial accelerometers and a gyroscope were

employed for measuring seat and body vibrations and inclination. Dynamic behavior and vibrations of the monoski were also investigated.



*Figure 2.11 - Instrumented Monoski*

Indoor tests demonstrated the foot load cell's capability to accurately measure both static and dynamic loads with high precision. The overall measurement systems provided reliable data, affirming the validity of the methods and instruments used.



### 3. Product Innovation

In the fast-paced and ever-evolving landscape of modern business, the concept of product innovation has become a driving force behind growth, competitiveness, and long-term sustainability. Innovation is not merely a buzzword but a strategic imperative that can redefine industries, empower companies to stay ahead of the curve, and improve the lives of consumers. It represents the pursuit of new ideas, processes, technologies, or methodologies that create value by addressing unmet needs or solving existing problems.

Innovation can be visualized as a pyramid, with different layers representing various stages of the process. The foundation of the pyramid comprises intelligence activities, which include gathering insights from diverse sources such as *voice of client analysis*, *competitive benchmarking*, and *technology scouting*. These activities serve as the bedrock upon which the innovation journey is built.

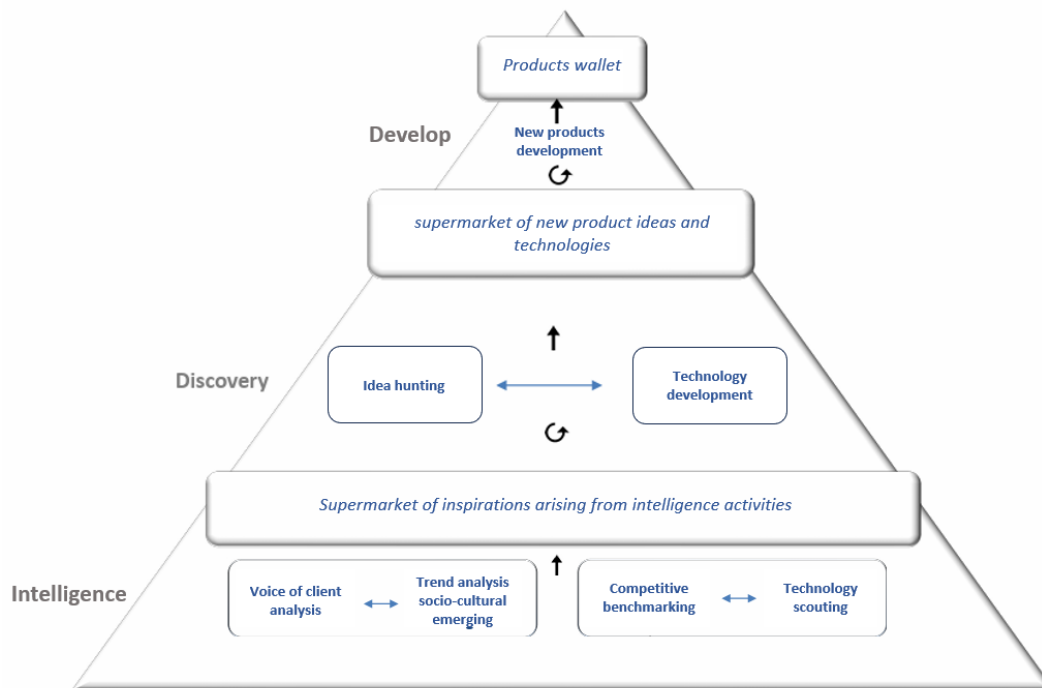


Figure 3.1 - Pyramid of innovation

The middle layer involves the discovery activities, where these insights are honed and shaped into viable concepts. *Technology development* in this phase involves the identification, exploration, and integration of new or existing technologies that can be leveraged to bring innovative ideas to fruition.

These technologies can range from software and hardware to materials and processes. On the other side of the discovery activities, there is *idea hunting*, a proactive and creative process aimed at identifying and generating innovative concepts that have the potential to address specific challenges or capitalize on emerging opportunities. It involves a combination of research, brainstorming, user feedback, and creative thinking techniques, and it is a dynamic and iterative process that can lead to breakthrough innovations.

While the apex of the pyramid signifies the development of a new product or innovation, which means the set of activities aimed at concretely creating products to be launched in the market, by transforming knowledge about customer needs, technological insights, and new product ideas into technologically feasible solutions that can be produced profitably on an industrial scale.

## 4. Competitive Benchmarking

Competitive benchmarking is a strategic practice in which a company assesses its performance relative to competitors to gain valuable insights.

The process begins by identifying both direct and indirect competitors in the industry; direct competitors offer similar products or services, while indirect competitors might fulfill the same needs through different means.

Establishing clear and relevant metrics and parameters is crucial. Subsequently, gathering data on the identified metrics becomes a comprehensive process.

The next step involves conducting a comparative analysis, which includes measuring the company's performance against that of competitors. This comparison could encompass various aspects, such as side-by-side evaluations of products, pricing models, marketing strategies, and customer experiences.

Benchmarking enables companies to identify industry best practices. By comprehending what competitors excel at, organizations can adopt and adapt these practices to enhance their own processes and outcomes.

With the insights gained, organizations can set both realistic and aspirational performance targets, aligning strategies with market expectations and driving continuous improvement.

Competitive benchmarking offers numerous benefits for this mechanical project. Through a careful analysis of existing mechanical projects in the market, it is possible to make design decisions that are not only innovative but also informed by the strengths and weaknesses observed in competitors' products.

This approach contributes to risk mitigation, allowing to proactively address potential challenges and ensure a smoother development and launch process. Additionally, efficient resource allocation is facilitated, ensuring that optimally deploys the limited resources in areas that will have the most significant impact on the project's competitiveness.

The starting point of this project is indeed a kinematic analysis of the products of the main competitors. Since there is no prior knowledge of sitski characteristics, an attempt was made to collect data from some existing systems, trying to identify a series of properties that could serve as a common thread among them. This was done to set target parameters for the system to be designed.

The sitskis identified as the main competitors are:

- Scarver by Tessier
- Tempo by Tessier
- Impact Evolution
- Monoski Racer by Alois Praschebrger

After a brief explanation of how the kinematic analysis of these monoskis was conducted, they will be analyzed individually and, finally, compared.

## 4.1. Kinematic Analysis

To perform the kinematic analysis of monoskis available on the market, a 2D simulation in the sagittal plane of the system is desired, using multibody simulation software. The goal is to evaluate the skier's movement during the sporting action, hoping to identify a repetitive behavior pattern for different systems, providing a set of targets during the design phase.

### Pixel Analysis Procedure

To conduct this analysis, several photographs of the aforementioned systems have been collected, and a dimensional analysis of the lengths of the main members of the articulated quadrilateral has been carried out using PC software. The procedure is as follows:

1. **Identify a Known Length:** Start by identifying a reference object in the photograph with a known length.
2. **Select Measurement Tool:** Open the photograph in an image editing software or a tool that allows pixel measurements.



3. **Calibrate the Measurement Tool:** Use the measurement tool to measure the pixel length of the reference object you identified in Step 1. Note down the pixel measurement.
4. **Calculate Pixels per Unit Length:** Divide the known length of the reference object by its pixel measurement. This gives the conversion factor, i.e., the number of pixels per unit length.

$$\textit{Pixel per Unit Length} = \frac{\textit{Known Length}}{\textit{Pixel Measurement}}$$

5. **Apply the Conversion Factor:** Now, it is possible to measure other objects or distances in the photograph using the conversion factor. Measure the pixel length of any other object or distance, and then multiply it by the conversion factor to get the actual length.

$$\textit{Actual Length} = \textit{Pixel Measurement} \cdot \textit{Pixels per Unit length}$$

This will give the real-world size of the object or distance in your photograph.

The accuracy of analysis depends on the precision of measurements and the quality of the reference object chosen for calibration. Additionally, perspective distortions in the photograph may introduce some errors in measurements.

### **Position Analysis of a planar mechanism**

In the study of mechanisms: solving the positional kinematic problem means explicitly expressing the relationships between the coordinates of the points in the mechanism and the free coordinates of the mechanism. The free coordinates or Lagrangian coordinates of a mechanism are parameters, freely chosen in a number equal to the degrees of freedom, provided they are independent, that define the configuration of the mechanism, i.e., the position of each of its points. When the study concerns a mechanism made up of rigid members, the positions, velocities, and accelerations of the points of the mechanism can be related, thanks to the fundamental relationships of rigid motions, to the position, velocity, and acceleration of the member to which the point belongs.

In the case of planar mechanisms, the position, velocity, and acceleration of a single member are functions of only three parameters (two translations and one angle) and their respective derivatives. We define driving members as those members in which at least one of the position parameters ( $x, y, \theta$ ) coincides with a free coordinate of the mechanism, and driven members as the others. The direct kinematic analysis of a mechanism consists of obtaining the parameters of interest (position, velocity, or acceleration) of the driven members from the corresponding parameters of the driving members (free coordinates and their first and second derivatives).

To formulate the positional kinematic problem, a vector equation, called the closure equation, is written, equating the sum of the vectors in the closure polygon to the zero vector. This equation expresses the fact that the vectors in the polygon form a closed path.

$$\sum_i \underline{z}_i = \underline{0}$$

If the mechanism has multiple loops, a vector equation is written for each loop.

To translate the vector closure equations into a system of scalar equations, we substitute the explicit expression of each vector with respect to an assigned reference system into the vector equations. If we choose, as the reference system, the one for which we have defined the angle of the vector ( $\varphi_i$ ), it results:

$$\sum_i \underline{a}_i \begin{Bmatrix} \cos\varphi_i \\ \sin\varphi_i \end{Bmatrix} = \underline{0}$$

This results in a system of  $m$  scalar equations, where  $m$  is equal to twice the number of independent loops in the mechanism:

$$f_i(\underline{x}, \underline{q}) = 0 \quad i = 1, \dots, m$$

where  $f_i = 0$  is the  $i$ -th equation of the system,  $\underline{q} \in \mathbb{R}^n$  is the vector of free coordinates,  $\underline{x} \in \mathbb{R}^m$  is the vector of dependent coordinates. The two vectors together contain all the variable terms (magnitudes and/or angles of vectors) present in the closure polygons, so the resulting system expresses the relationships between the position variables of the mechanism.

## 4.2. Models Implementation in MSC Adams

MSC Adams is a multibody dynamics simulation software used for analyzing and simulating the motion and behavior of mechanical systems. Adams allows users to model and simulate complex mechanical systems consisting of interconnected rigid and flexible bodies. It enables the analysis of how these systems move and interact with each other over time. The software can perform dynamic analyses, including kinematic and kinetic studies, to understand the motion, forces, and torques within a mechanical system.

One of the main advantages of performing a kinematic analysis of a mechanism using multibody simulation software is that the software assigns a local coordinate system (attached to the member) to each mechanism member and automatically constructs the transformation matrices to switch between these local coordinates and the absolute system coordinates. To define the Lagrangian coordinates of a rigid body, it is convenient to choose a reference frame attached to the rigid body and use the position of the frame's origin (3 variables) and the orientation of its axes (expressible with 3 variables) as free coordinates. The kinematic analysis of any system is, therefore, straightforward as it only requires creating rigid bodies with the correct lengths and inclinations and connecting them with the appropriate constraints.

### **Scarver by Tessier**

The Scarver represents Tessier's flagship model and is considered a benchmark in competitions. This monoski is predominantly constructed from aluminum and allows for numerous adjustments. Scarver has 3 possible kinematic configurations:

In position 1, when the damper compresses, the suspension movement is almost vertical, which is ideal for slalom, freeride and Dualski use.

In position 3, the centre of gravity of the frame moves forward when the shock absorber compresses. This moves the centre of gravity forward to compensate for the rear imbalance produced by skiing in a “carving” style and recharges the tip of the ski so that it bites through its entire length.

Position 2 is an intermediate, versatile position that will suit most people [6]. The analysis of the scarver has been performed with the connecting rods in configuration 2.

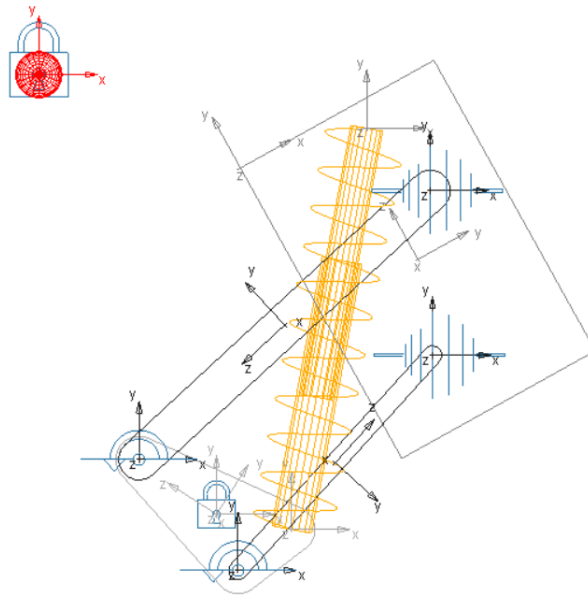


*Figure 4.1 – Scarver's kinematic configurations*

The reference system is defined by a left-handed tri-orthogonal coordinate system, with the X-axis oriented in the direction of ski advancement and the Z-axis perpendicular to the ground entering into this area.

In total, 5 rigid bodies have been created:

- A triangular plate for the base, connected to the two connecting rods and the monoshock. The plate is fixed to the "ground" body with a fixed joint.
- Two connecting rods created with "beam" rigid bodies, connecting the lower triangular plate and the upper rectangular plate. Revolute joints are used at the bottom, constraining 5 degrees of freedom, and spherical joints are used at the top, constraining 3 degrees of freedom while leaving all rotations free. It is important to construct a statically determinate system with 1 degree of freedom to avoid issues with the solver.
- An upper rectangular plate for constructing attachments to the frame. It is fixed to the connecting rods with two spherical joints.
- A sphere positioned at the center of gravity of the system, in accordance with the calculations in Giovanni Colla's thesis.



*Figure 4.2 – Scarver Adams Model*

The shock absorber has been recreated using the dedicated Adams function. The values of the spring stiffness constant  $k$  and the damping constant  $c$  do not influence the analysis in any way, so default values have been retained. The motion is imparted by a Motion applied to the 'Revolute Joint' between lower beam and the lower triangle with a specific motion law.

The model outputs include the movement along the X-axis and along the Z-axis of the sphere representing the athlete's center of gravity.

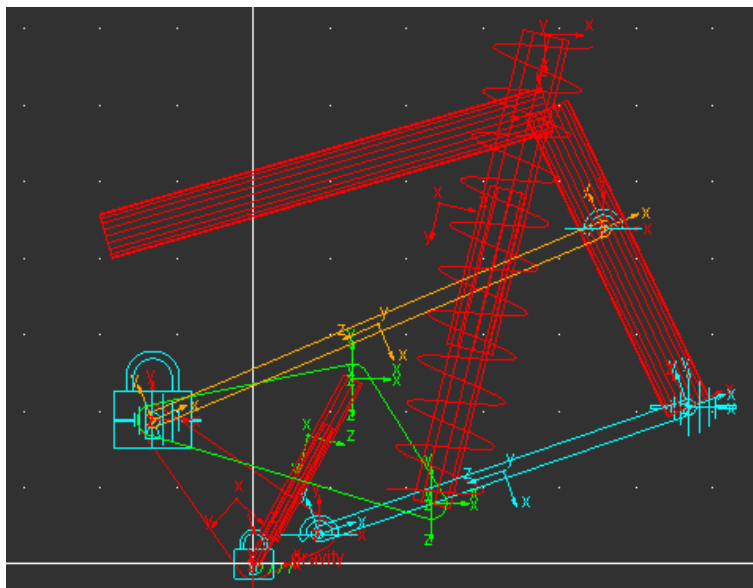
## **Tempo by Tessier**

Tempo represents the model designed for amateur skiers produced by Tessier. In its basic version, it comes equipped with an adjustable shock absorber, allowing for pre-load adjustments through a lever with three different positions. The lift system for the chairlift is assisted by two gas pistons. It is available in both Uniski and Dualski versions, with no changes in the longitudinal plane kinematics for the two variants. The frame is made of steel tubes, and the weight, including the seat and skis, hovers around 20kg.

The kinematic analysis of the Tempo is conducted in a manner almost analogous to that of the Scarver, with the distinction that, for this model, it has been possible to kinematically recreate the lifting mechanism as well.



*Figure 4.3 - Tessier Tempo*



*Figure 4.4 - Adams Model for Tessier Tempo*

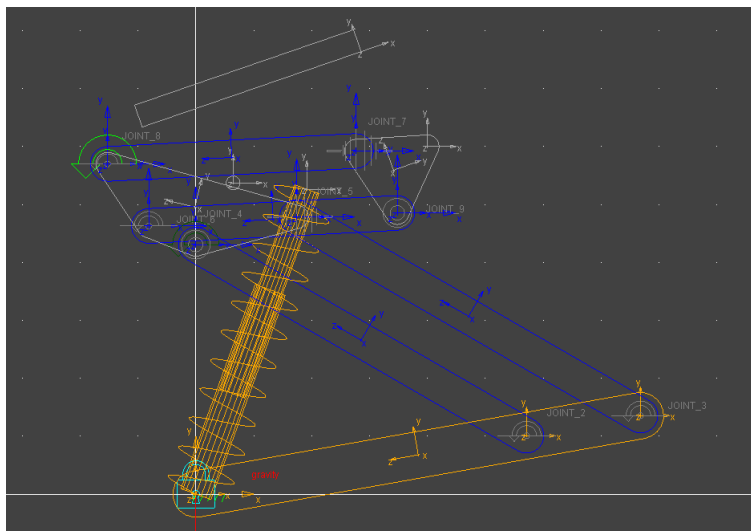
To recreate the lifting mechanism, a second plate (green in Figure 4.4) has been created, hinged at a point on the lower triangle. If one wishes to simulate the forward kinematics, the hinge is transformed into a "fixed joint." In the case of simulating the lifting kinematics, it is sufficient to revert the "fixed joint" back into a "revolute joint" and apply motion to the hinge.

## Impact Evolution

"Impact Evolution" is a monoski manufactured by the Swedish company Länna Svets & Mekaniska Verkstad AB. There is limited information available about this monoski. It is constructed entirely from aluminum, and it features a high-end Ohlins shock absorber.

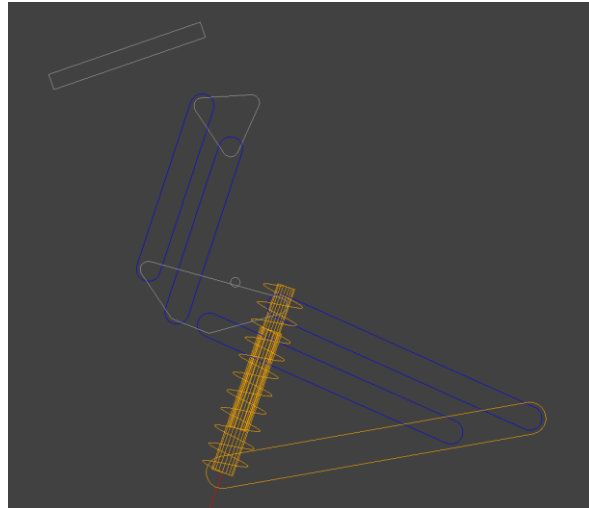


*Figure 4.5 - Impact Evolution*



*Figure 4.6 - Adams Model for Impact Evolution*

The construction of the "Impact Evolution" immediately stands out from all other monoskis: the single shock absorber and the two linkages are no longer attached to a triangular base but along a rod. The two linkages form an angle between  $90^\circ$  and  $180^\circ$  counterclockwise with respect to the x-axis. Above this mechanism, another one has been built, also based on an articulated quadrilateral, to manage the lifting mechanism.



*Figure 4.7 - Impact evolution lifted up*

As with the Tempo, here too, motions are applied to the Revolute Joints to move the system and record its kinematics.



## Monoski Racer by Alois Praschberger

The Monoski Racer is a model of monoski produced by the Austrian company Alois-Praschberger. Currently, it is one of the most affordable monoskis on the market, thanks to its steel frame. It features an entry-level spring shock absorber, a remote-controlled chairlift release system, and has a relatively low weight (approximately 13kg).



Figure 4.8 - Monoski Racer by Alois-Praschberger

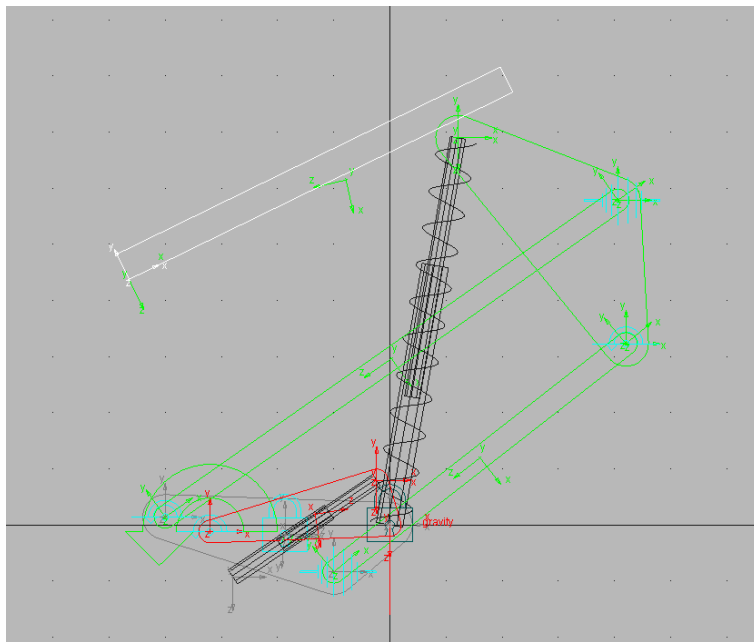
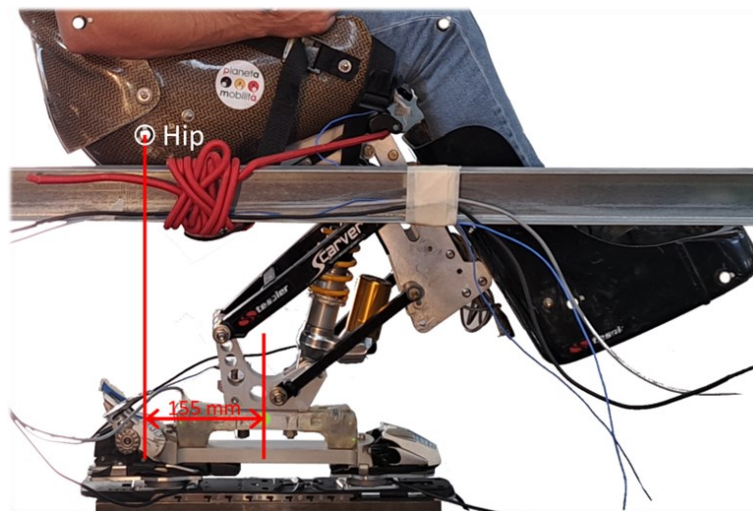


Figure 4.9 - Adams Model for Monoski Racer

Here, too, the model has been completely reconstructed, including the "easy-up system." It is noticeable that the model appears very similar in construction to that of the Tempo. In fact, the lower and upper parts of the system are connected at three points: two points where the linkages attach and one point for the shock absorber. The lifting system consists of a plate that rotates counterclockwise relative to the foot, moving the attachment of the spring-damper along a circular trajectory, assisted by two gas pistons.

## Results and Comparison

To obtain comparable results, a marker was placed at the hip joint calculated by Giovanni Colla for a skier on a monoski in all models. The method certainly has some limitations, as in a different monoski model, the hip may be positioned differently than in the monoski considered. However, given the difficulties in determining the actual position in each model, this is an approximation that we can accept since the analysis serves only to provide a rough idea of the movement that each mechanism allows.



*Figure 4.10 – Position of hip joint with respect to the Reference System*

Measurements of the displacement along the x-axis (horizontal displacement) and along the z-axis (vertical displacement) have been included and are shown in the following graph (Figure 4.11). The data refers to a compression of the monoski of 70mm.

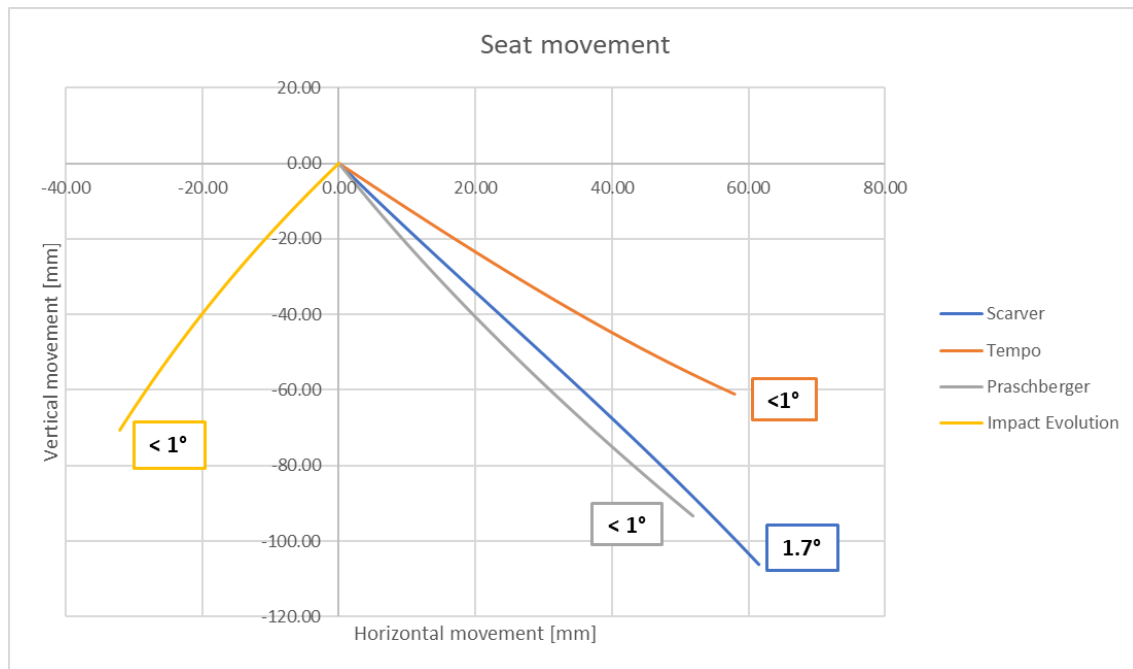


Figure 4.11 - Seat movement comparison

Values in colored text box refers to the seat rotation of each monoski that undergoes during monoshock compression.

The first observation that immediately stands out is how Impact Evolution moves in a completely different way from the 3 competitors. In fact, during the monoski compression phase, the seat descends and moves, almost without rotation, towards the rear of the ski. It was not possible to collect feedback from users of this system; however, it seems to disagree with the results obtained in the previously mentioned theses, where it was observed that it was necessary to move the COP (Center of Pressure) towards the front of the ski to be able to turn better and more quickly.

The other investigated monoskis, in fact, during the shock absorber compression phase, move consistently with the results observed in the theses, towards the front of the ski and downward.

It is interesting to note how the trajectory of Scarver, unlike that of Tempo and Monoski Racer, forms a line with concavity downward. This certainly depends on the position of the linkages, but a possible explanation is that, from the first millimeters of travel, an effort was made to move the center of pressure forward.

Differently in Monoski Racer and, in a much more pronounced way, in Tempo, the trajectory of the seat draws a line with concavity upward, which translates into a more vertical movement in the first millimeters of suspension travel.

Evaluating, instead, the numerical values of the displacement, it is noted that the 3 positively evaluated monoskis move the seat forward in a range between 50mm (Monoski Racer) and 63mm (Scarver). Conversely for the amount of sinking, where data are more dispersed: Scarver sinks by over 100mm, Monoski Racer sinks by 90mm, while Tempo sinks by only 60mm. This last value is certainly due to the particular configuration of its linkages: it is noted that the angle formed by these with the x-axis is smaller than that formed by the linkages of Scarver or Monoski Racer.

A logical deduction can be made: with the linkages oriented at an angle to the x-axis, of about 45 degrees, the maximum sinking with respect to the available travel is obtained. This is because, established that with this type of kinematics, the seat follows a circular trajectory, where the tangent to the trajectory has the steepest slope, the greater the sinking will be.

### 4.3. 2x2 Comparison Matrices

Comparison matrices, often employed in analytical frameworks, provide a structured approach to evaluating and contrasting elements within a 2x2 matrix. This format consists of two axes intersecting to create four quadrants, each representing a distinct set of criteria or variables.

Within this matrix, relationships and differences between elements become visually apparent, facilitating a comprehensive understanding of their comparative attributes. The simplicity of a 2x2 matrix lends itself well to scenarios where distinctions along two dimensions are pivotal for analysis.

This tool is frequently utilized in diverse fields such as business strategy, decision-making processes, and risk assessment. The horizontal and vertical axes can signify different dimensions, such as cost and benefit, risk and reward, or urgency and importance.

The upper left quadrant might represent situations with low risk and high reward, while the lower left quadrant could denote high risk and low reward. Such visualizations aid in prioritization, allowing for strategic focus on specific areas.

Effective utilization of 2x2 comparison matrices requires thoughtful consideration of the chosen dimensions, ensuring that the intersection of these elements conveys meaningful insights. Whether used in project management, product development, or strategic planning, 2x2 matrices serve as powerful tools for enhancing decision-making processes and fostering a nuanced understanding of complex relationships.

In the pursuit of a comprehensive evaluation of sit-skis, it is employed two distinct 2x2 comparison matrices, each focusing on key dimensions crucial for decision-making. The first matrix scrutinized the sit-skis based on their performance-price ratio, where the horizontal axis represented the price level and the vertical axis depicted the corresponding performance. This visual representation allowed for a clear assessment of the value proposition offered by each sit-ski in relation to its cost. The second matrix delved into the realm of adjustability-price, juxtaposing the extent of price flexibility against the degree of adjustability provided by each sit-ski. This approach facilitated a nuanced examination of the adaptive features in relation to the

associated cost. By employing these matrices, the evaluation process was not only structured but also visually intuitive, enabling a thorough analysis of sit-ski options based on essential criteria.

The sit-skis evaluated in these comparison matrices are:

- Scarver by Tessier
- Tempo by Tessier
- Impulse Boost by Unicent GmbH
- Monoski Racer by Alois – Prascherbegr
- Impact Evolution

The 2x2 comparison matrices in figures 4.12 and 4.13 highlight market segments that are not currently covered, and they aim to become the target market for the sitski addressed in this thesis.

It is noticeable that there is a lack of a sitski that offers decent performance at a modest purchase price. Among current competitors, systems capable of delivering "racing" performance come with almost prohibitive purchase prices. The market segment intended for amateurs is well-covered, but due to certain design choices in these sitskis, the purchase price remains high.

Analyzing the Adjustability-Price matrix, it is evident that high-end sitskis offer skiers a wide range of solutions to personalize and adapt the sitski to their needs. In contrast, models intended for amateurs provide few or no adjustment possibilities, making it challenging for a ski school to purchase a system adaptable to multiple people. One of the objectives of the sitski in this thesis is to offer, at a sustainable price, a system capable of providing a modest range of adjustments that can cater to a broad range of users.

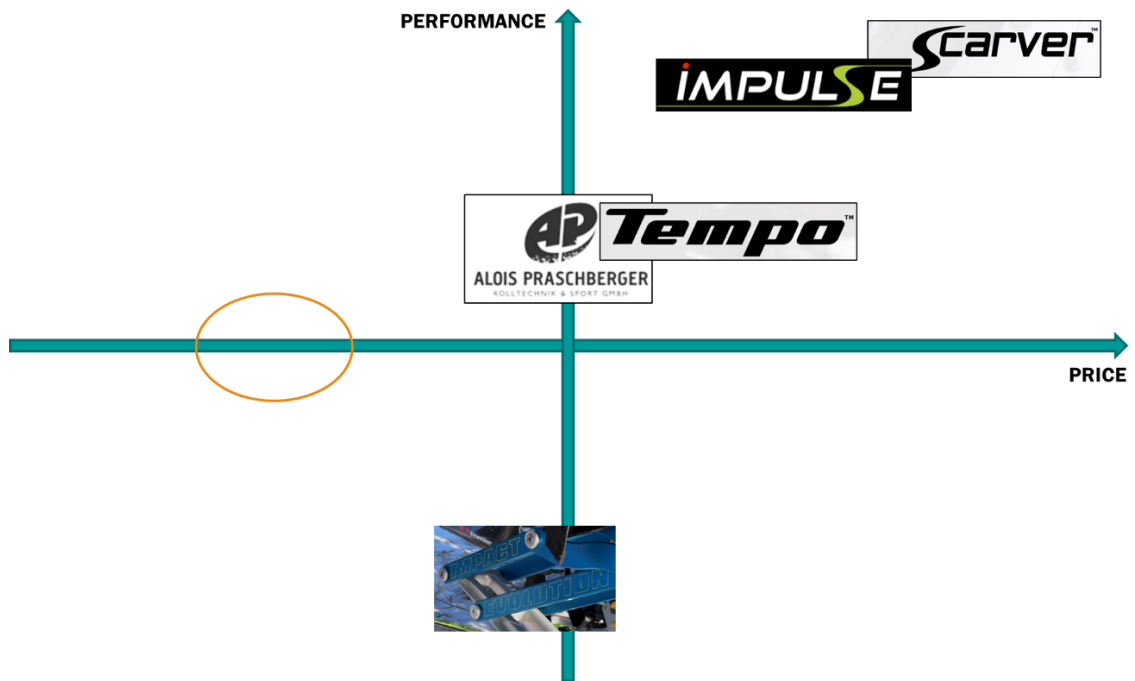


Figure 4.12 - Price - Performance Comparison Matrix

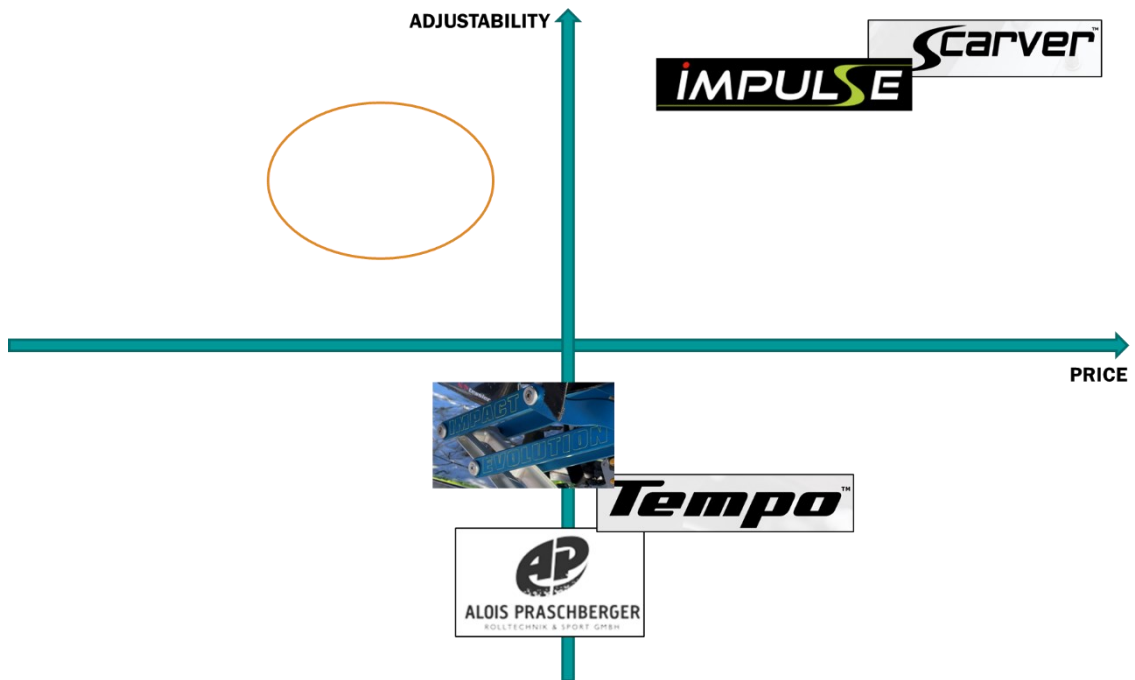


Figure 4.13 - Price - Adjustability Comparison Matrix





## 5. Technology Scouting

Technology scouting is a strategic business practice that involves actively searching for and identifying external technologies, innovations, or solutions that have the potential to enhance a company's competitiveness, drive innovation, or address specific business needs. It's a proactive approach to staying informed about developments in the broader technological landscape, both within and outside the industry, with the goal of gaining a competitive advantage.

Key aspects of technology scouting include identification of opportunities from external sources, such as startups, research institutions, industry conferences, patents, and technology publications. This involves looking beyond a company's internal R&D efforts to identify technologies that align with strategic goals and business objectives.

Technology scouting plays a crucial role in driving innovation by accelerating innovation cycles and introducing new products or services more rapidly. It helps companies maintain competitiveness by keeping them aware of emerging trends and ensuring they don't fall behind in the rapidly evolving technological landscape.

Additionally, technology scouting often leads to the establishment of partnerships, collaborations, or licensing agreements with external entities possessing the desired technologies. This can be a mutually beneficial way to leverage expertise and reduce R&D risks.

Successful technology scouting involves continuous monitoring of technological trends, breakthroughs, and market dynamics. It also includes looking beyond the immediate industry to draw inspiration or solutions from other sectors that may have relevance or applicability.

Intellectual property considerations are an integral part of technology scouting, requiring an understanding of existing patents and potential barriers to adopting or developing certain technologies.

Advanced data analytics and tools can be employed in technology scouting to sift through vast amounts of information, identify patterns, and generate actionable insights. Companies engaged in technology scouting often foster a culture of innovation within their organizations,

encouraging employees to actively explore external technologies and bring forward innovative ideas.

Overall, technology scouting is a proactive and strategic initiative that helps organizations stay at the forefront of technological advancements, foster innovation, and position themselves for long-term success in their respective industries.

## 5.1. Monoshock Absorber

In assessing the shock absorbers of commercially available monoskis, a careful examination revealed that the predominant models on the market often feature costly spring shocks. The inconvenience of changing a coil spring prompted a technological scouting effort to explore alternative solutions.

Notably, within the realm of downhill mountain biking, air shock absorbers have gained prominence for their versatility and adaptability. The utilization of air shocks in the biking industry has demonstrated superior adjustability, providing riders with the flexibility to fine-tune their suspension according to specific preferences and terrains. The exploration of this technology suggests that incorporating air shock absorbers into monoski designs could offer a more customizable and efficient solution for adaptive skiers. This insight from the technology scouting process may pave the way for enhanced performance and user experience in the realm of adaptive skiing equipment.



*Figure 5.1 – MTB with air Monoshock*

The air system for suspension consists of a sealed air spring chamber housed within an outer casing attached to the bike or motorcycle frame. The air spring chamber contains pressurized air, and the amount of air pressure determines the stiffness of the suspension. The piston, connected to a shaft, moves within the air spring chamber in response to external forces, compressing or decompressing the air to provide suspension. Damping mechanisms, such as rebound and compression damping circuits, control the speed of compression and rebound. These mechanisms often involve oil flow through valving to regulate the shock's movement.

Air shocks, compared to coil spring shocks, offer several advantages in terms of performance, adjustability, and overall versatility.

- *Variable Spring Rate:* Air shocks allow for a more easily adjustable spring rate. By simply adjusting the air pressure, users can fine-tune the suspension to match their weight, riding style, and terrain preferences. This level of customization is often challenging to achieve with coil spring shocks.
- *Lighter Construction:* Air shocks are generally lighter than their coil spring counterparts. The use of air eliminates the need for heavy metal coil springs, contributing to reduced overall weight on the bike or, in the context of monoskis, on adaptive skiing equipment.
- *Progressive Compression:* Air shocks exhibit a progressive compression rate. As the shock compresses, the air pressure increases, providing a more nuanced and controlled response to varying impacts. This progressive resistance can enhance the shock's ability to handle a wider range of terrains.
- *On-the-Fly Adjustments:* Adjusting air pressure can often be done on the fly, allowing riders to adapt to changing trail conditions without the need for specialized tools. This contrasts with coil spring shocks, where adjustments may require changing out the coil itself.
- *Simplified Maintenance:* Air shocks generally involve simpler maintenance compared to coil spring shocks. The absence of metal coils eliminates concerns related to sagging or fatigue over time. Regular maintenance often involves checking and adjusting air pressure.

- *Responsive and Sensitive:* Air shocks are known for their responsiveness and sensitivity to small bumps and impacts. This can contribute to a smoother ride, especially in situations where rapid and precise adjustments to the suspension are crucial.
- *Tailored to Rider Preferences:* The adjustability of air shocks allows riders to tailor the suspension to their specific preferences. This level of customization is particularly beneficial for adaptive skiers or bikers with unique requirements.

## 5.2. Release System

Quick release systems, commonly known as QR systems, are mechanisms designed for rapid and tool-free assembly and disassembly of components. The primary purpose of quick release systems is to facilitate swift and convenient adjustments, replacements, or removals without the need for specialized tools.

In the specific case of monoskis, it is crucial to design a system that allows for quick and easy unlocking of the seat when requested by the skier, usually with the aim of getting on a chairlift. Typically, the height and inclination of the seat from the ground do not allow for the use of such a service.

Analyzing the most commonly used monoskis, however, reveals that these systems, although user-friendly, practically translate into rather complex mechanical systems, involving cams, hooks, levers, and more.

Therefore, a technological scouting operation was conducted outside the monoski world, searching for a convenient, functional, easy, and cost-effective quick-release system. Attention turned to the agricultural sector, specifically focusing on quick coupling and uncoupling systems for agricultural trailers with tractors. This is crucial for farmers and operators who frequently need to switch between different tools based on the tasks at hand.

An American farmer, in particular, created a system that allowed him to change trailers independently and very quickly. The system caught the attention of friends and neighboring farmers who encouraged him to patent and commercialize the idea. The system, available in the market but less common among European farmers, is called Pat's Easy Change.

As can be seen in the figure below (Figure 5.2), Pat's Easy Change consists of a cast steel body that has the shape of a hook at the front, where the towing pin is inserted. A closing handle, held in place by a spring, keeps the pin securely fastened.

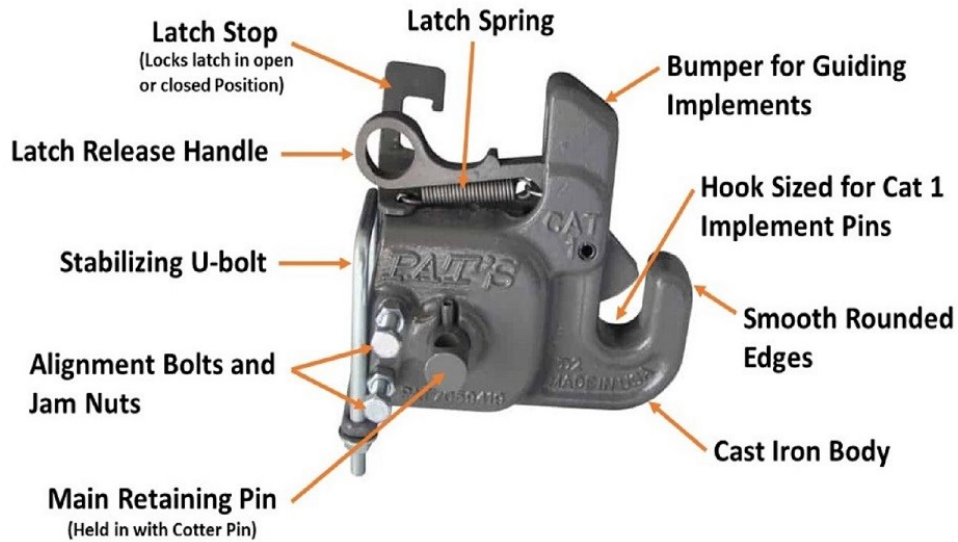


Figure 5.2 - Pat's Easy change

It is possible to implement a system of this kind in monoskis as well, scaling down the dimensions and selecting the necessary features. The final result will be presented in the chapter dedicated to design.



## 6. Definition of the kinematic scheme of the monoski

### 6.1. Constraints and Target

To define the kinematic scheme of a new monoski, it was important to establish constraints and design objectives from the very beginning. The main constraint is represented by the choice of the mono-shock absorber: low-end gas shock absorbers for bicycles do not reach the strokes and interaxles that the shock absorbers commonly mounted on monoskis achieve. The choice fell on a commercial shock absorber with the following characteristics:

- Wheelbase: 190 mm
- Stroke: 51 mm

From here, design objectives were defined based on the data obtained during the competitive benchmarking phase, identifying a range of values within which the forward and downward movement of the seat should fall. The objectives are listed in the table below (Table 6.1):

*Table 6.1 – Kinematic target value*

<b>Kinematic Parameter</b>	<b>Target Behave</b>	<b>Target Values [mm]*</b>	<b>Current Behave</b>	<b>Current Value [mm]*</b>
<b>Horizontal movement</b>	Forward	50 - 60		
<b>Vertical Movement</b>	Downward	70 - 100		
<b>Seat Rotation</b>	Counterclockwise	0° - 1°		
<b>Lift-up mechanism</b>	Upward	150 - 200		

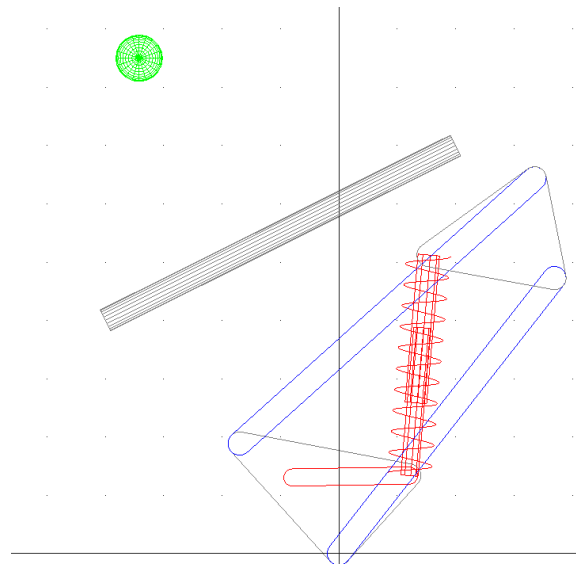
\*Values refer to the movement of the seat relative to the maximum compression of the mono-shock absorber.

Seat rotation refers to the amount of rotation imparted to the seat during the downward movement.

Lift-up mechanism, on the other hand, refers to how many vertical millimeters the reference marker must move during the lift for the chairlift. However, it is necessary to make a clarification here: the target values should be taken into context, assessing the limitations provided by external factors. As will be explained in the chapter on mechanical design, it is necessary for the lowest point of the frame to be 60cm above the ground to ensure that it is always possible to take the chairlift. The value indicated in the table, therefore, serves as an indicative target, based on the actual dimensions of commercial monoskis.

## 6.2. Final Design Scheme

To achieve a design capable to meet the required targets, the Trial-and-Error method was employed. To expedite the procedure, a Multibody model with rigid bodies was created, and the kinematic dimensions were parameterized.



*Figure 6.1 - Parametric Model in Adams*

It is possible to control the lengths and angles of the lower triangle, thus varying the positions of the attachment points of the linkages and the mono-shock absorber.



It is then possible to vary the length and inclination of the linkages, the interaxle distance, and the inclination of the mono-shock absorber.

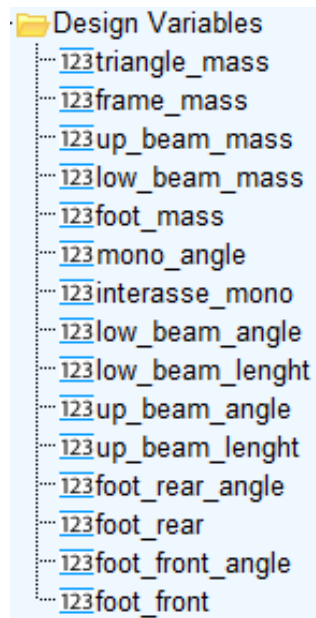


Figure 6.2 - Design Variables List

- Mono\_angle refers to the angle of the mono-shock absorber relative to the x-axis, calculated counterclockwise.
- Low\_beam\_angle refers to the angle of the lower linkage relative to the x-axis, calculated counterclockwise.
- Up\_beam\_angle refers to the angle of the upper linkage relative to the x-axis, calculated counterclockwise.
- Foot\_rear\_angle refers to the angle that the rear segment (on the left in the image) of the lower triangle forms with the x-axis, calculated clockwise.
- Foot\_rear refers to the length of the mentioned segment.
- Foot\_front\_angle refers to the angle that the front segment (on the left in the image) of the lower triangle forms with the x-axis, calculated counterclockwise.
- Foot\_front refers to the length of the mentioned segment.

These kinematic dimensions essentially characterize the Monoski system. The constraints used are essentially those used for the models described in the competitive benchmarking chapter.

The final mechanism has the characteristics listed in the following table (Table 6.2).

Table 6.2 - Design Variables values

Design Variable	Value
foot front length	90 mm
foot front angle	48 deg
foot rear length	127 mm
foot rear angle	48 deg
upper beam length	340 mm
upper beam angle	42 deg
lower beam length	300 mm
lower beam angle	52 deg
Monoshock wheelbase	190 mm
Monoshock angle	85 deg

It will be analyzed in chapter 6.3.

### 6.3. Results and comparison

Just like the Monoski models analyzed in the chapter dedicated to competitive benchmarking, the performance of the system obtained with the data reported in Table 6.3 is evaluated based on the movement of the seat during the compression phase of the mono-shock absorber.

The results are visible in the graph below (Figure 5.4).



Figure 6.3 - Monoski Unipd seat movement comparison

The data for Scarver, Tempo, Monoski Racer, and Impact Evolution are related to 70mm of shock absorber travel. Monoski Unipd, on the other hand, refers to the maximum travel of the chosen shock absorber, which is 51mm.

It is observed that the reference model follows a linear trajectory during the compression of the shock absorber. The model's sink exceeds 100mm, while the advancement slightly exceeds 30mm.

*Table 6.3 - Target and Current Values*

<b>Kinematic Parameter</b>	<b>Target Behave</b>	<b>Target Values [mm]*</b>	<b>Current Behave</b>	<b>Current Value [mm]*</b>
<b>Horizontal movement</b>	Forward	50 - 60	Forward	33
<b>Vertical Movement</b>	Downward	70 - 100	Downward	100
<b>Seat Rotation</b>	Counterclockwise	0° - 1°	Counterclockwise	~6°
<b>Lift-up mechanism</b>	Upward	150 - 200	Upward	179

It is observed that the seat undergoes a counterclockwise rotation of about 6° during the sinking, while the target value was almost zero rotation. For passenger comfort, it is suggested to keep this angle as close to zero as possible. [7]. However, it was decided to accept a slight rotation to increase the perceived sinking for the skier, providing a greater sense of what happens in the Monoski system. Choosing to keep the sinking value high has forced limiting the seat's forward movement. In the design phase, it will be essential to consider the limited forward movement of the system's center of gravity (COG). Therefore, it will be necessary to create a system with a relatively advanced COG projection onto the ground compared to the ski, making it easy to load into its front part and allowing for easy turning.



## 7. Mechanical design

### 7.1. Introduction

Within the previous chapter, the definition of the basic kinematic scheme of the sitski was discussed. Specifically, the characteristic dimensions of the articulated quadrilateral system were identified, determining the lengths of the linkages as well as the geometric parameters of the attachment points to the foot and the frame. Finally, the attachment points of the shock absorber and the length of the system allowing for disengagement when necessary to ascend on a chairlift were chosen.

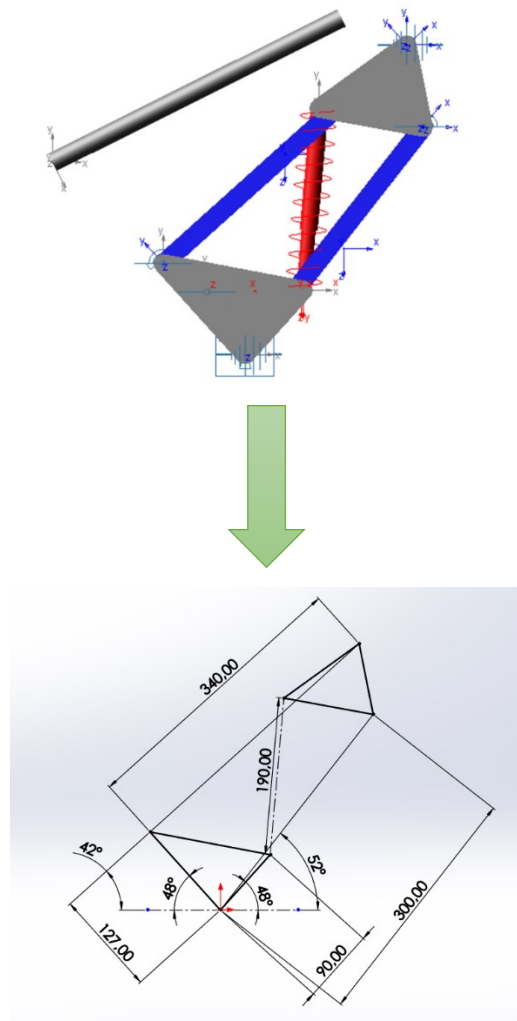


Figure 7.1 - Kinematic scheme of the Sitski

Starting from these geometric dimensions, three concept designs have been developed, which will be presented in detail later on. These are incomplete drawings from every perspective; however, they allow for a series of evaluations. From a single basic design, indeed, an infinite (or nearly infinite) number of conceptual designs can be developed. These designs must be compared with the project objectives and the available resources.

Before proceeding with the analysis of these three designs, it is necessary to make some preliminary considerations: the goal set by this thesis project is to create a sitski with the primary constraint of being cost-effective to produce. In order to meet this constraint, some a priori decisions have been made regarding the choice of materials and production systems.

## 7.2. Production System

Competition sitskis are mostly made with complex aluminum components processed using CNC machining. CNC-machined aluminum parts offer a combination of precision, versatility, and material advantages and are widely used across industries where lightweight, durable, and intricately designed parts are essential. The cost of CNC-machined aluminum parts can vary based on several factors, including the complexity of the part, the quantity being produced, material specifications, and the intricacy of the machining process.



*Figure 7.2 - on the left Scarver by Tessier, on the right Impulse Boost by Unicent GmbH*

In the automotive world, instead, the technique of aluminum die casting is increasingly being used. Aluminum die casting is a manufacturing process that allows for the production of complex and high-precision metallic components using pressure to force molten metal into a mold. This technique is widely employed in the industry to produce lightweight components with intricate geometries. Die casting is a rapid and efficient process and ensures high dimensional accuracy and repeatability. It is a process that proves to be very advantageous from many perspectives; however, the costs are extremely high for the production of a single prototype, which is why it has been discarded regardless.



*Figure 7.3 - Motorcycle components made by die casting*

The final method considered involves the creation of a prototype using metal profiles, sheet metal, and welding, aiming to minimize the number of parts to be machined on tooling machines and reduce waste.

There are a lot of benefits: for example, the use of readily available metal profiles and sheet metal, combined with efficient welding techniques, facilitates a relatively quick prototyping process compared to more intricate manufacturing methods. Furthermore, metal profiles, sheet metal are widely available in various grades and sizes, contributing to the accessibility of materials for the prototyping process.

Table 7.1 - Productive System Comparison Matrix

Criteria	CNC Machined Parts	Die-Cast Parts	Metal Profiles/Sheet Metal
<b>Material Options</b>	Wide range of materials, including metals, plastics, and composites.	Limited to materials suitable for casting, typically metals like aluminum, zinc, and magnesium.	Broad range of metals and alloys for profiles and sheet metal.
<b>Production Volume</b>	Suitable for both low and high volumes.	Economical for high volumes; tooling costs may impact low-volume production.	Suitable for both low and high volumes, cost-effective for low volumes.
<b>Complexity of Geometry</b>	Excellent for intricate and complex geometries.	Good for complex shapes but may have limitations compared to CNC.	Limited complexity compared to CNC; suitable for many shapes.
<b>Tooling Costs</b>	Generally lower tooling costs for prototypes and low-volume production.	Higher initial tooling costs; amortized over high production runs.	Lower tooling costs; especially beneficial for prototypes.
<b>Surface Finish</b>	High-quality surface finish achievable.	Excellent surface finish; may require minimal post-processing.	Good surface finish; additional processes may be needed.
<b>Tolerances</b>	High precision achievable; tight tolerances possible.	Good tolerances, but may be less precise than CNC.	Moderate tolerances; may require additional machining for tight tolerances.
<b>Material Waste</b>	Produces material waste	Generates minimal material waste in the casting process.	May produce more waste, especially in cutting and shaping processes.
<b>Lead Time</b>	Moderate lead times for prototypes and small batches.	Moderate lead times; tooling setup may take longer.	Short lead times for prototypes and small to medium batches.
<b>Cost for Prototypes</b>	Generally expensive	Higher initial cost for prototypes due to tooling; cost-effective for mass production.	Cost-effective for prototypes; lower tooling costs.
<b>Weight</b>	Can be lightweight depending on material choice.	Lightweight, especially for thin-walled sections.	Weight can vary based on material; generally moderate.
<b>Strength and Durability</b>	Excellent strength and durability, material-dependent.	Good strength; depends on the casting material.	Good strength, especially with welding; material-dependent.
<b>Applications</b>	Versatile for a wide range of applications.	Widely used in automotive, aerospace, and consumer goods.	Commonly used in construction, industrial equipment, and prototypes.



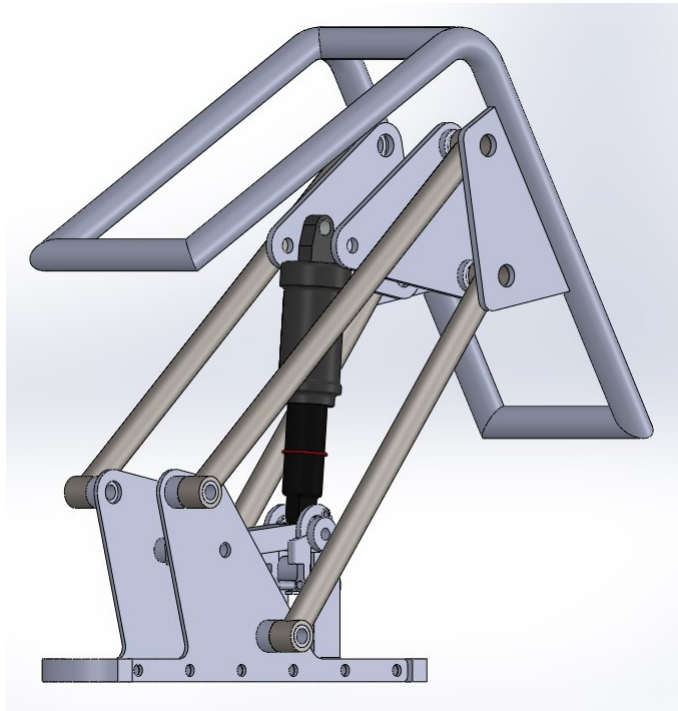
Considering the availability and costs of materials, the accessibility of mechanical processes, as well as the speed of prototype production, it was decided to opt for a sitski constructed using steel sheets and profiles. The aim was to employ processing methods that minimally required CNC machining, reducing material waste, and minimizing the hours needed for welding wherever possible.

Hence arises the idea of creating a tubular frame and the kinematics using tubular profiles and appropriately shaped metal sheets.

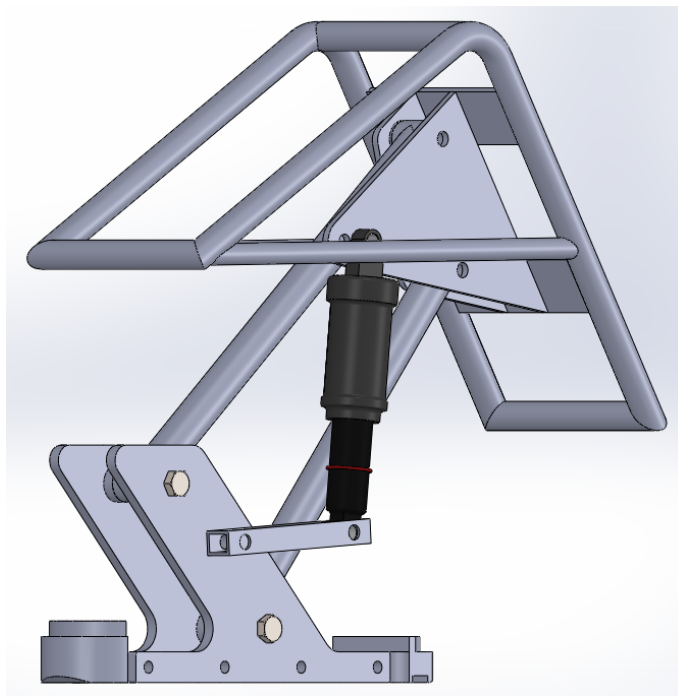
### **7.3. Design Concept**

The first design concept (Figure 7.4) involved constructing the frame using two bent side tubes, cut at  $45^\circ$  at the ends, welded to three transverse reinforcement tubes. The linkages were built using tubes, also angled at the ends, welded to two bushings obtained by turning a cylinder to create a seat for needle bearings. The upper triangle comprised two welded external plates cut into the frame and two internally drilled plates for connecting to the shock absorber. The lower triangle consisted of two shaped plates bolted to the side of the monoski foot. The lifting system, finally, consists of a rectangular-sectioned boxed tube, bolted to the lower triangle on one side and to the shock absorber on the other, free to disengage and rotate around the pivot that fixes it to the lower system.

The second design concept (Figure 7.5) was conceived to overturn the classical monoski concept, which involves the adoption of two lateral quadrilaterals and the positioning of the shock absorber at their center. This, in fact, envisages the use of a single linkage positioned along the longitudinal axis of the system and the decentralization of the damping system. The lower triangle remains bolted to the side of the foot, while the frame-upper triangle superstructure is completely overhauled. The welded plates cut into the frame tube are eliminated, and two sheets are added fixed transversely to it, on which the upper triangle rests.

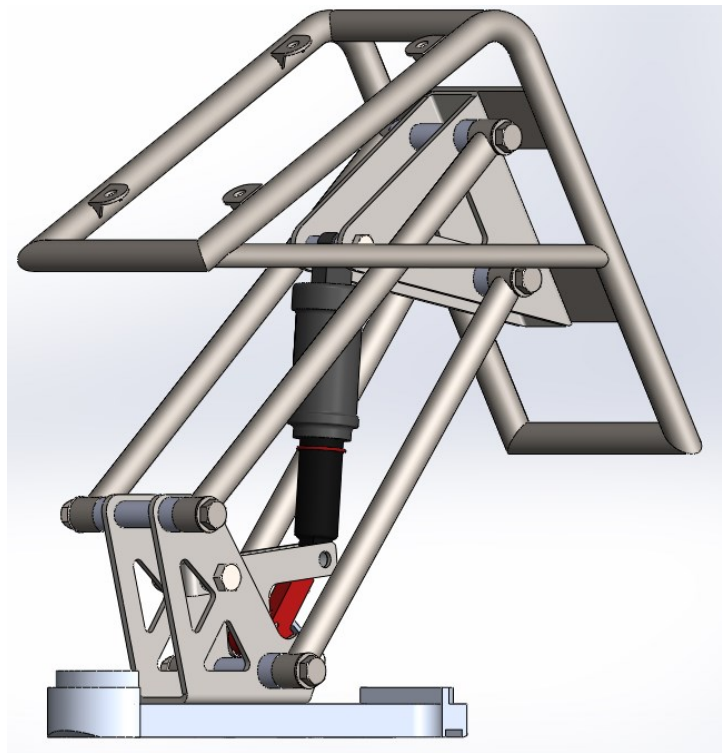


*Figure 7.4 - First Concept Design*



*Figure 7.5 - Second Concept Design*

The third and final Design Concept (Figure 7.6) arises as a fusion of the first and second, retaining the best ideas from both and significantly improving certain aspects. Like in the first concept, it maintains the adoption of two lateral linkages with the shock absorber at the center. The frame retains the welded transverse plates on which the upper triangle, consisting of a U-shaped bent sheet, is bolted. In the lower area, the same production line is followed, and the lower triangle also adopts the U-shaped bent sheet. The linkages are the same as those in the first design concept.



*Figure 7.6 - Third Concept Design*

The third solution appears to be the most structurally sound. The first one, in fact, severely limits the width of the frame or would require very long spacers to create an offset between the lower triangle and the upper plates. This would result in the transmission of large moments on the pins. Furthermore, the welded cutting plates create significant stress concentrations at a point that would make sizing the frame very difficult.

On the other hand, the second concept design introduces significant complexities both structurally, giving rise to forces that are discharged asymmetrically into the frame, and geometrically, requiring the quick-release mechanism for the chairlift grip to be moved outside the foot's ground projection.

The third design, finally, allows freedom in choosing the frame dimensions, does not create transport moments or asymmetric forces, and structurally seems to be the best to develop.

Below is a summary table (table 7.2), which evaluates the concept designs from 1 to 5 according to some criteria identified by the designer, known as the Pugh Matrix for concept testing.

Table 7.2 - Concept Scoring Matrix

		CONCEPT DESIGN					
		I		II		III	
Attributes	Weight	RATING	SCORE	RATING	SCORE	RATING	SCORE
Chassis Design	15.00%	2	0.3	5	0.75	5	0.75
Joints and Connection	8.00%	2	0.16	2	0.16	4	0.32
Adjustability	14.00%	4	0.56	4	0.56	4	0.56
Suspension System	10.00%	4	0.4	3	0.3	4	0.4
Weight Distribution	5.00%	5	0.25	1	0.05	5	0.25
Release System	13.00%	3	0.39	2	0.26	4	0.52
Modularity	7.00%	3	0.21	5	0.35	5	0.35
Ease of Assembly	6.00%	3	0.18	5	0.3	2	0.12
Forces Distribution	10.00%	4	0.4	2	0.2	4	0.4
Constructive Freedom	12.00%	3	0.36	5	0.6	5	0.6
FINAL SCORE			3.21		3.53		4.27
RANKING			3		2		1

In the table, each attribute is assigned a specific weight that is multiplied by the assigned value ranging from 1 to 5. Finally, the scores are summed, resulting in the ranking of concept designs and identifying the best starting design.

$$Final\ score_{cd} = \sum_{i=1}^n Rating_i \cdot Weight_i \quad with\ cd = I, II, III$$

n attributes.

The model developed from the third concept design is analyzed in the following chapters.

## 7.4. Foot

The sitski foot is the part that allows the connection of the system with the ski. It must possess the same geometry and characteristics as the shell of a ski boot, as it should enable insertion into traditional ski bindings.



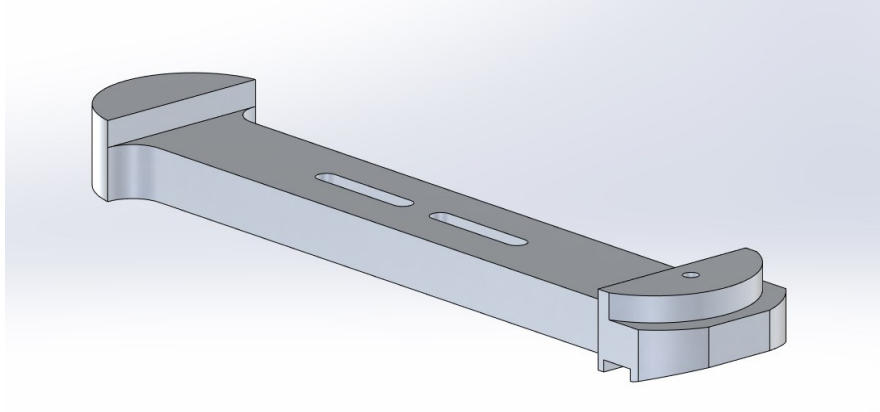
*Figure 7.7 - Ski Boot*

The crucial parts to replicate, particularly the toe and the heel, are important because it is thanks to their shape that insertion and disengagement in the ski binding are allowed. Due to the irregular shape and required stiffness, the decision was made to machine the foot from a solid block of Aluminum 7075 (Ergal) measuring 323x70x30 mm. The toe (highlighted in yellow in Figure 7.8) and the heel (highlighted in orange in Figure 7.8) require a height of 30mm, while the central part is lightened by maintaining an external thickness of 20mm and creating pockets on the bottom.

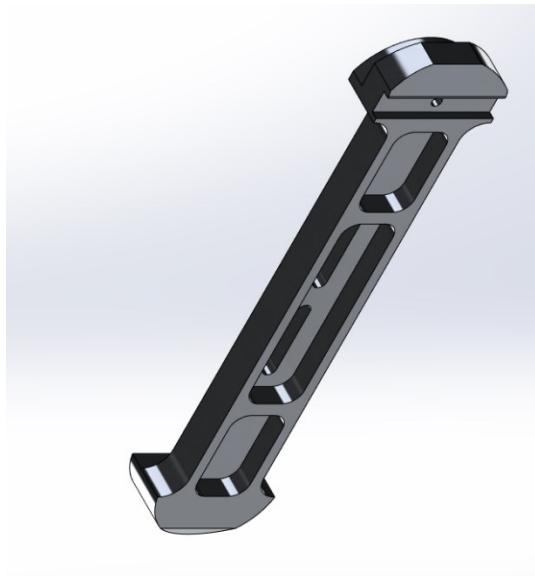


*Figure 7.8 - Sitski "foot"*

The two slots on the bottom are for securing the lower triangle and allow adjustment of its position forward or backward in the sagittal plane. Fastening is done using two flanged hex head bolts M8x25, class 8.8, made of galvanized steel (DIN 6921). The total length of the slot is 40mm.



*Figure 7.9 - Details of "foot": the slots*

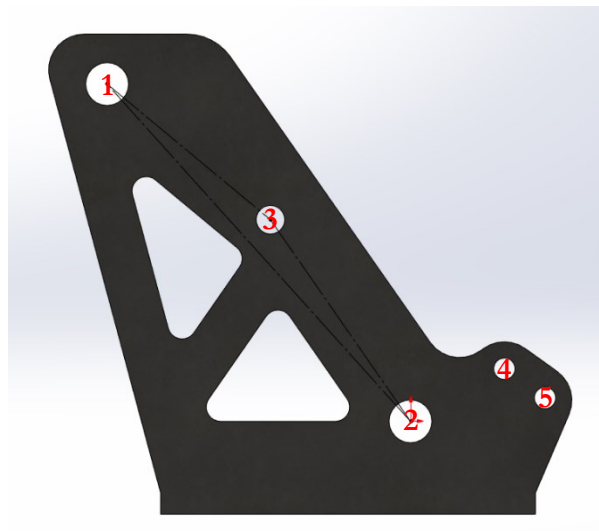


*Figure 7.10 - Details of "foot": pockets*

The verification of the bolted connection with the lower triangle will be further examined in Chapter 8.

## 7.5. Lower Triangle

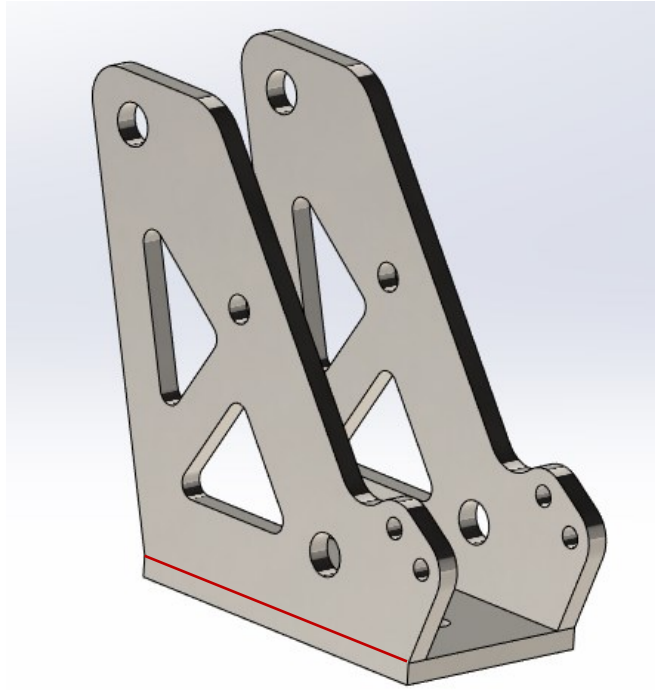
The lower triangle is the component of the monoski bolted beneath the foot, allowing, laterally, the attachment of the linkages and internally the attachment of the lifting system. The nomenclature 'triangle' refers to the initial sketch on the sagittal plane, obtained by connecting the attachment point of the upper linkage, the attachment points of the lower linkage, and the attachment point of the lifting system.



*Figure 7.11 - Lower Triangle*

Holes **1** and **2**, with a diameter of 12mm, accommodate the pins of the linkages. In hole **3**, with a diameter of 8mm, the pin of the lifting mechanism is inserted, which will be described later. Bolts M6 are inserted into holes **4** and **5** for fastening the quick-release mechanism (Figure 7.11). Finally, two lightening windows have been created in the component.

Initially, the component was designed to be water-cut from a 6mm thick sheet of Fe360 steel, and then bent to form a U with a width (distance between the inner walls) of 46mm. However, due to difficulties in maintaining hole alignment during bending, the decision was made to cut two side plates to be welded onto the lower plate. The welding bead line is marked in red in Figure 7.12.



*Figure 7.12 - Isometric view of Lower Triangle*

During the prototype construction, due to the ease of sourcing the material, the lower triangle was made from an 8mm sheet of Avional EN AW 2017. The yield strength of this aluminum is equivalent to that of Fe360 (275Mpa), despite being much lighter (7850 kg/m<sup>3</sup> vs 2780 kg/m<sup>3</sup>). Although it was necessary to widen the lower triangle for space considerations and construct it from an 8mm sheet, the weight of the component decreased from 1130g (Fe360) to 550g (Avional EN AW 2017). However, the specific cost of aluminum is more than double that of steel, so it is suggested to use steel for a more economical model and aluminum for a more performance-oriented, lightweight, and expensive model.



## 7.6. Lift up System

The lift-up system is the assembly of components that connect the lower triangle with the shock absorber and the quick-release system. In particular, it consists of two shaped and lightened water-cut steel plates (1), a spacer with shoulders (2), a locking pin (3), four radial ball bearings (4 - 5), and a torsional spring (Figure 7.13).

The system is mobile, and when activated by the skier, it must rotate around the pivot connecting it to the lower triangle, allowing the rear part of the frame to lift for the purpose of accessing ski lift facilities.

The two plates are water-cut from the same 6mm thick Fe360 steel sheet, from which the lower triangle is also derived. However, they need further machining on a milling machine to create the shoulder and the seat for the bearings, which are inserted with an interference fit.

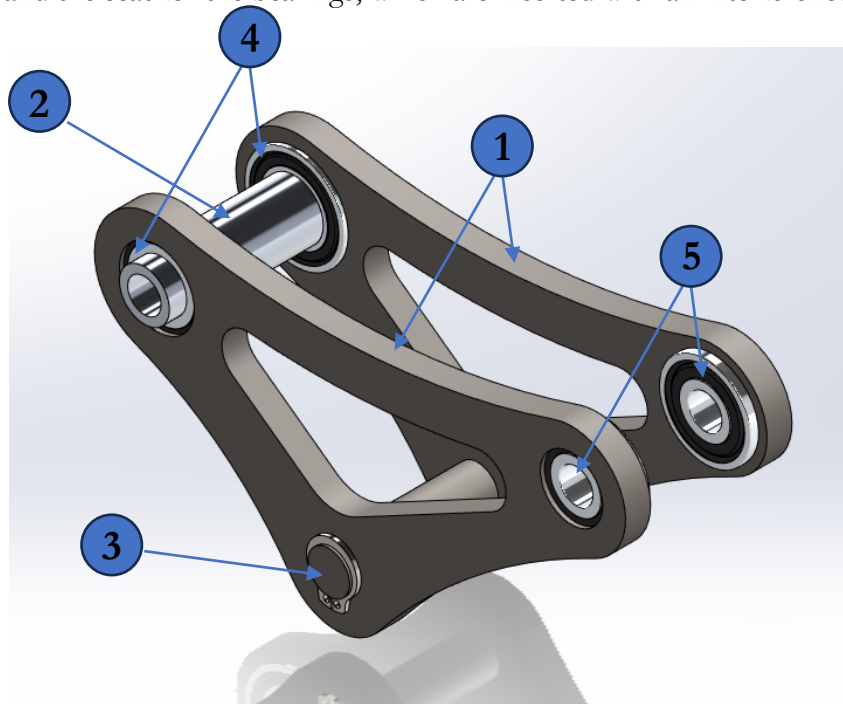
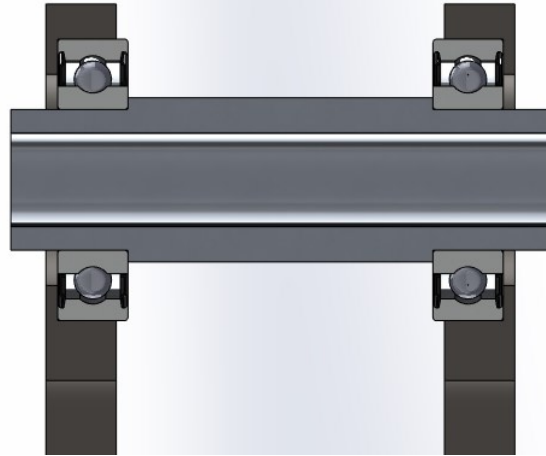


Figure 7.13 - Lift up System

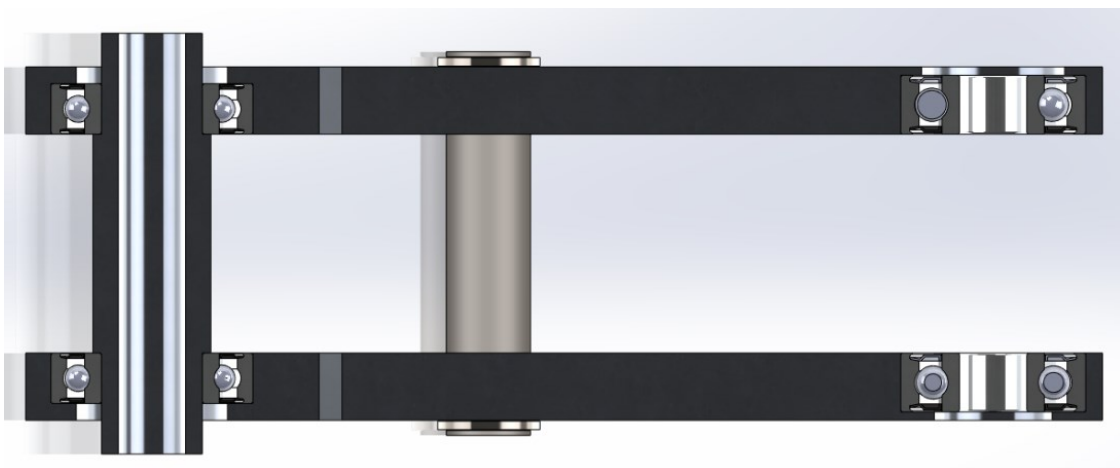
The locking pin is a ground pin made of C40 steel, with a diameter of 10mm, on which seats for retaining rings (DIN 470 – 10 x 1) are machined. These rings serve the function of keeping the pin in place.



*Figure 7.14 - Section view of lift up System*

On the spacer, shoulders are machined to prevent the two plates from collapsing inwards. This spacer is coupled with the bearings with clearance. This solution was chosen with assembly in mind, aiming for simplicity and speed.

Similar to the lower triangle, these triangles were also produced during the prototype construction using an 8mm sheet of Avional EN AW 2017. The increased thickness of these triangles allows for the creation of seats for bearings that fully contain them (Figure 7.15). The weight of each individual triangle decreased from 144g (6mm, Fe360) to 68g (8mm, Avional EN AW 2017).

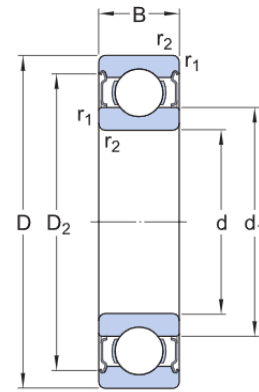


*Figure 7.15 - Lift Up System in Aluminium*

The rear bearings (4) were chosen from the SKF catalog and have the code 61901 – 2Z. Dimensions and calculation data are reported in table 7.3, below.

Table 7.3 - SKF 61901 2Z Data

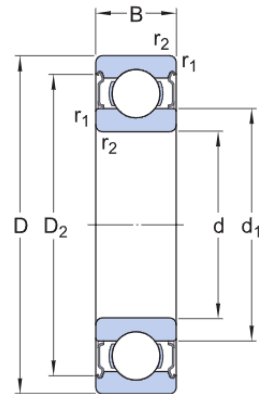
Deep groove ball bearing		61901 2Z	
<b>DIMENSIONS</b>			
Bore Diameter	d	12	mm
Outside Diameter	D	24	mm
Width	B	6	mm
<b>CALCULATION DATA</b>			
Basic Dynamic Load Rating	C	2.91	kN
Basic Static Load Rating	$C_0$	1.46	kN
Fatigue Load Limit	$P_u$	0.062	kN
Minimum Load Factor	$k_r$	0.02	
Calculation Factor	$f_0$	14.5	



The front bearings (5), on the other hand, have the code 608 – 2Z and come from the SKF catalog. Dimensions and calculation data are reported in the table 7.4, below:

Table 7.4 - SKF 608 2Z Data

Deep groove ball bearing		608 2Z	
<b>DIMENSIONS</b>			
Bore Diameter	d	8	mm
Outside Diameter	D	22	mm
Width	B	7	mm
<b>CALCULATION DATA</b>			
Basic Dynamic Load Rating	C	3.45	kN
Basic Static Load Rating	$C_0$	1.37	kN
Fatigue Load Limit	$P_u$	0.057	kN
Minimum Load Factor	$k_r$	0.025	
Calculation Factor	$f_0$	12	



For the verification of the bearings, please refer to the next chapter.

## 7.7. Quick Release System

The quick-release system is a set of components with the dual function of holding the lifting system in place during skiing and, when requested by the skier, allowing it to detach freely.

This part of the sitski is particularly critical and crucial: the release must be guaranteed at any time, easy to activate, and as simple as possible, in line with a sustainable sitski.

The first choice to be made concerned the positioning: it can be positioned either above the mono-shock absorber or below it. Both solutions have advantages and disadvantages:

- Placing it above has the advantage of protecting the system from compacted and frozen snow that could block it. Additionally, it reduces the need to reach the actuator with cables or other linkage systems, which are subject to wear and breakage.
- On the other hand, placing the system below has the advantage of reducing bulk in the frame area, facilitating the attachment of components, and simplifying the system.

It was decided to opt for the second option, keeping in mind the disadvantages it brings.

As seen in the paragraph dedicated to technological scouting, the idea comes from the world of agricultural machinery, where quick and secure coupling and uncoupling of trailers to tractors is necessary.

The system consists of three main components: the hook, the closing handle, and the return spring. The pin (3 in figure 7.13) rests in the hook and is locked by the closing handle during skiing.

By actuating a steel cable, it is possible to rotate the closing handle, thus freeing the closure pin (Situation 2, Figure 7.16). The return spring will then bring the closing handle back to its position (Situation 1, Figure 7.16). During reattachment, the pin will fall onto the closing handle, which, being shaped, will open spontaneously and then close over the pin thanks to the return spring.

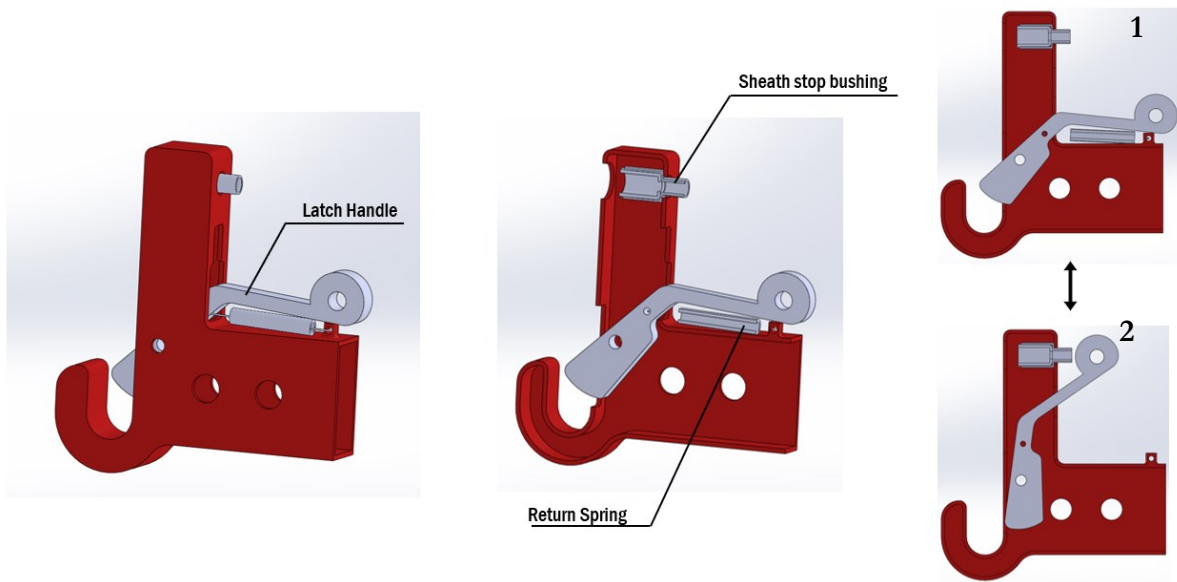


Figure 7.16 – Section View of Release System

For the realization of the piece, it was decided to divide the component into two semi-parts. On an 8mm Fe360 sheet, the closing handle and two hooks are shaped, then appropriately milled to create the housing for the handle.

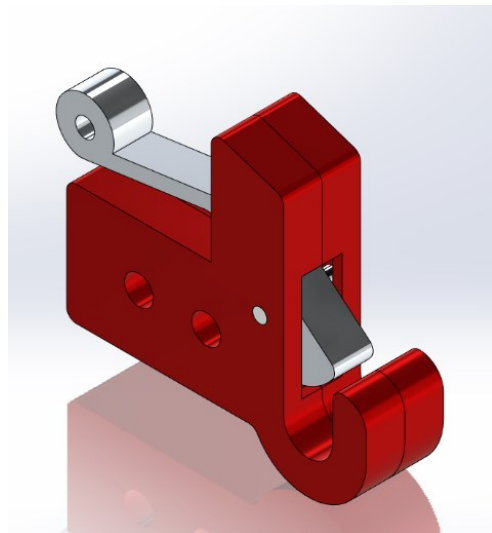
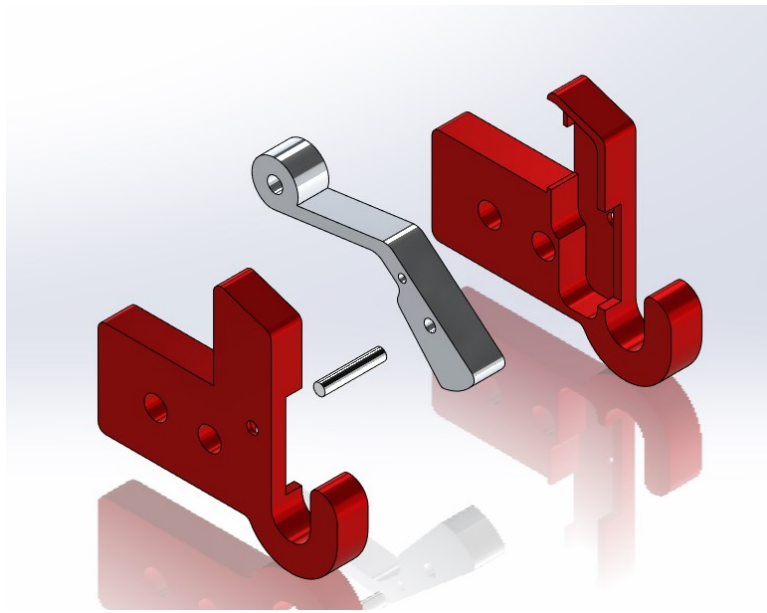


Figure 7.17 – Release System Assembly

The two halves of the piece are held together, in part, by fixing bolts to the lower triangle, pivoting around the axis about which the closing handle rotates. The shaft-hole coupling has clearance between the handle's pivot and the handle itself, with a slight interference between the handle's pivot and the body of the hook. In this way, the component must be tapped in with a mallet and will remain in position during use, while still allowing the handle to rotate freely without uncomfortable friction.



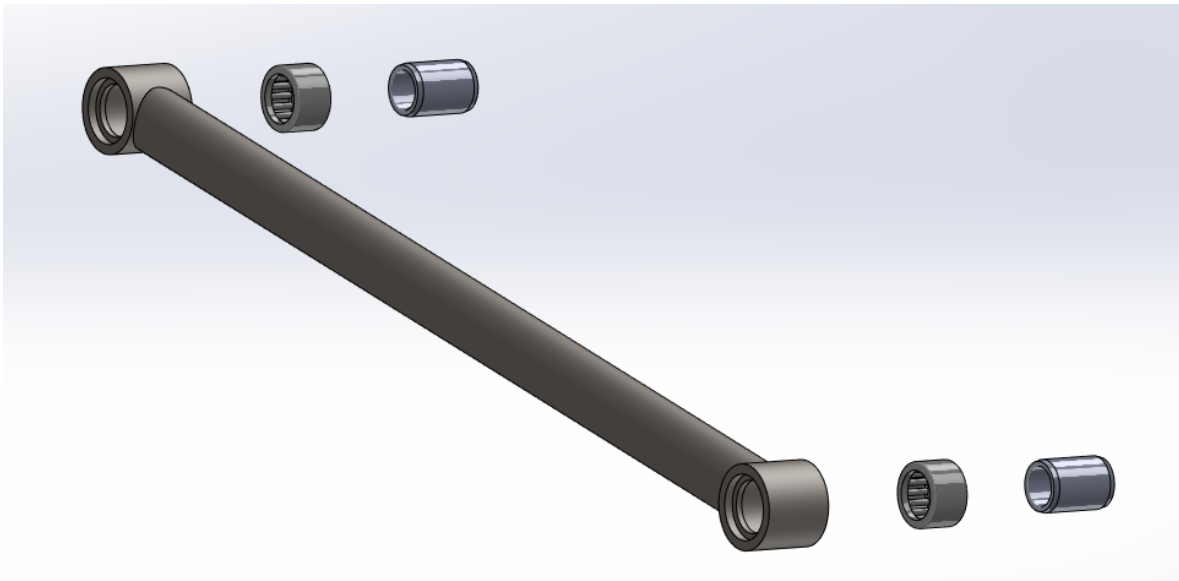
*Figure 7.18 – Exploded View of Release System*

The attachment to the lower triangle is better described in paragraph 7.11.

## 7.8. Beams

Beams constitute a fundamental part of the articulated quadrilateral system that determines the movement of the sitski. They connect the lower part of the system (foot, lower triangle, release system, etc.) with the upper part (upper triangle and frame). In order to avoid complicating the geometry of these components and minimize production costs, they have been designed using 25CrMo4 steel tubes, chamfered at the ends, and welded to bushings. These bushings are lathe-worked to create the seat for a needle roller bearing.

The choice of bearings in these cases is particularly crucial, as it is necessary to ensure the tightening of bolts while allowing relative motion between the components.

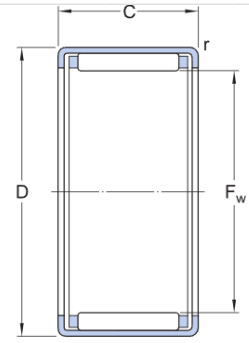


*Figure 7.19 – Exploded View of the Assembly of a beam*

It has been chosen to use SKF HK1612 needle roller shells, equipped with a thin-walled outer ring, cold-formed. Needle roller shells are typically used in applications where the housing bore cannot be used as a track for the roller and cage assembly, and instead, a very compact and economical bearing arrangement is required. These bearings are mounted with an interference fit locked in the housing. This allows for a simple and economical design of the housing bore [8].

Table 7.5 – SKF HK1612 Data and Dimension

Drawn cup needle roller bearing		HK 1612	
<b>DIMENSIONS</b>			
Diameter under rollers	$F_w$	16	mm
Outside Diameter	$D$	22	mm
Width	$C$	12	mm
<b>CALCULATION DATA</b>			
Basic Dynamic Load Rating	$C$	7.37	kN
Basic Static Load Rating	$C_0$	9.8	kN
Fatigue Load Limit	$P_u$	1.12	kN



Internally, however, an inner ring is housed (IR 12X16X22). Inner rings are typically combined with needle roller and cage assemblies or drawn cup needle roller bearings in applications where the shaft cannot be hardened and ground.

The inner ring protrudes by two tenths of a millimeter on each side axially. This creates axial play for the connecting rods but brings the bolts and nuts into contact directly with the inner ring, avoiding the constraint of the connecting rods (Figure 7.20).

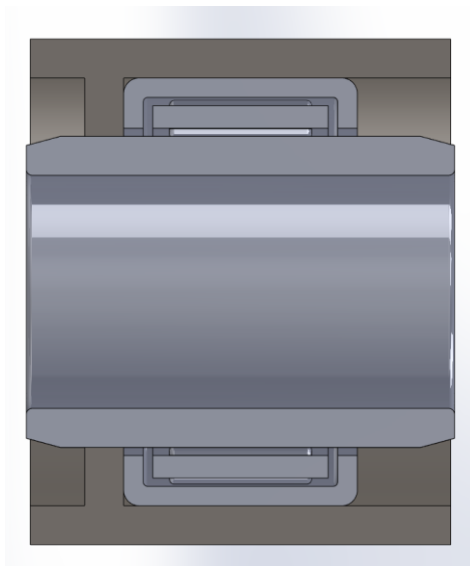


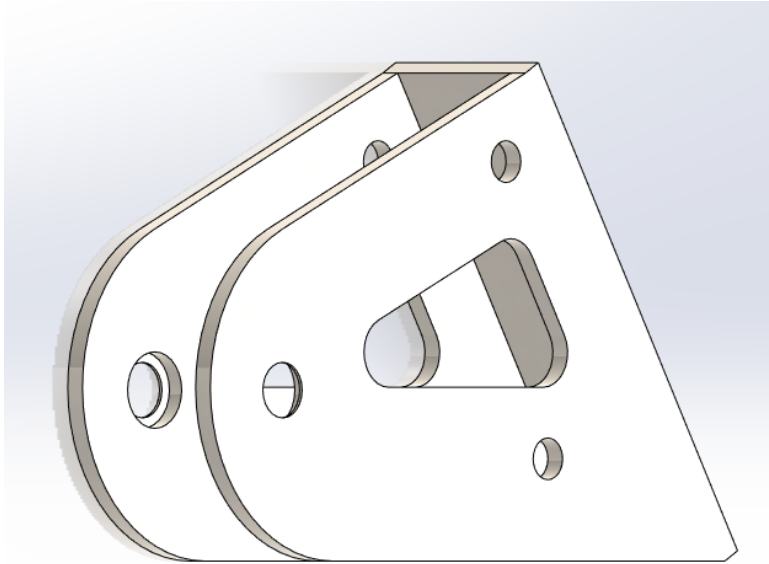
Figure 7.20 - Details of bearing

Due to spatial constraints, the connecting rods are mounted with 10mm spacers on the triangles. This certainly poses a disadvantage from a structural perspective, but it is preferable to having to produce bent connecting rods.



## 7.9. Upper Triangle

The upper triangle provides the upper attachment points for the mono-shock absorber and the connecting rods. For its construction, the same considerations as those made for the lower triangle apply. It is therefore built by water cutting a 6mm Fe360 sheet, obtaining two side plates to be welded onto a plate that serves as the base (Figure 7.21).



*Figure 7.21 – Upper Triangle*

The component has also been designed to fulfill the function of protecting the mono-shock absorber from impacts caused by the chairlift. Similar to the lower attachment point of the mono-shock absorber, bearings are intended to be positioned at the upper attachment point to ensure the correct relative motion between the shock absorber and the component.

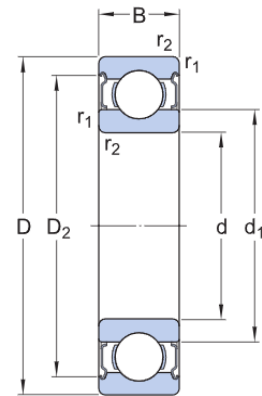
The seat for the bearing is created by milling the two side plates before being welded onto the backing plate. The bearing shoulder has a thickness of 1 mm. The bearing used is the same ball bearing mounted on the lower attachment point of the mono-shock absorber. It is sourced from the SKF catalog and has the code 608 – 2Z.

Dimensions and calculation data are reported in table 7.6, on the next page.

For the verification of the bearings, please refer to the next chapter.

Table 7.6 - SKF 608 2Z Data

Deep groove ball bearing		608 2Z	
<b>DIMENSIONS</b>			
Bore Diameter	d	8	mm
Outside Diameter	D	22	mm
Width	B	7	mm
<b>CALCULATION DATA</b>			
Basic Dynamic Load Rating	C	3.45	kN
Basic Static Load Rating	$C_0$	1.37	kN
Fatigue Load Limit	$P_u$	0.057	kN
Minimum Load Factor	$k_f$	0.025	
Calculation Factor	$f_0$	12	



During the prototype construction, the upper triangle was made from an 8mm sheet of Avional EN AW 2017. There is a significant weight reduction, decreasing from 2005g (6mm, Fe360) to 947g (8mm, Avional EN AW 2017). As with the triangles of the Lift-Up System, the thickening of the sheet from which the component is made allows the creation of seats that fully contain the bearings.

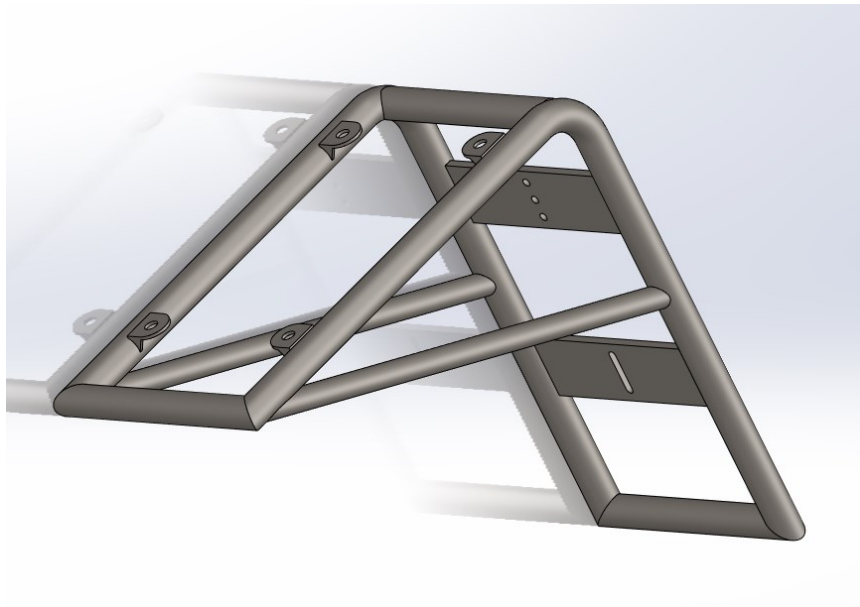
## 7.10. Frame

The frame constitutes one of the most important parts of the entire sitski system. It serves as the interface between the skier and the monoski, accommodating the seating system on it and connecting to the upper triangle at the bottom.

It is a crucial part as the skier's position depends on its geometry, influencing the overall feeling, comfort, and Center of Pressure of the entire system. Given that the sitski is targeted at beginners and enthusiasts, a moderate seating inclination of about 30 degrees from the horizontal was chosen.

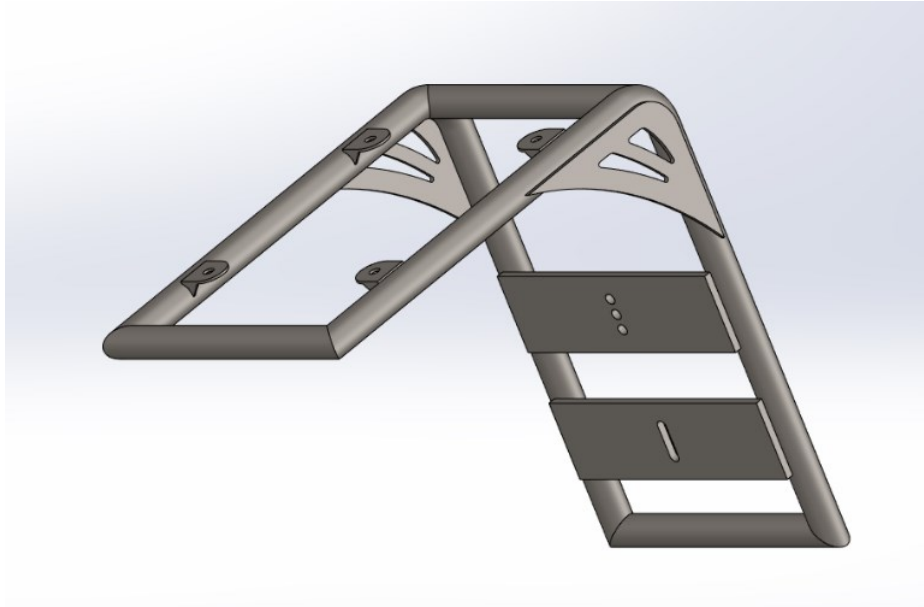
Another design consideration was the positioning of the upper triangle, which cannot be arbitrarily placed. It is necessary to ensure that, when in the raised position, the frame's lower part, under the seat, is 600mm above the ground. Italian chairlifts have a boarding and disembarking seat height of 45cm +/- 5cm [2]. The distance is measured at the center of the seat width at the front edge. This distance must account for the thickness of the snow needed for operation.

In the first version, the frame appeared as in the image below (Figure 7.22).



*Figure 7.22 – First frame version*

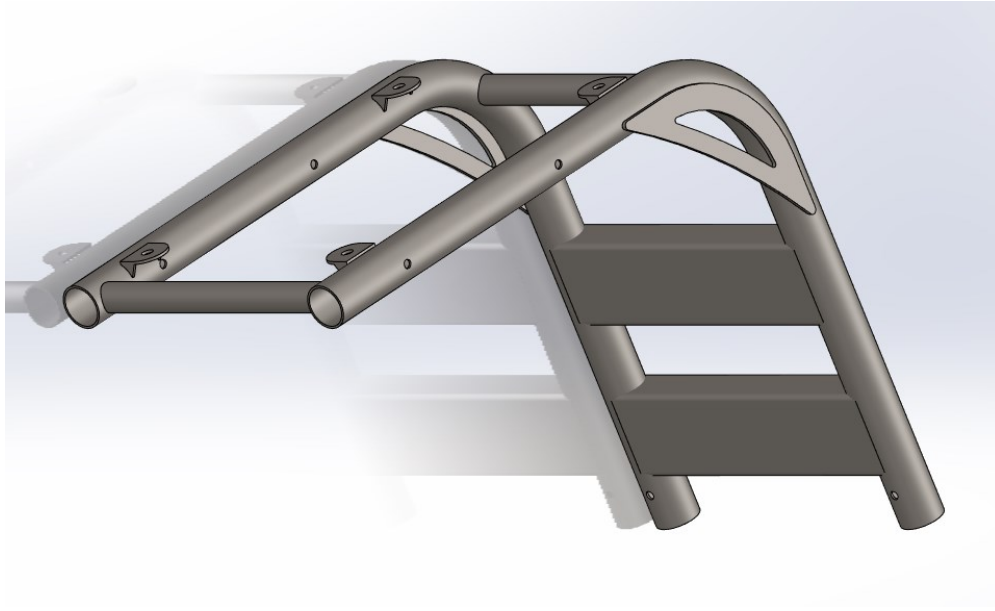
The plates are welded in the middle of the tube, and a reinforcing tube is used. In a second version (Figure 7.23), the plates were placed on the inner face of the tubes to induce bending stress. The reinforcing tubes, allowing the sitski to ascend on the chairlift, were replaced by a plate, which is externally welded along the tube's centerline.



*Figure 7.23 – Second frame version*

In the final version, the plates were replaced by rectangular-sectioned boxed tubes welded onto the main tubes. The bend radius was increased to 90mm to meet the manufacturer's requirements. The reinforcing plate made of Fe360 with a thickness of 3mm was retained.

The lateral tubes are made of 25CrMo4 with an outer diameter of 30mm and a thickness of 1.5mm. Two crosspieces, made of 25CrMo4 tubes with an outer diameter of 20mm and a thickness of 1.5mm, have been added. The ends of the 30mm lateral tubes are left free to accommodate an adjustable platform on one side and a handle for teaching discipline on the other.



*Figure 7.24 – Final frame version*

Above the frame, a perforated plate is placed for bolting the seat.

## 7.11. Assembly

Below are some images of the complete assembly of the system in order to make some observations about the system.



*Figure 7.25 – Assembly with Monosbock totally uncompressed*



*Figure 7.26 - Assembly with Monosbock totally compressed*

The seat has been scanned from a real one. Under the frame, in the seat area, a plastic plate is fixed to create a smooth support surface for the chairlift.

In the sagittal plane view, it is evident how the upper triangle protects the mono-shock absorber from potential collisions with the chairlift.

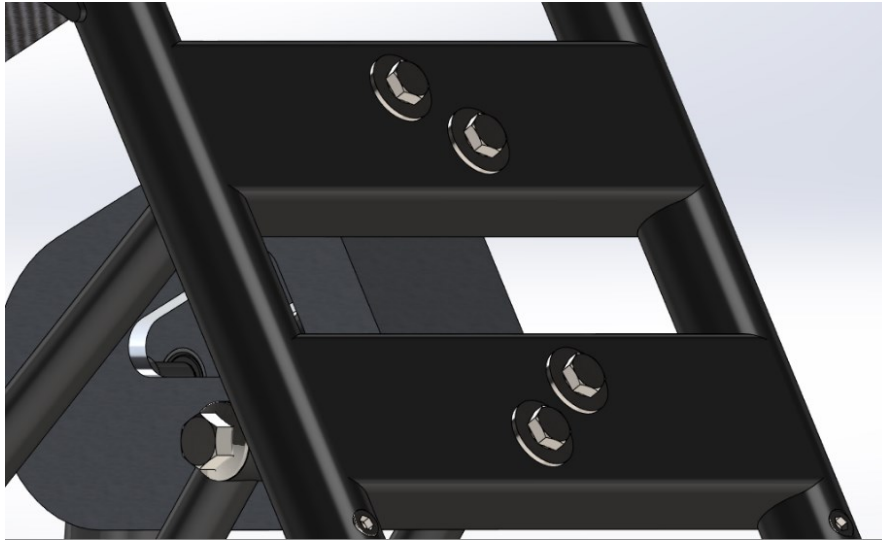
On the foot of the sitski, a plastic element is attached to protect the quick-release system from potential snow accumulation in that area, which could block the system.

Below (Figure 7.27), the system is also presented in the raised configuration. The plate under the seat of the frame is 58cm above the ground.

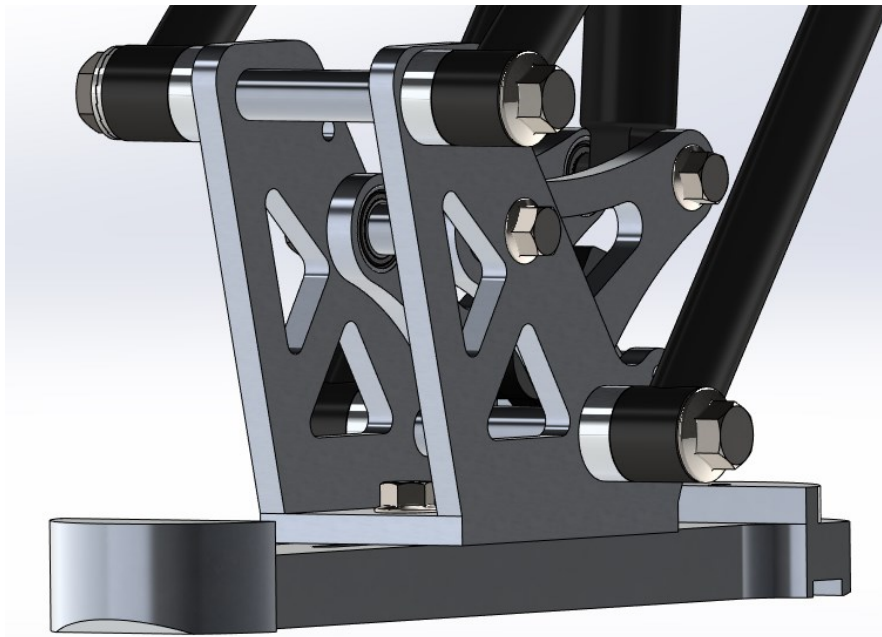


*Figure 7.27 – Monoski in raised configuration*

Since in the prototype the upper triangle is made of aluminum, while the frame is made of steel, and considering the difficulty of welding steel with aluminum, a bolted joint has been provided using 4 Hex Head Bolts partially threaded Coarse Thread Class 8.8 DIN 931 M8, as shown in the figure below (Figure 7.28). The joint will be better presented and verified according to standards in the following chapter.



*Figure 7.28 – Bolted joint between frame and Upper triangle*



*Figure 7.29 – Assembly of the Monoski's lower part from behind*



Figure 7.29 shows a detail of the assembled lower part of the monoski. Hex Head Bolts with partially threaded shank Coarse Thread Class 8.8 DIN 931 M12x140mm are used to join the links to the lower triangle. For the secure fastening of the bolts, Nord-Lock wedge-locking washers and low hexagon nuts (DIN 936) are used. Nord-Lock wedge-locking washers utilize tension instead of friction to secure bolted joints. [9].



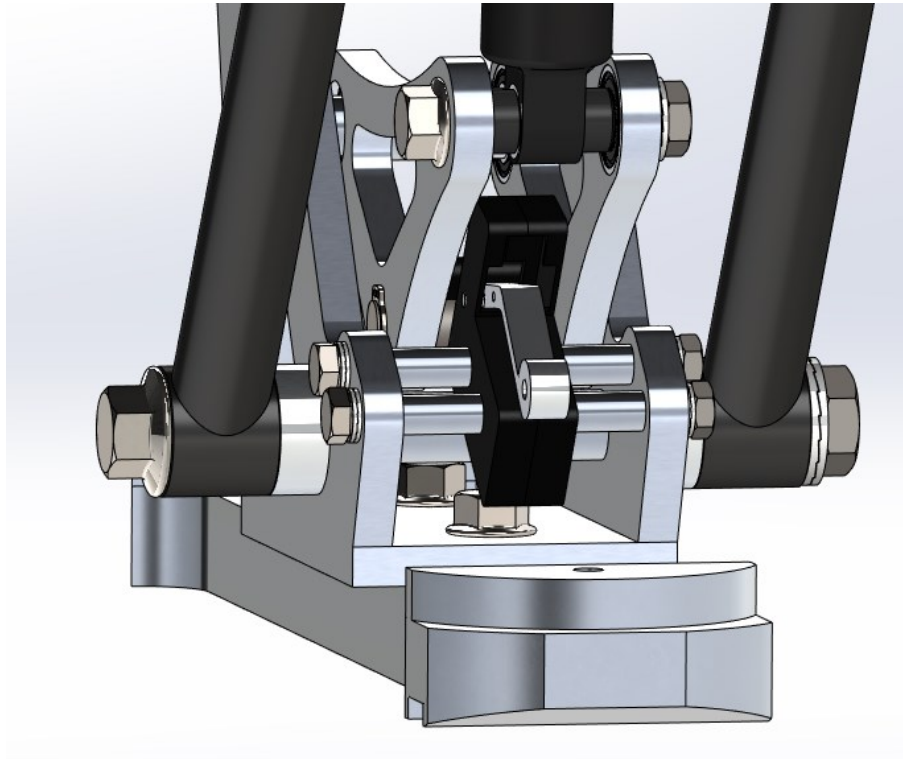
*Figure 7.30 - Nord Lock washers*

The use of standardized fasteners allows for considerable cost savings compared to the production of custom pins. As visible in the figure, the use of spacers between the internal walls of the lower and upper triangles is also anticipated. This figure also shows a detail of the bolted joint that connects the lower triangle and the foot, as described in the "foot" section. For verification according to regulations, please refer to the next chapter.

The quick-release system is fixed using two Hex Head Bolts with partially threaded shank Coarse Thread Class 10.9 DIN 931. The locking of the bolts is ensured by using NordLock washers under the head of the screw and under the low M6 hex nut (DIN 936). The hook is held in place by using 4 aluminum spacers. The verification of the screws will be addressed in the next chapter.

The mono-shock absorber is fixed with Hex Head Bolts with partially threaded shank Coarse Thread Class 8.8 DIN 931 M8. To keep it in place, specific commercial aluminum spacers for the chosen shock absorber are used.

Observing figures 7.29 and 7.31, it is possible to notice the spacers used to separate the rods from the lower and upper triangles, mentioned in the "beams" section. This is necessary to create space for the heads of the screws that are directly fixed to the triangle.



*Figure 7.31 – Assembly of the Monoski's lower part from front*

In the following chapter, structural checks are presented, carried out to verify the integrity and safety of the prototype during the testing phase.

## 8. Structural calculations

### 8.1. FEA Analysis

The Finite Element Analysis (FEA) is the simulation of any given physical phenomenon using the numerical technique called the Finite Element Method (FEM).

In the field of machine construction, the Finite Element Method is a numerical technique for evaluating the stress state of a body based on the principle of discretization into elements. This involves dividing the structure into elementary parts connected by nodes.

Standard procedure for FEM analysis is the following:

#### 1. Problem Definition:

- **Geometry:** Define the physical geometry of the mechanical structure or component.
- **Material Properties:** Specify the material properties, such as elasticity, thermal conductivity, and density.
- **Loading Conditions:** Identify and apply the external loads, including forces, pressure, or thermal loads.
- **Boundary Conditions:** Prescribe constraints, such as fixed supports or specified displacements, to represent the physical constraints of the system.

#### 2. Mesh Generation:

- **Discretization:** Divide the geometry into smaller, interconnected elements. The choice of element type (e.g., triangles, quadrilaterals, tetrahedra, hexahedra) depends on the complexity of the geometry and the nature of the problem.
- **Node Placement:** Assign nodes at the vertices of the elements. Nodes are the points where displacements and other quantities are computed.

### 3. **Mathematical Modeling:**

- **Element Equations:** Derive mathematical equations that represent the behavior of each element. This involves considering material properties, geometric properties, and loading conditions. The equations are often based on principles like equilibrium, compatibility, and material constitutive relations.
- **Assembly:** Assemble the individual element equations into a global system of equations that represents the entire mechanical structure. This involves combining the stiffness matrices and load vectors of each element.

### 4. **Application of Boundary Conditions:**

- **Constraint Implementation:** Modify the global system of equations to incorporate the specified boundary conditions. This is done by adjusting rows and columns corresponding to fixed degrees of freedom (displacements).
- **Load Application:** Incorporate the effects of applied loads into the system.

### 5. **Solution of System Equations:**

- **Solving Linear Equations:** If the problem is linear, solve the system of linear equations using methods like direct solvers or iterative solvers.

$$\{F\} = [K] \cdot \{f\}$$

Where  $\{F\}$  It is the vector containing the forces applied to each node;  $[K]$  is the stiffness matrix of the structure, and  $\{f\}$  is the vector containing the nodal displacements.

- **Nonlinear Analysis:** If the problem is nonlinear (due to material or geometric nonlinearity), iterative solution techniques are typically employed.

### 6. **Post-Processing:**

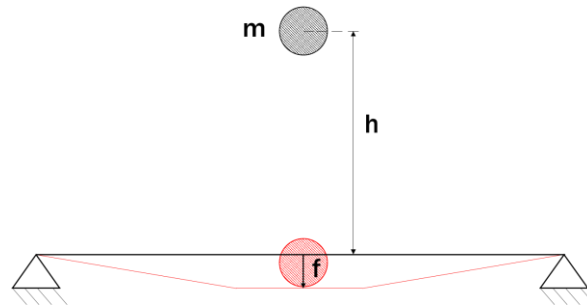
- **Nodal Displacements:** Obtain the nodal displacements from the solution.

- Calculating Engineering Quantities: Use the displacements to calculate other engineering quantities of interest, such as stresses, strains, and reactions.
- Visualization: Represent the results through graphical visualization, including contour plots, deformed shapes, and animations.

## 8.2. Load Calculations

### Impulsive shock effects on structures

The effect of the fall of a mass  $m$  from a height  $h$  on a supported beam is evaluated.



The beam, at the point of contact between the mass and the beam, behaves like a spring. To determine the deflection  $f$  and the maximum dynamic load  $F$  on the beam, the conservation of energy equation can be used.

*Potential energy of the mass = Elastic potential energy*

$$mg(h + f) = \frac{1}{2} F \cdot f$$

Since  $F = k \cdot f$ , with  $K$  = stiffness of the structure at the impact point.

$$mg(h + f) = \frac{1}{2} KF^2$$

$$F = \frac{(mg) \pm \sqrt{(mg)^2 + 2K \cdot mg \cdot h}}{K}$$

$$F = k \cdot f = mg \left( 1 + \sqrt{1 + \frac{2k \cdot h}{mg}} \right)$$

If  $h = 0$ , then  $F = 2 \cdot mg$

### Static Load Size

Based on what was observed for the simple case of impacts on a beam, considered as the foot of the sitski, and considering the rough and possibly hard surface that can be encountered on a ski slope, impacts at 2g are assumed as a plausible target value.

The dynamic load thus obtained is then multiplied by a safety factor of 1.5 to provide the dimensioning load for static analysis.

$$F = 2 \cdot mg \cdot 1.5 \approx 3000N$$

The chosen load is confirmed by the experimental data recorded in the on-slope tests conducted by Matteo Ferrari. [2] Dario Vanzetto [3].

Vanzetto tested a high-level Paralympic skier doing giant slalom. Since the accelerations and thus forces produced by the skier are key factors in the performance, then as expected Vanzetto had bigger values of loads. Vanzetto could not measure My with his instrumentation so was used the data from Ferrari.

The loads calculated are the following:

*Table 8.1 - Loads calculated by Dario Vanzetto*

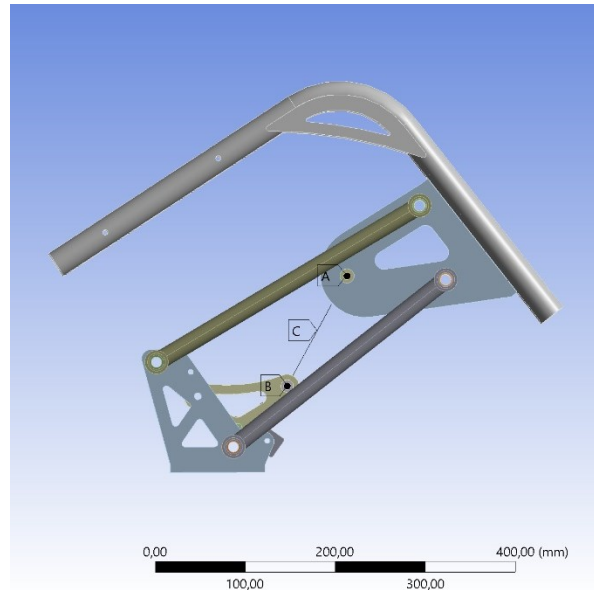
	x	y	z	mag	
Force	0	160	-2500	2505	N
Moment	8.00E+04	3.00E+05	0.00E+00	3.10E+05	Nmm

### 8.3. Stress on main structural parts

The calculation software used for FEM simulations is Ansys®.

In the Ansys Workbench working environment, a simplified CAD model in .STP format of the Monoski Assembly was imported. This model has been simplified to lighten the analysis as much

as possible. The monoski foot has been removed, as well as all the screws, which will be analyzed separately. Finally, the bearings have been modeled as simple cylindrical bodies (Figure 8.1).



*Figure 8.1 – FEM Assembly Model*

The mono-shock absorber was brought to the length it would have if fully compressed, then it was suppressed and replaced by Remote Points A, B, and C.

All contacts between the pieces are of the bonded type.

Between the bushings of the beams and the corresponding spacer that separates it from the triangle, a revolute joint was inserted to simulate the real behavior that would occur with the bearing (Figure 8.2).

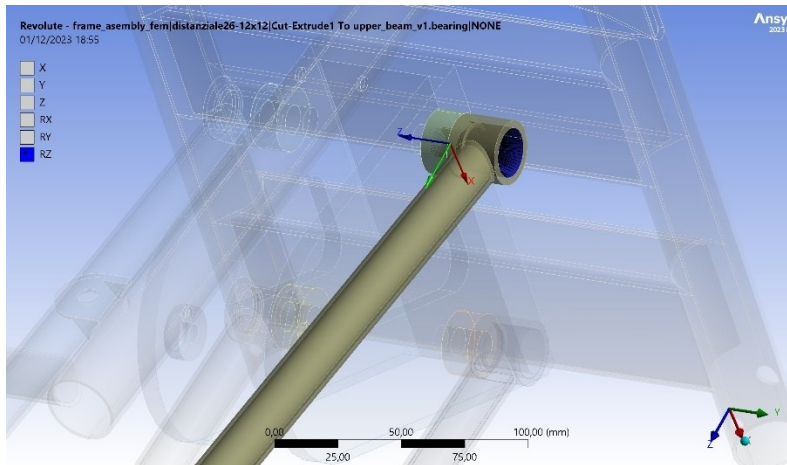


Figure 8.2 - Revolute Joint

The mesh used is quadratic tetrahedral with element size of 3mm and active adaptive sizing.

The boundary conditions involve applying a fixed support on the lower face of the lower triangle and applying 3000N vertically on the seat.

## FEM Results

The total deformation of the system is as follows:

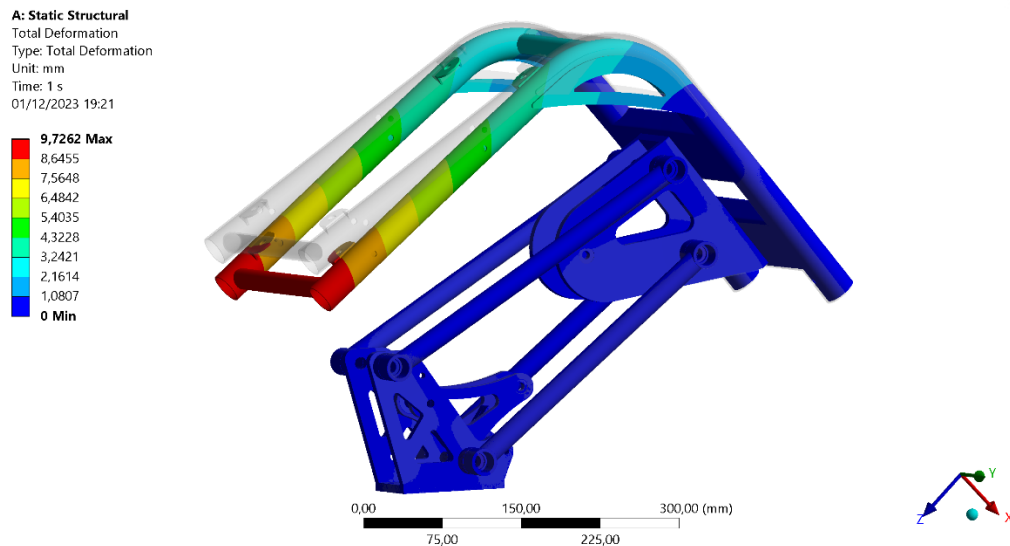


Figure 8.3 - Total Deformation 4,0X



The deformation is consistent with what is expected. It is noted that the deformation introduces an additional angular rotation of the seat, estimated at around  $1.4^\circ$ , which adds to the  $6^\circ$  introduced by the monoski's kinematics. However, this is still a limit value, which occurs only under extreme loads.

Overview on the Equivalent Stress (von Mises):

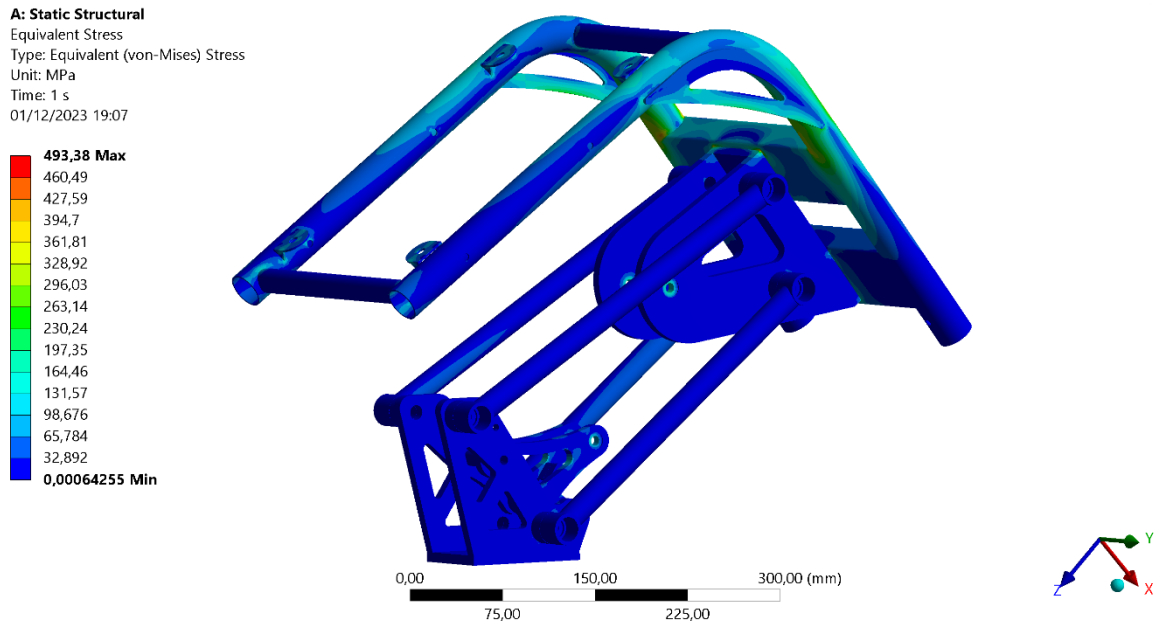


Figure 8.4 - Stress on the model (1)

The equivalent stress values remain below the critical value (Yield Strength).

The safety factors for each component are expressed in Table 8.2.

Among the most stressed components there are the frame, the lift-up system, and the quick-release system, as visible in Figures 7.8 and 7.9. On the frame, in particular, there are some stress concentration zones corresponding to discontinuities in the 3D model, which will be eliminated with the welding process. Welding creates a transition that distributes stresses; therefore, in the calculation of static safety factors, the stress value at the point of discontinuity is not considered.

**A: Static Structural**  
 Equivalent Stress  
 Type: Equivalent (von-Mises) Stress  
 Unit: MPa  
 Time: 1 s  
 01/12/2023 19:08

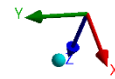
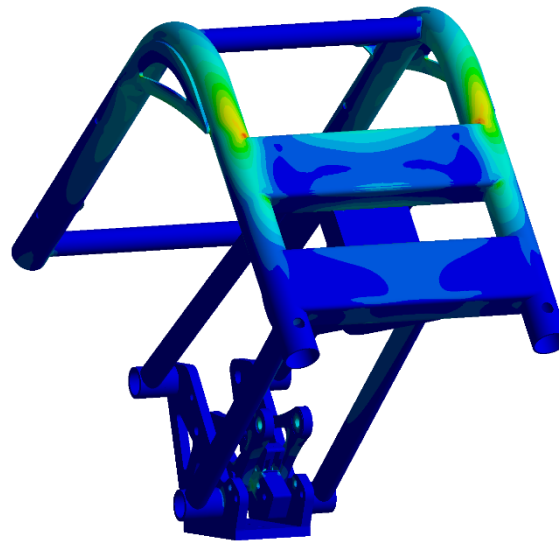
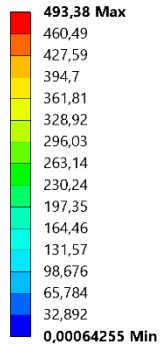


Figure 8.5 - Stress on the model (2)

Static Safety Factors are calculated as follows:

$$v_s = \frac{\sigma_{yield}}{\sigma_{eq,VM}}$$

It is common practice for the static safety factor to remain above 1.5.

Table 8.2 - Static Safety Factors

Component	Material	Yield Strength [Mpa]	Max Stress value [MPa]	Static safety factor
Frame	25CrMo4 Steel	540	364	1.48
Upper Triangle	Avional EN AW 2017	275	69	3.99
Upper Beam	25CrMo4 Steel	540	15	36.00
Lower Beam	25CrMo4 Steel	540	52	10.38
Lower Triangle	Avional EN AW 2017	245	93	2.63
Lift Up System	Avional EN AW 2017	245	115	2.13
Quick Release System	Fe360	245	108	2.27
Closing Pivot	11SMnPb37 (AVP)	440	251	1.75

Points of interest:

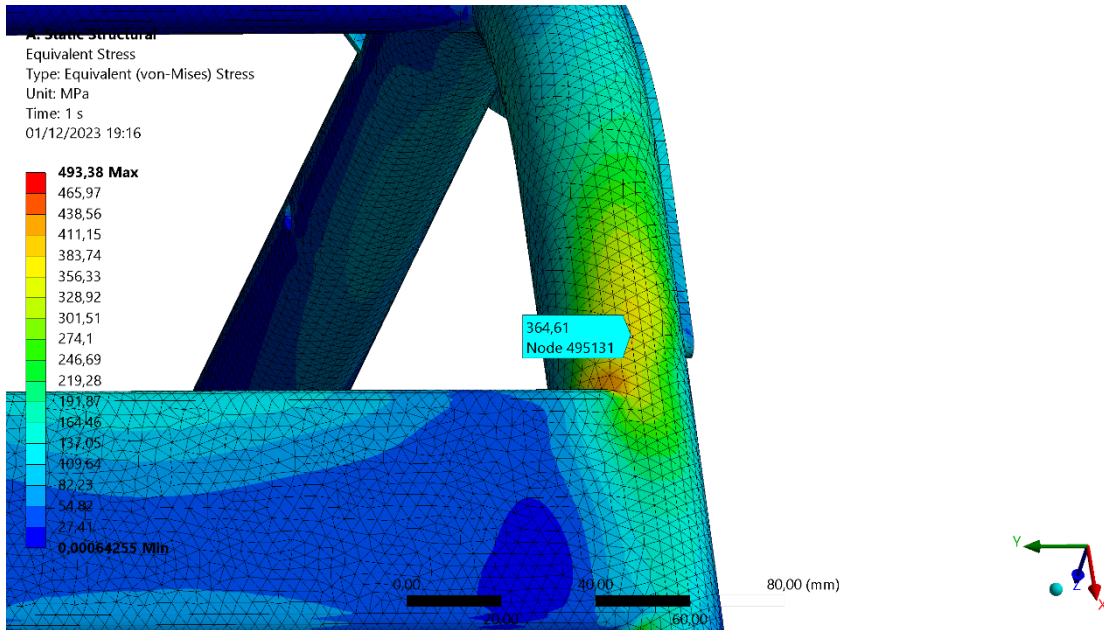


Figure 8.6 - "external" face of frame

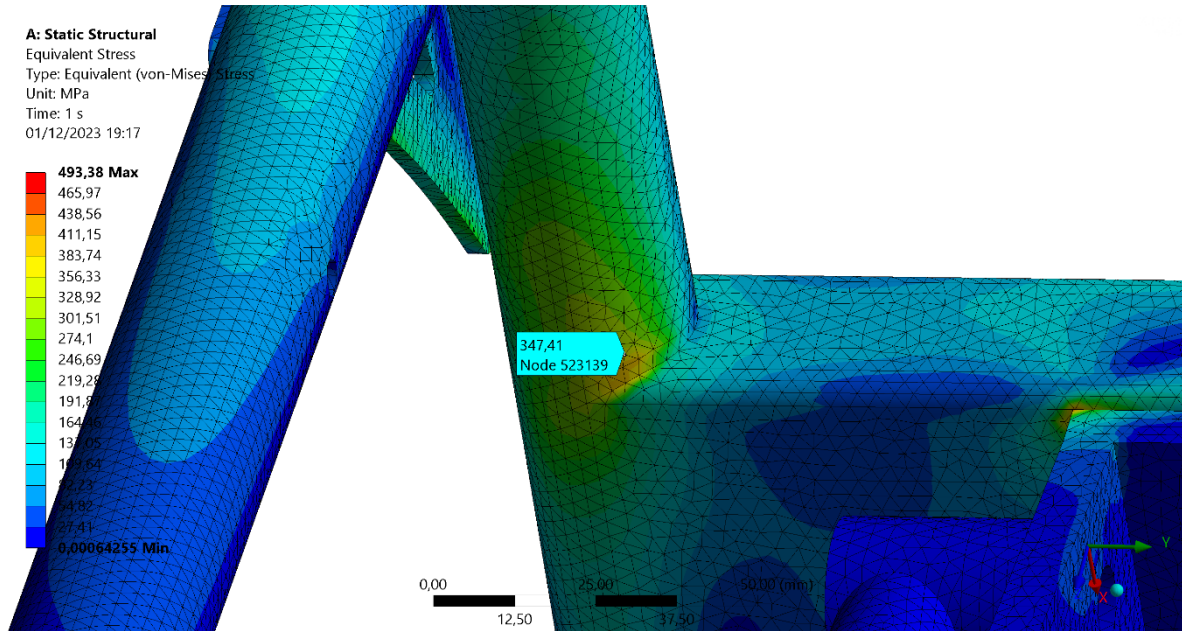


Figure 8.7 - "Internal" face of frame



Figure 8.8 – Stress on Lift Up System

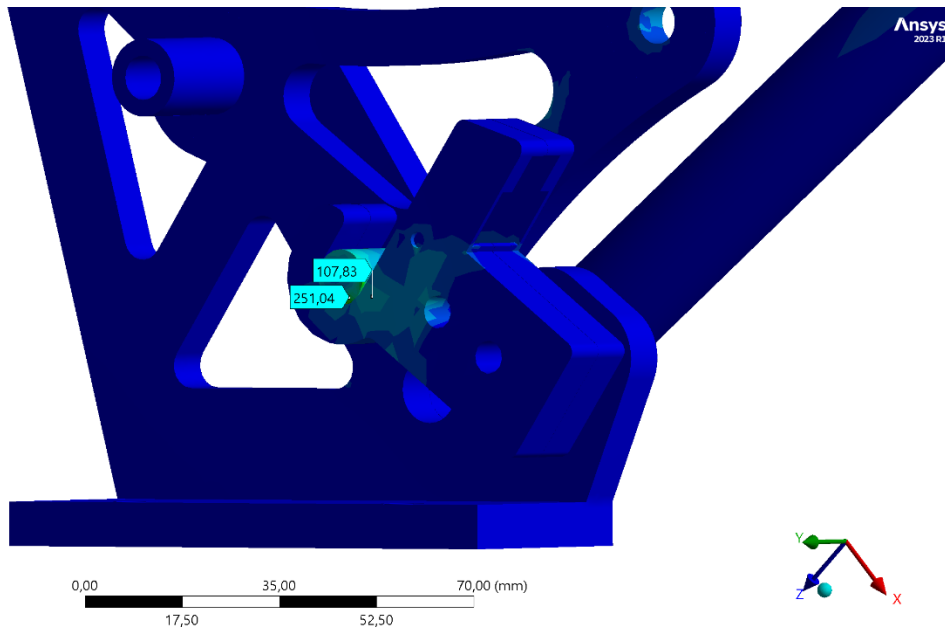


Figure 8.9 – Stress on quick release System

## 8.4. Bearings verification

Assuming the case of load at low speed ( $n < 10$  r/min) ball bearing size should be selected or verified based on the static load that the bearing can accommodate, taking into account the possible effects of permanent deformation. [10]

The basic static load rating  $C_0$  is defined in ISO 76 as the load that results in a certain value of contact stress at the centre of contact of the most heavily loaded rolling element/raceway. The contact stress values are:

- 4 600 MPa for self-aligning ball bearings
- 4 200 MPa for all other ball bearings
- 4 000 MPa for all roller bearings

These stress values produce a total permanent deformation of the rolling element and raceway that is approximately 0,0001 of the rolling element diameters.

Loads comprising radial and axial components that are to be evaluated in relation to the static load rating  $C_0$ , must be converted into an equivalent static bearing load. This is defined as that hypothetical load (radial for a radial bearing and axial for a thrust bearing) which, when applied would cause the same maximum rolling element load in the bearing as the actual loads to which the bearing is subjected. It is obtained from the general equation:

$$P_0 = X_0 F_r + Y_0 F_a$$

Where:

- $P_0$  equivalent static bearing load [kN]
- $F_r$  actual radial bearing load (see below) [kN]
- $F_a$  actual axial bearing load (see below) [kN]
- $X_0$  radial load factor for the bearing
- $Y_0$  axial load factor for the bearing

The static safety factor  $s_0$  is given by:

$$s_0 = C_0/P_0$$

Where:

- $s_0$  static safety factor
- $C_0$  basic static load rating [kN]
- $P_0$  equivalent static bearing load [kN]

Guideline values for the static safety factor  $s_0$ , based on experience, are listed for ball bearings in the table 8.3 and for roller bearings in table 8.4 [11].

Table 8.3 – static safety factor for ball bearings

Guideline values for the static safety factor $s_0$ – for continuous and/or occasional loads – ball bearings				
Certainty of load level	Continuous motion			Infrequent motion
	Permanent deformation acceptance			Permanent deformation acceptance
	Yes	Some	No	Yes
<b>High certainty</b> For example, gravity loading and no vibration.	0,5	1	2	0,4
<b>Low certainty</b> For example, peak loading.	$\geq 1,5$	$\geq 1,5$	$\geq 2$	$\geq 1$

Table 8.4 - static safety factor for roller bearings

Guideline values for the static safety factor $s_0$ – for continuous and/or occasional loads – roller bearings <sup>1)</sup>				
Certainty of load level	Continuous motion			Infrequent motion
	Permanent deformation acceptance			Permanent deformation acceptance
	Yes	Some	No	Yes
<b>High certainty</b> For example, gravity loading and no vibrations.	1	1,5	3	0,8
<b>Low certainty</b> For example, peak loading.	$\geq 2,5$	$\geq 3$	$\geq 4$	$\geq 2$

## SKF 608 – 2Z

According to the simulation made with a vertical Force of 3000N on the seat, each bearing experiences a radial load of 1475 N.

$$P_0 = X_0 F_r + Y_0 F_a = 1475 \text{ N}$$

$$s_0 = \frac{C_0}{P_0} = 0.93 > 0.4$$

Considering that the bearings have infrequent movement and given that the load case is already significantly overestimated, the bearing is deemed verified.

## SKF 61901 2Z

According to the simulation made with a vertical Force of 3000N, very few forces are discharged on these bearings, therefore, the load case is considered inadequate for the verification of the bearings.

So, a finite element analysis was carried out with the monoski in the raised position, a situation in which the load is greater on these bearings. A force of 1500N was applied perpendicular to the seat, sizing for a skier weighing 100kg with a dynamic factor of 1.5 during a challenging descent from the chairlift.

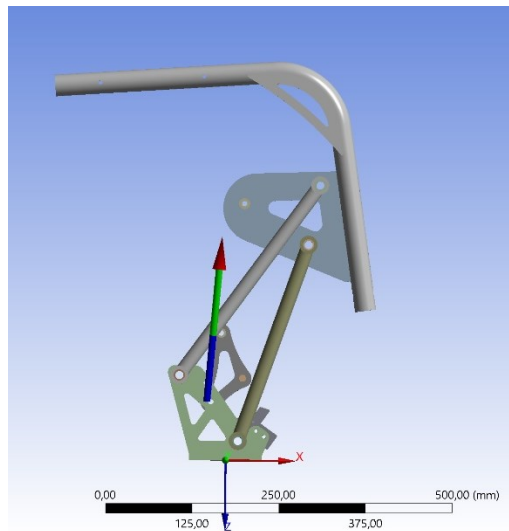


Figure 8.10 - FEA in raised position

On the bearing, a radial load of 1078N is calculated.

$$P_0 = X_0 F_r + Y_0 F_a = 1078 \text{ N}$$

$$s_0 = \frac{C_0}{P_0} = 1.35 > 0.4$$

The bearings are verified.

### **SKF HK 1612**

According to the simulation made with a vertical Force of 3000N on the seat, the most stressed bearings are the ones of the lower beams. They experience a radial load of 1444 N.

$$P_0 = X_0 F_r + Y_0 F_a = 1444 \text{ N}$$

Static Load Factor is:

$$s_0 = \frac{C_0}{P_0} = 6.79 > 3$$

The basic rating life of a bearing in accordance with ISO 281 is:

$$L_{10} = \left(\frac{C}{P}\right)^p = (5.1)^{\frac{10}{3}} = 228$$

Where:

- $L_{10}$  basic rating life (at 90% reliability) [millions of revolutions]
- $C$  basic dynamic load rating [kN]
- $P$  equivalent dynamic bearing load [kN]
- $p$  exponent of the life equation = 10/3 for roller bearings



## 8.5. Verification of bolted joints – CNR-UNI 10011 - 1988

### Lower Triangle – Foot

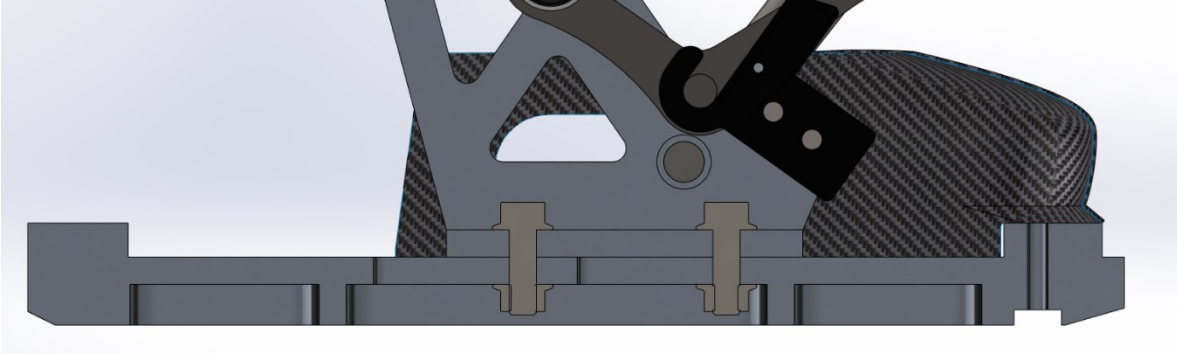


Figure 8.11 – Lower Triangle – Foot bolted joint

2 Hexagon socket head cap screws with flange and serrations CL.8.8 DIN 6921 Z.B.

$$\sigma_r = f_t = 8 * 100 = 800 \text{ Mpa}$$

$$\sigma_s = f_y = 8 * 8 * 10 = 610 \text{ Mpa}$$

Project resistance:

$$f_{k,N} = \min\{f_y ; 0.7 * f_t\} = 560 \text{ Mpa}$$

Allowable stresses:

$$\sigma_{b,adm} = \frac{f_{k,N}}{\nu} = 373 \text{ Mpa}$$

$$\tau_{b,adm} = \frac{\sigma_{b,adm}}{\sqrt{2}} = 264 \text{ Mpa}$$

Tightening of the screws:

$$N_s = 0.8 * f_{k,N} * A_{res} = 16396.8 \text{ N}$$

$$T_s = 0.2 * N_s * d = 26234.88 \text{ Nmm} \cong 26 \text{ Nm}$$

- Forces

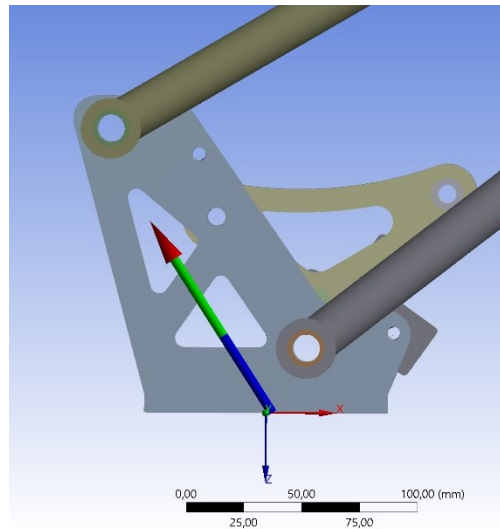


Figure 8.12 – Force acting on “Lower Triangle – Foot” bolted joint

The Force Reaction and Moment Reaction are reported in the table below.

Table 8.5 – Forces acting on the “Lower Triangle - Foot” joint

	x	y	z	mag	
Force	-1630	0	-2520	3001	N
Moment	0	4.55E+05	0	4.55E+05	Nmm

- Shear strength verification of the joint.

The following condition must be satisfied:

$$\left( \frac{\sigma_b}{\sigma_{b,adm}} \right)^2 + \left( \frac{\tau_b}{\tau_{b,adm}} \right)^2 \leq 1$$

With

$$\sigma_b = \frac{N}{A_{res}} = 191 \text{ Mpa} \text{ and } \tau_b = \frac{F_x}{n_b * n_d * A_{res}} = 22.3 \text{ Mpa}$$

Where  $n_b$  = number of bolts,  $n_d$  = number of resistant areas for every bolt and  $N=N'+N''$

$$N' = \frac{F_z}{n_b} = 1260 \text{ N and } N'' = \frac{M_y}{n_f * \sum y_i^2} * y_2 = 5732 \text{ N}$$

Where  $n_f$  = number of rows of bolts and  $y_i$  is the distance between the screw I and the tipping point.

It is obtained:

$$\left( \frac{\sigma_b}{\sigma_{b,adm}} \right)^2 + \left( \frac{\tau_b}{\tau_{b,adm}} \right)^2 = 0.27 < 1$$

The joint is checked for shear.

- **Tensile strength check of the sheet metal**

The criterion for checking the sheet metal for tearing is as follows:

$$\sigma = \frac{F_x}{(w - n_f * \varphi) * t_p} \leq \sigma_{adm}$$

Where  $w$  = sheet width,  $\varnothing$  = hole diameter,  $t_p$  = sheet thickness and  $\sigma_{adm}$  = material yield strength.

Sheet of Lower Triangle:

$$\sigma = 3.51 \text{ Mpa} < 245 \text{ Mpa}$$

Sheet of Foot:

$$\sigma = 3.77 \text{ Mpa} < 503 \text{ Mpa}$$

- **Frictional Joint Verification**

In order to verify the frictional joint, it is necessary to ensure that the load to be transmitted is less than or equal to the frictional load-carrying capacity.

$$V_f = \frac{F_x}{n_b * n_s} \leq V_{f,N} = \mu \frac{N_s}{\gamma_s} * \left( 1 - \frac{N}{N_s} \right)$$

Where  $n_s$  = number of friction surfaces,  $\gamma_s$  = Safety factor against slippage = 1.25,  $\mu$  = friction coefficient.

Additionally, it must be:

$$N \leq 0.8 * N_s$$

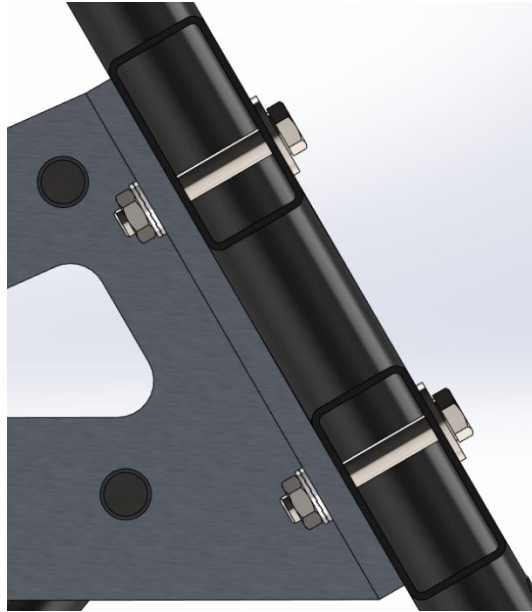
It is obtained:

$$V_f = 810 N < V_{f,N} = 2257.2 N$$

$$N = 6992 N < 0.8 * N_s = 13117 N$$

The joint is also checked for friction.

## Upper Beam – Frame



*Figure 8.13 – Sectioned view of “Lower Triangle - Frame” bolted joint*



*Figure 8.14 – View of “Lower Triangle – Frame” bolted joint*

Bolts are M8 CL 8.8, so the same considerations made in previous paragraph are still valid.

## Forces

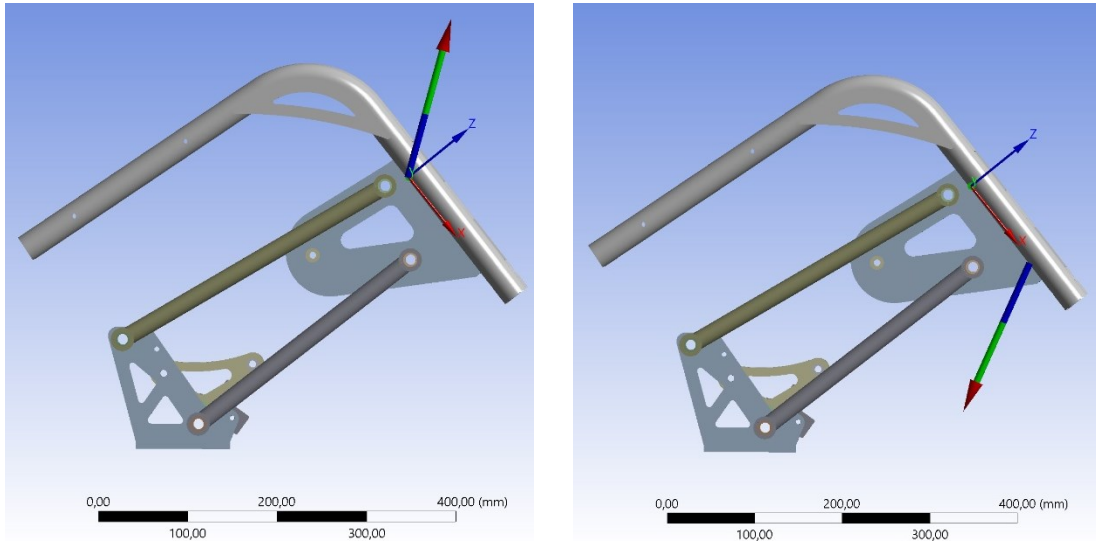


Figure 8.15 - Reaction forces on frame-upper triangle bolted joint

The Force Reaction and Moment Reaction are reported in the table below.

Table 8.6 – Forces acting on upper crosspiece

	x	y	z	mag	
Force	-4073.4	202.4	5647.4	6966	N
Moment	5.13E+04	1.88E+05	14497	1.95E+05	Nmm

Table 8.7 – forces acting on lower crosspiece

	x	y	z	mag	
Force	2100	-42.4	-4112.3	4618	N
Moment	1.03E+04	-1.62E+04	3.88E+03	1.96E+04	Nmm

Since the bolting is identical for the upper crosspiece and the lower crosspiece, the verification will be carried out only for the upper crosspiece.

- **Shear strength verification of the joint.**

$$\sigma_b = \frac{N}{A_{res}} = 136.7 \text{ Mpa} \text{ and } \tau_b = \frac{\frac{F_x}{n_b * n_d}}{A_{res}} = 55.64 \text{ Mpa}$$

Where  $n_b$  = number of bolts,  $n_d$  = number of resistant areas for every bolt and  $N=N'+N''$

$$N' = \frac{F_z}{n_b} = 2823.7 \text{ N and } N'' = \frac{M_y}{n_f * \sum y_i^2} * y_2 = 2180.4 \text{ N}$$

Where  $n_f$  = number of rows of bolts and  $y_i$  is the distance between the screw I and the tipping point.

It is obtained:

$$\left( \frac{\sigma_b}{\sigma_{b,adm}} \right)^2 + \left( \frac{\tau_b}{\tau_{b,adm}} \right)^2 = 0.18 < 1$$

The joint is checked for shear.

- **Tensile strength check of the sheet metal**

The criterion for checking the sheet metal for tearing is as follows:

$$\sigma = \frac{F_x}{(w - n_f * \varphi) * t_p} \leq \sigma_{adm}$$

Where  $w$  = sheet width,  $\varphi$  = hole diameter,  $t_p$  = sheet thickness and  $\sigma_{adm}$  = material yield strength.

Sheet of Upper Triangle:

$$\sigma = 10.2 \text{ Mpa} < 245 \text{ Mpa}$$

Sheet of Upper crossection:

$$\sigma = 40.73 \text{ Mpa} < 275 \text{ Mpa}$$

- **Frictional Joint Verification**

In order to verify the frictional joint, it is necessary to ensure that the load to be transmitted is less than or equal to the frictional load-carrying capacity.

$$V_f = \frac{F_x}{n_b * n_s} \leq V_{f,N} = \mu \frac{N_s}{\gamma_s} * \left( 1 - \frac{N}{N_s} \right)$$

Where  $n_s$  = number of friction surfaces,  $\gamma_s$  = Safety factor against slippage = 1.25,  $\mu$  = friction coefficient.

Additionally, it must be:

$$N \leq 0.8 * N_s$$

It is obtained:

$$V_f = 2036.7 \text{ N} < V_{f,N} = 2187.3 \text{ N}$$

$$N = 5004.1 \text{ N} < 0.8 * N_s = 13117 \text{ N}$$

The joint is also checked for friction.



## Conclusions and future development

The thesis aimed to develop the design of a sustainable and innovative monoski. To achieve this, kinematic targets for the mechanism were set based on observations of some commercial models. The kinematic synthesis was then carried out through trial-and-error to create a mechanism that best met these targets while considering certain design constraints, particularly the choice of the shock absorber. The kinematic scheme of the monoski was translated into a CAD model, keeping in mind that for economic sustainability, it should be simple to produce with easily obtainable parts and minimal mechanical processing. Finally, the monoski was tested through finite element analysis and compliance with standard procedures.

The production of a prototype has already been initiated, but due to timing constraints, it was not possible to present it within the thesis. Upon completion of the prototype, it will be crucial to estimate manufacturing costs and possibly create a Business Model to verify the project's actual sustainability. Simultaneously, the prototype will be tested on ski slopes to assess the loads acting on the structure and identify any structural weaknesses that may need reinforcement. In this regard, it is recommended to verify the frame at points subjected to the highest stresses using strain gauges. Additionally, measuring certain kinematic-related data, such as shock absorber usage, and kinetic data, such as center of pressure during skiing, is important. These data should be compared with the skier's sensation to introduce any necessary improvements at the setup level.



## Bibliography

- [1] D. Piccinin, «Kinematic and kinetic analysis of a paralympic skier during slalom,» 2016.
- [2] M. Ferrari, «Design and validation of a dynamometric load cell for the measurement of loads acting on a Paralympic monoski,» 2016.
- [3] D. Vanzetto, «Acquisition and analysis of kinematic and kinetic data on a top Paralympic skier during giant slalom,» 2017.
- [4] G. Colla, «Development and validation of an Instrumented Monoski for kinematic and kinetic data collection,» 2022.
- [5] N. Petrone, D. Vanzetto, G. Marcolin, B. Bruhin e M. Gilgien, «The effect of foot setting on kinematic and kinetic skiing parameters during giant slalom. A single subject study on a paralympic gold medalist sit skier.,» *J Sci Med Sport*, 2021.
- [6] Tessier, “Scarver - 3 damping kinematics,” Tessier Adaptive Sports, [Online]. Available: <https://www.tessier-adaptive-sports.com/en/scarver-uniski-monoski-dualski-competition-freeride-sitski/>.
- [7] M. Cavacece, F. Smarrini, P. Valentini and L. Vita, “Kinematic and dynamic analysis of a sit-ski to improve,” University of Rome ‘Tor Vergata’, Department of Mechanical Engineering, Italy, Rome, 2005.
- [8] SKF, «Drawn cup needle roller bearings,» SKF, [Online]. Available: <https://www.skf.com/group/products/rolling-bearings/roller-bearings/needle-roller-bearings/drawn-cup-needle-roller-bearings>.

- [9] "NordLock," Nord-Lock S.r.L, [Online]. Available: <https://www.nord-lock.com/nord-lock/products/washers/>.
- [10] SKF, «Size selection based on static load,» SKF, [Online]. Available: <https://www.skf.com/group/products/rolling-bearings/principles-of-rolling-bearing-selection/bearing-selection-process/bearing-size/size-selection-based-on-static-load>.
- [11] SKF, «Bearing Size,» SKF, [Online]. Available: <https://www.skf.com/us/products/rolling-bearings/principles-of-rolling-bearing-selection/bearing-selection-process/bearing-size>.
- [12] Ministero delle infrastrutture e dei trasporti, «REGOLAMENTO DI ESERCIZIO FUNIVIA MONOFUNE A COLLEGAMENTO TEMPORANEO in servizio pubblico per il trasporto di persone,» [Online].

## List of figures

Figure 2.1 - Dynafoot.....	8
Figure 2.2 – Results of Ferrari’s test.....	8
Figure 2.3 – Dynaplate .....	9
Figure 2.4 – Mean values of force peaks .....	10
Figure 2.5 - Stella's 3rd wide run.....	11
Figure 2.6 - Varotto's 2nd wide run .....	11
Figure 2.7 - Mean values of XCOP .....	12
Figure 2.8 – Results from run 302.....	14
Figure 2.9 - GRF (left/right) - position of COP.....	15
Figure 2.10 – Amplified Load Cell.....	16
Figure 2.11 - Instrumented Monoski .....	17
Figure 3.1 - Pyramid of innovation .....	19
Figure 4.1 – Scarver’s kinematic configurations.....	26
Figure 4.2 – Scarver Adams Model .....	27
Figure 4.3 - Tessier Tempo.....	28
Figure 4.4 - Adams Model for Tessier Tempo .....	28
Figure 4.5 - Impact Evolution.....	29
Figure 4.6 - Adams Model for Impact Evolution .....	29
Figure 4.7 - Impact evolution lifted up.....	30
Figure 4.8 - Monoski Racer by Alois-Praschberger .....	31
Figure 4.9 - Adams Model for Monoski Racer.....	31
Figure 4.10 – Position of hip joint with respect to the Reference System .....	32

Figure 4.11 - Seat movment comparison.....	33
Figure 4.12 - Price - Performance Comparison Matrix.....	37
Figure 4.13 - Price - Adjustability Comparison Matrix .....	37
Figure 5.1 – MTB with air Monoshock .....	40
Figure 5.2 - Pat's Easy change.....	43
Figure 6.1 - Parametric Model in Adams.....	46
Figure 6.2 - Design Variables List .....	47
Figure 6.3 - Monoski Unipd seat movement comparison .....	48
Figure 7.1 - Kinematic scheme of the Sitski .....	51
Figure 7.2 - on the left Scarver by Tessier, on the right Impulse Boost by Unicent GmbH.....	52
Figure 7.3 - Motorcycle components made by die casting .....	53
Figure 7.4 - First Concept Design .....	56
Figure 7.5 - Second Concept Design .....	56
Figure 7.6 - Third Concept Design .....	57
Figure 7.7 - Ski Boot.....	59
Figure 7.8 - Sitski "foot" .....	59
Figure 7.9 - Details of "foot": the slots.....	60
Figure 7.10 - Details of "foot":pockets.....	60
Figure 7.11 - Lower Triangle.....	61
Figure 7.12 - Isometric view of Lower Triangle.....	62
Figure 7.13 - Lift up System .....	63
Figure 7.14 - Section view of lift up System .....	64
Figure 7.15 - Lift Up System in Aluminium.....	64
Figure 7.16 – Section View of Release System.....	67

Figure 7.17 – Release System Assembly .....	67
Figure 7.18 – Exploded View of Release System.....	68
Figure 7.19 – Exploded View of the Assembly of a beam .....	69
Figure 7.20 - Details of bearing .....	70
Figure 7.21 – Upper Triangle .....	71
Figure 7.22 – First frame version .....	73
Figure 7.23 – Second frame version.....	74
Figure 7.24 – Final frame version.....	75
Figure 7.25 – Assembly with Monoshock totally uncompressed .....	76
Figure 7.26 - Assembly with Monoshock totally compressed.....	76
Figure 7.27 – Monoski in raised configuration.....	77
Figure 7.28 – Bolted joint between frame and Upper triangle.....	78
Figure 7.29 – Assembly of the Monoski’s lower part from behind.....	78
Figure 7.30 - Nord Lock washers .....	79
Figure 7.31 – Assembly of the Monoski’s lower part from front.....	80
Figure 8.1 – FEM Assembly Model .....	85
Figure 8.2 - Revolute Joint.....	86
Figure 8.3 - Total Deformation 4,0X.....	86
Figure 8.4 - Stress on the model (1) .....	87
Figure 8.5 - Stress on the model (2) .....	88
Figure 8.6 - "external" face of frame.....	89
Figure 8.7 - "Internal" face of frame.....	89
Figure 8.8 – Stress on Lift Up System .....	90
Figure 8.9 – Stress on quick release System.....	90

Figure 8.10 - FEA in raised position.....	93
Figure 8.11 – Lower Triangle – Foot bolted joint .....	95
Figure 8.12 – Force acting on “Lower Triangle – Foot” bolted joint.....	96
Figure 8.13 – Sectioned view of “Lower Triangle - Frame” bolted joint.....	99
Figure 8.14 – View of “Lower Triangle – Frame” bolted joint .....	99
Figure 8.15 - Reaction forces on frame-upper triangle bolted joint.....	100

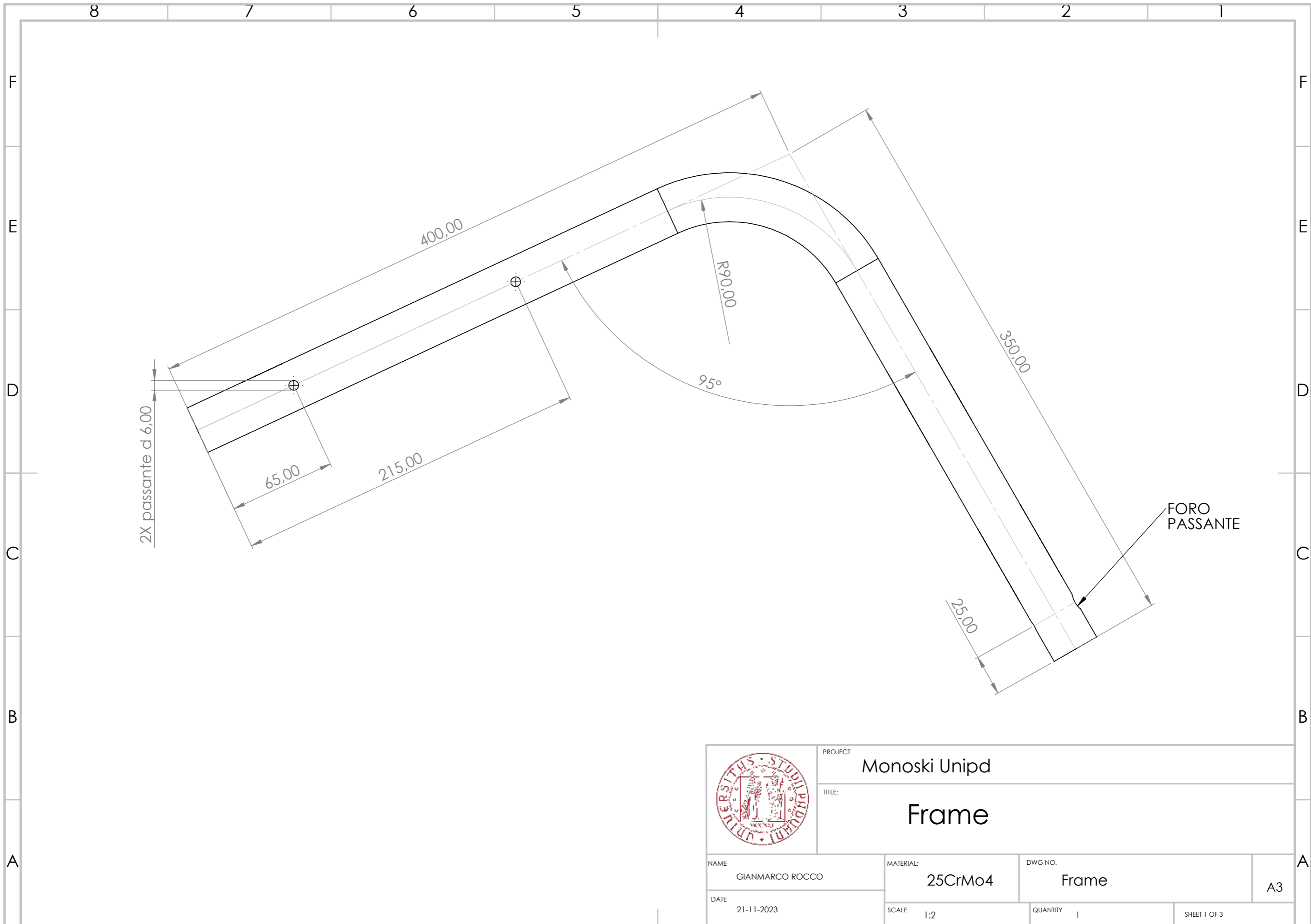



## List of Tables

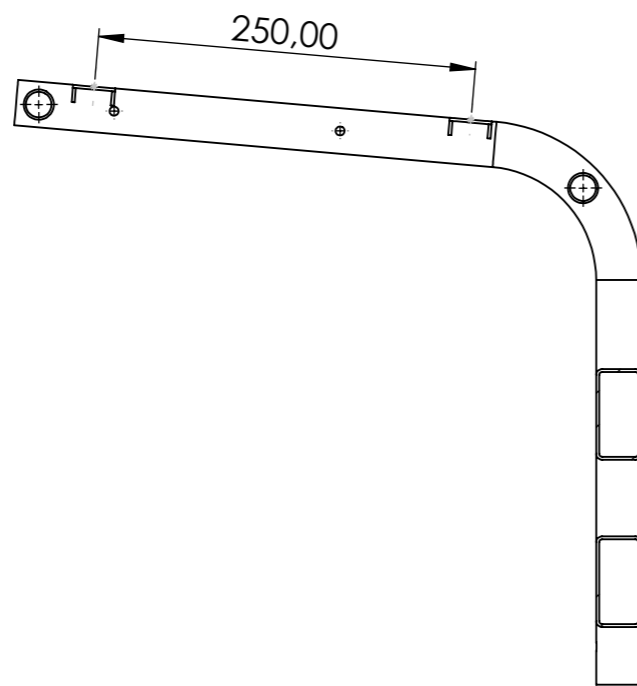
Table 6.1 – Kinematic target value.....	45
Table 6.2 - Design Variables values.....	48
Table 6.3 - Target and Current Values.....	49
Table 7.1 - Productive System Comparison Matrix.....	54
Table 7.2 - Concept Scoring Matrix.....	58
Table 7.3 - SKF 61901 2Z Data.....	65
Table 7.4 - SKF 608 2Z Data.....	65
Table 7.5 – SKF HK1612 Data and Dimension.....	70
Table 7.6 - SKF 608 2Z Data.....	72
Table 8.1 - Loads calculated by Dario Vanzetto.....	84
Table 8.2 - Static Safety Factors.....	88
Table 8.3 – static safety factor for ball bearings.....	92
Table 8.4 - static safety factor for roller bearings.....	92
Table 8.5 – Forces acting on the “Lower Triangle - Foot” joint.....	96
Table 8.6 – Forces acting on upper crosspiece.....	100
Table 8.7 – forces acting on lower crosspiece.....	100



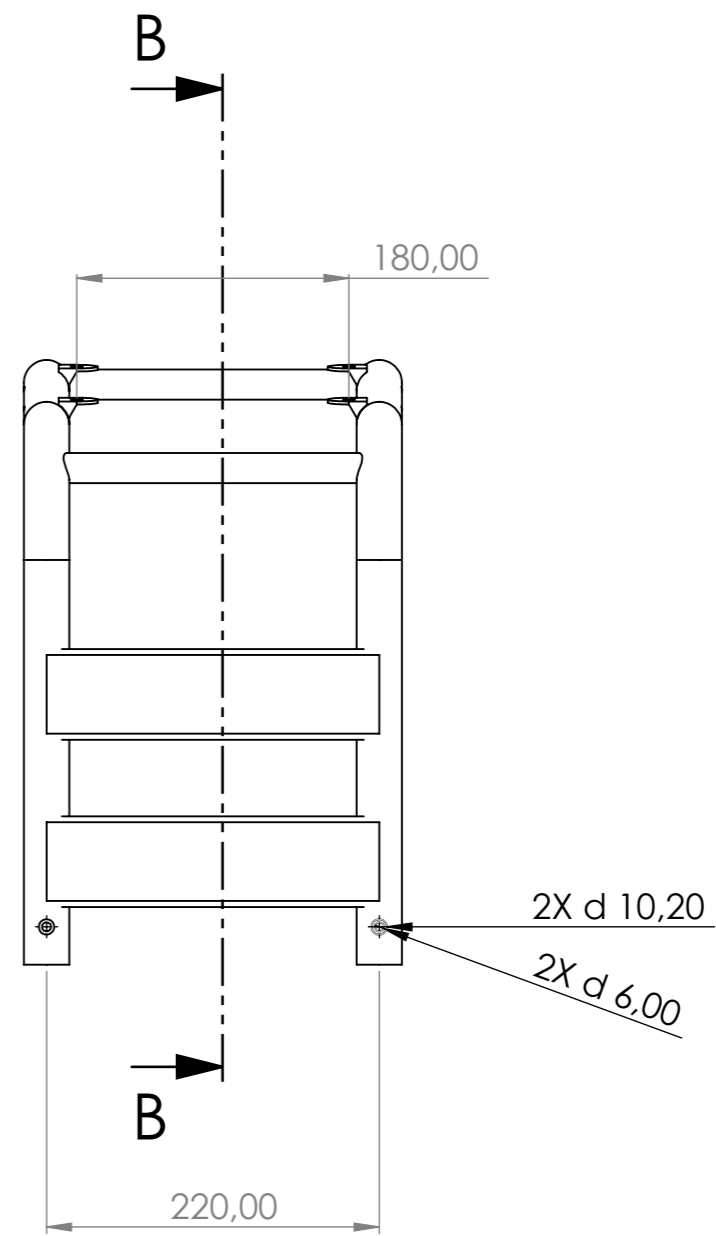
## Appendix A – Drawings



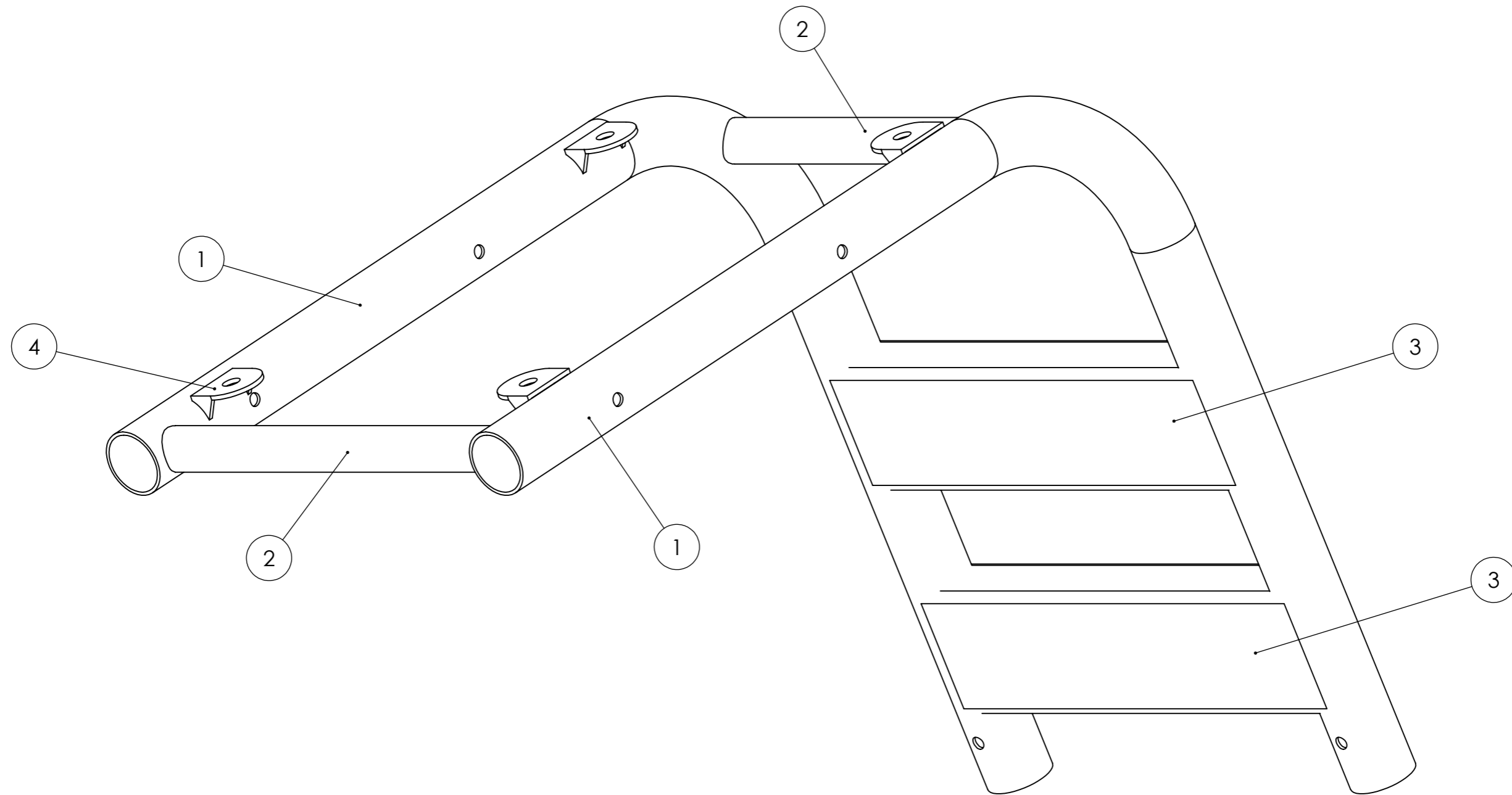
	PROJECT Monoski Unipd		
	TITLE: Frame		
NAME GIANMARCO ROCCO	MATERIAL: 25CrMo4	DWG NO. Frame	A3
DATE 21-11-2023	SCALE 1:2	QUANTITY 1	SHEET 1 OF 3




SECTION B-B

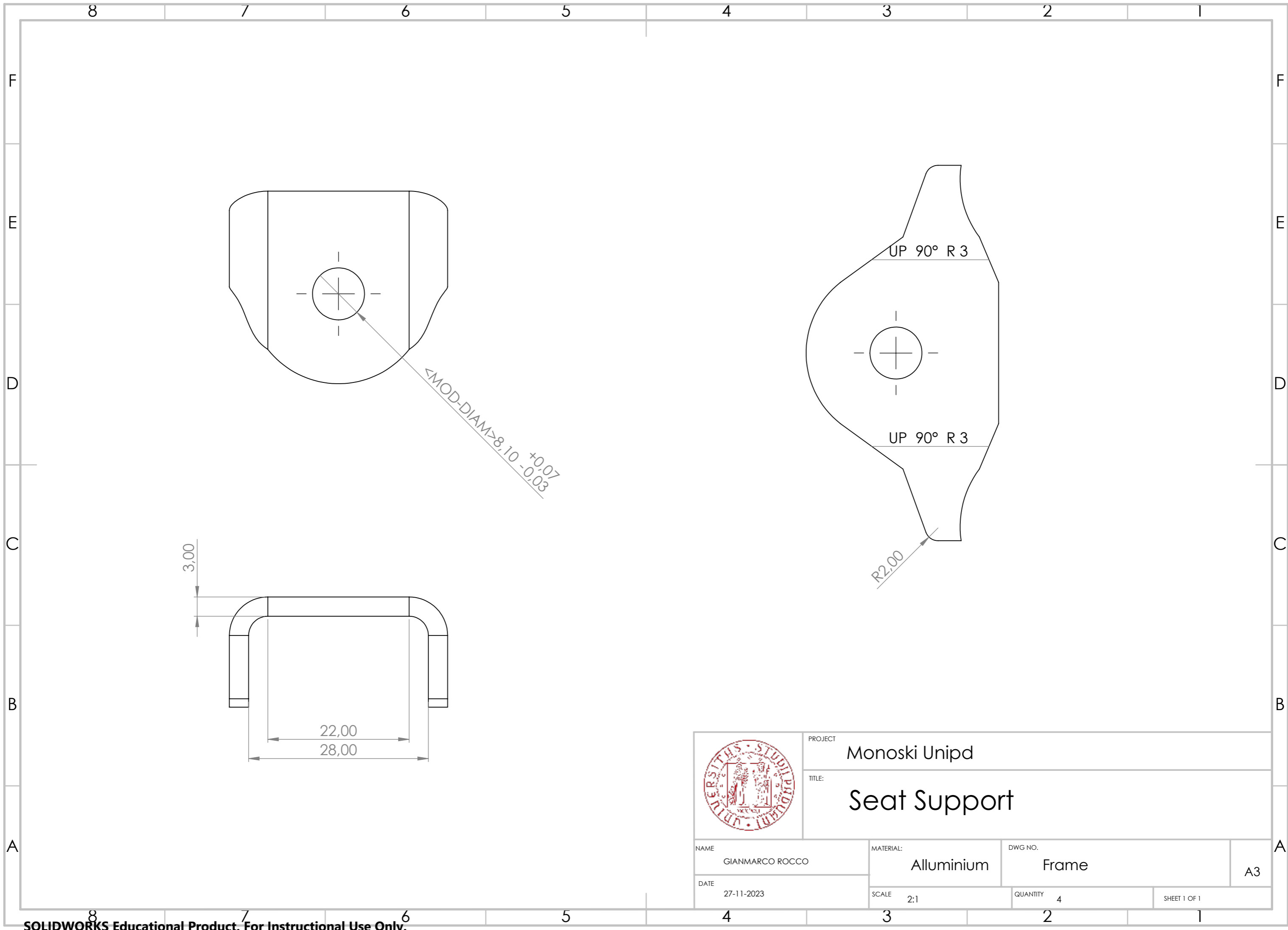


	PROJECT Monoski Unipd		
	TITLE: Frame		
NAME GIANMARCO ROCCO	MATERIAL: 25CrMo4	DWG NO. Frame	A3
DATE 18-11-2023	SCALE 1:5	QUANTITY 1	SHEET 2 OF 3



ITEM NO.	DESCRIPTION	QTY.
1	d 30mm, s 1.5mm	2
2	d 20mm, s 1.5mm	2
3	BxA 60x30mm, s 2mm	2
4	Seat supports	4

	PROJECT Monoski Unipd		
	TITLE: Frame		
NAME GIANMARCO ROCCO	MATERIAL: 25CrMo4	DWG NO. Frame	
DATE 18-11-2023	SCALE 1:2	QUANTITY 1	A3
		SHEET 3 OF 3	



PROJECT: Monoski Unipd

TITLE: Seat Support

NAME: GIANMARCO ROCCO

MATERIAL: Alluminium

DWG NO.: Frame

A3

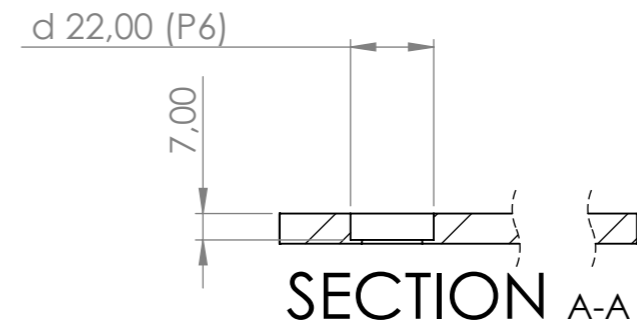
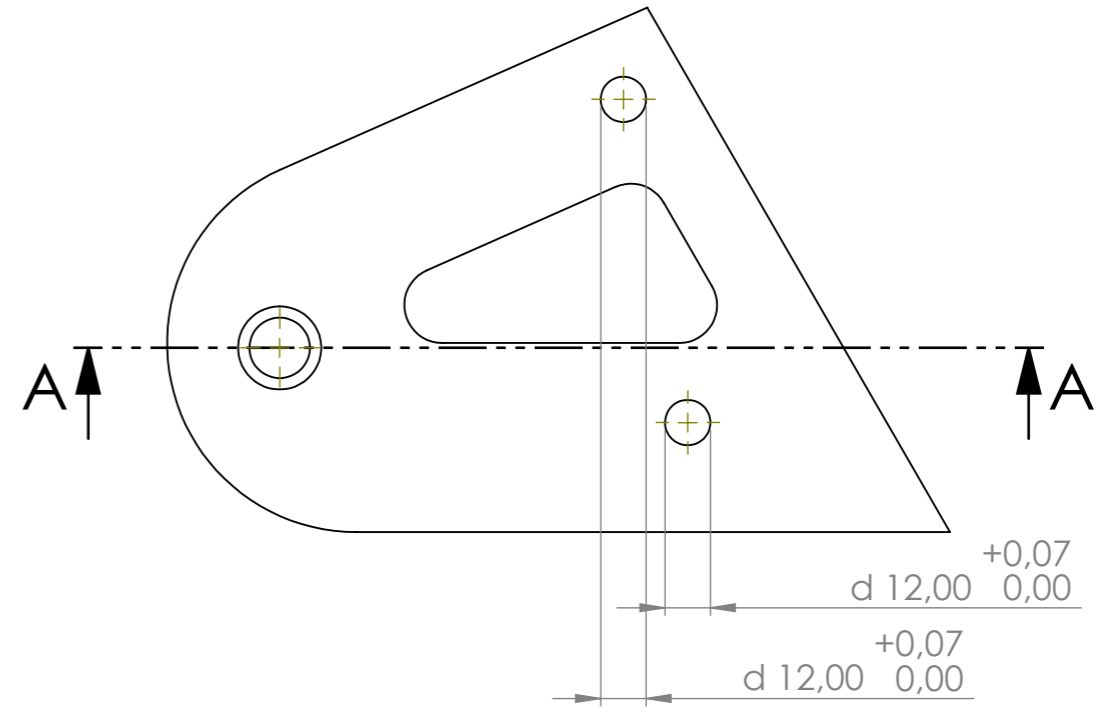
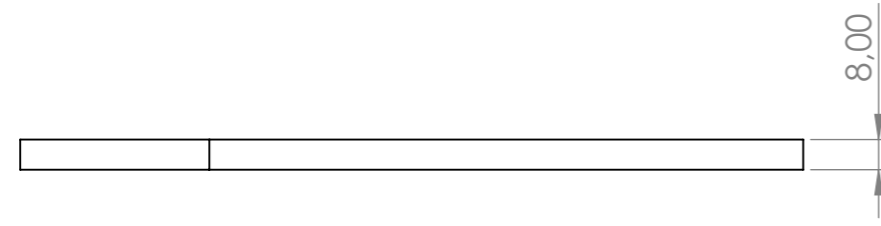
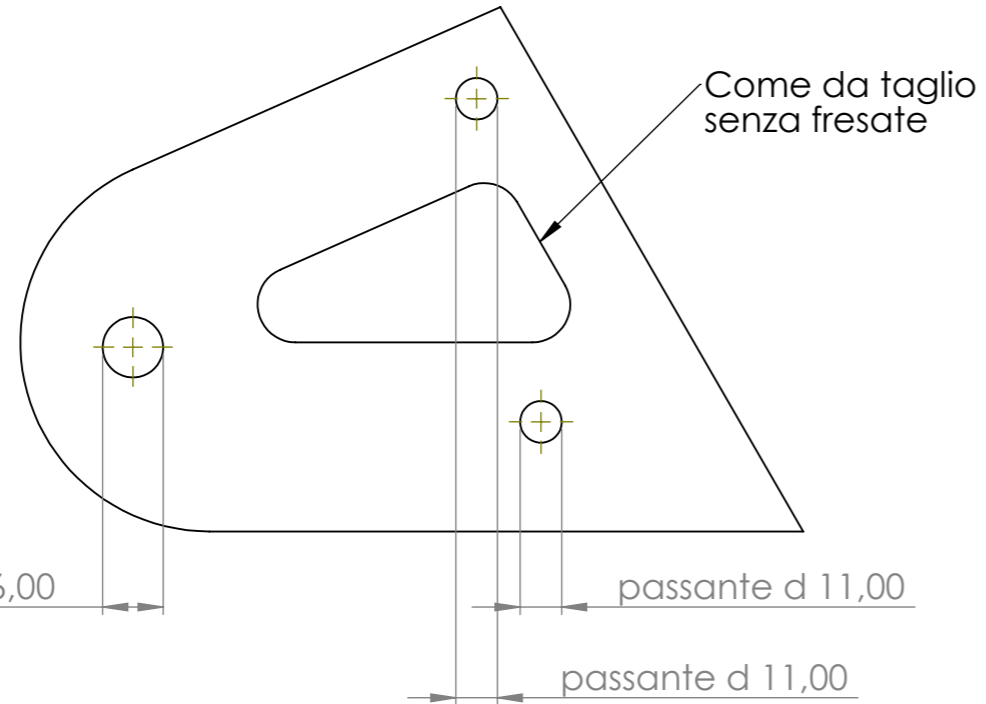
DATE: 27-11-2023


SCALE: 2:1

QUANTITY: 4

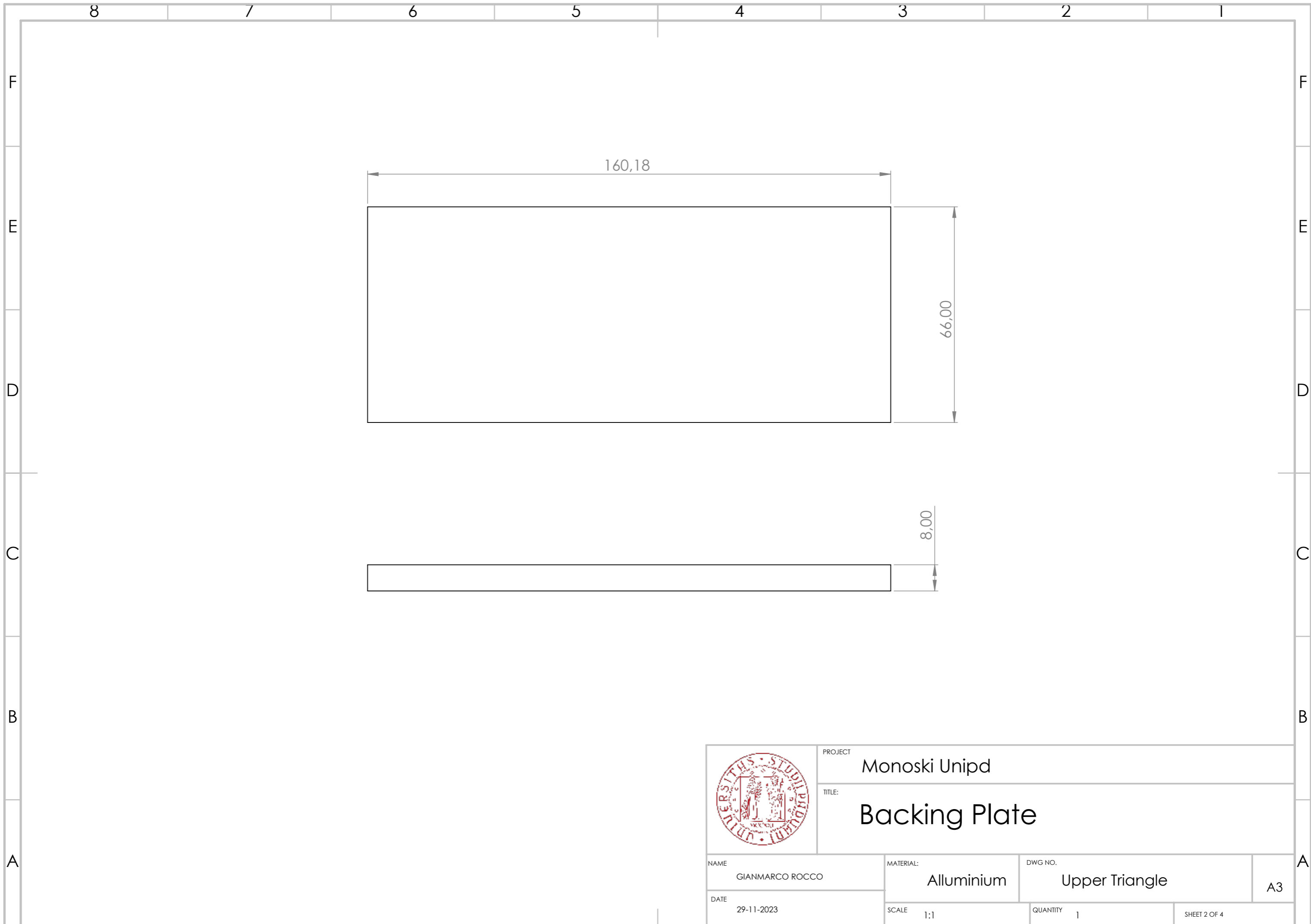
SHEET 1 OF 1


VERSIONE TAGLIO  
AD ACQUA

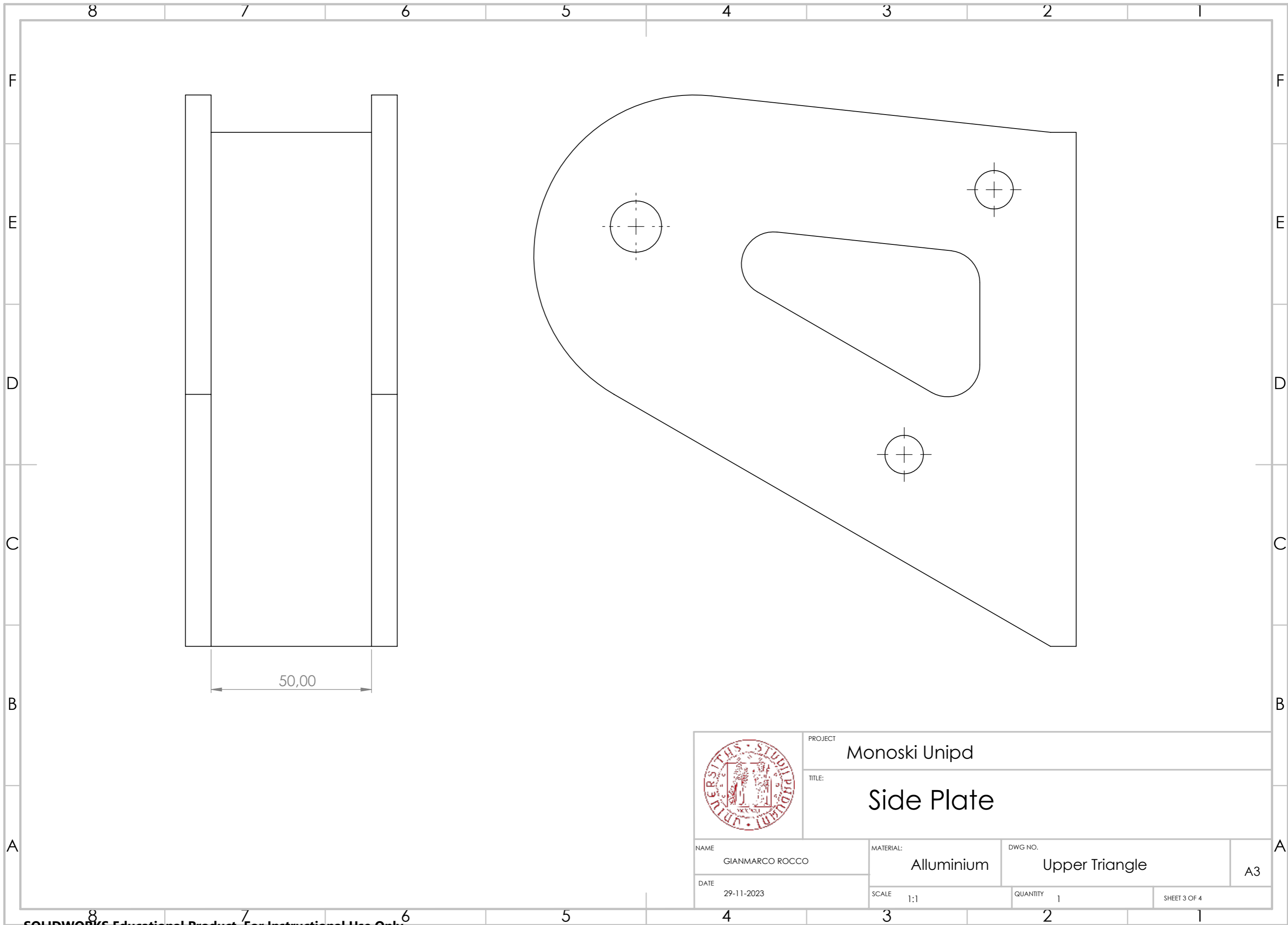


	PROJECT Monoski Unipd		
	TITLE: Side Plate		
NAME GIANMARCO ROCCO	MATERIAL: Alluminium	DWG NO. Upper Triangle	A3
DATE 29-11-2023	SCALE 1:2	QUANTITY 2	SHEET 1 OF 4





	PROJECT Monoski Unipd		
	TITLE: Backing Plate		
NAME GIANMARCO ROCCO	MATERIAL: Alluminium	DWG NO. Upper Triangle	A3
DATE 29-11-2023	SCALE 1:1	QUANTITY 1	SHEET 2 OF 4



50,00



PROJECT  
Monoski Unipd

TITLE:  
Side Plate

NAME  
GIANMARCO ROCCO

MATERIAL:  
Alluminium

DWG NO.  
Upper Triangle

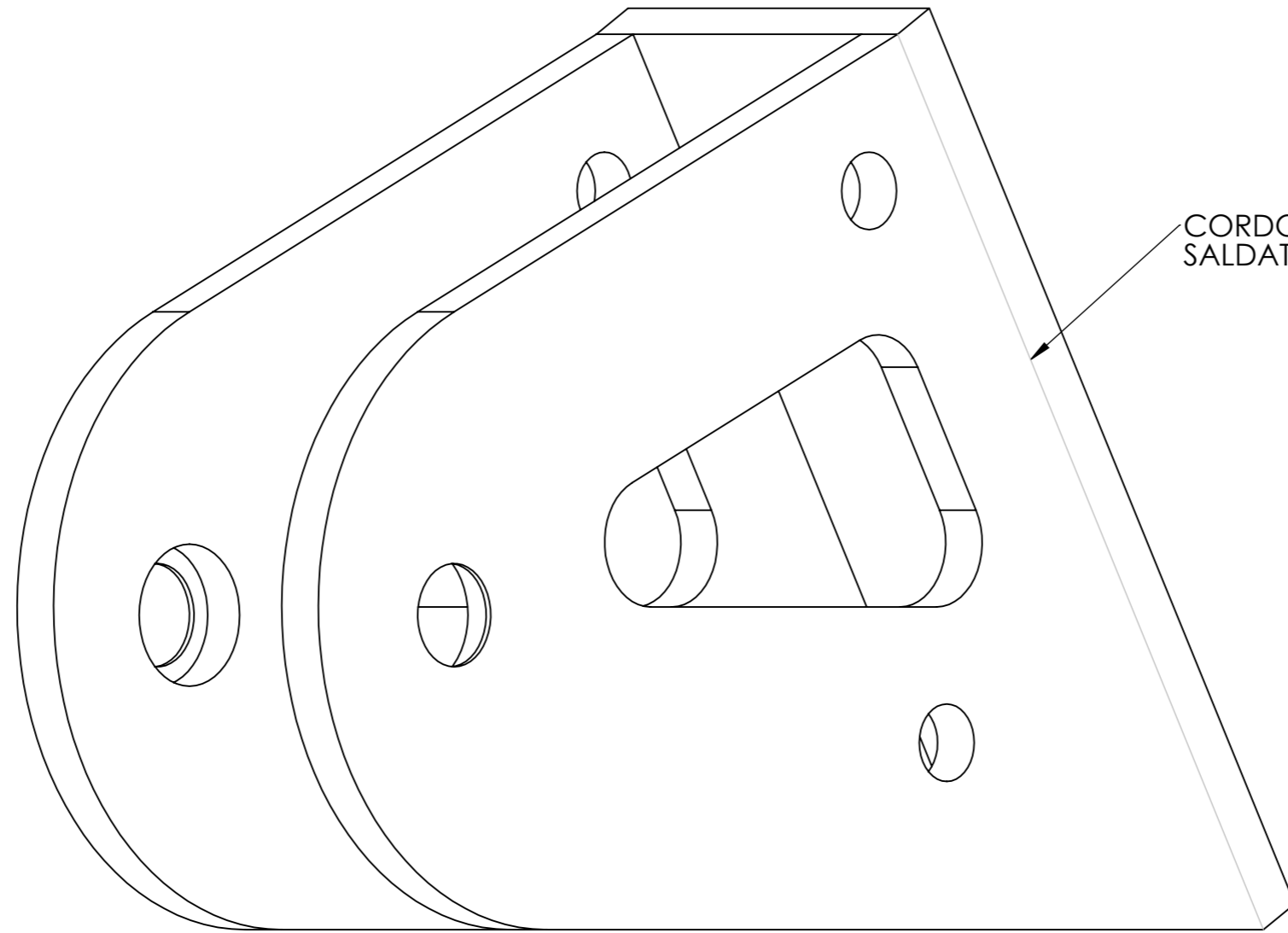
A3

DATE  
29-11-2023

SCALE  
1:1

QUANTITY  
1

SHEET 3 OF 4



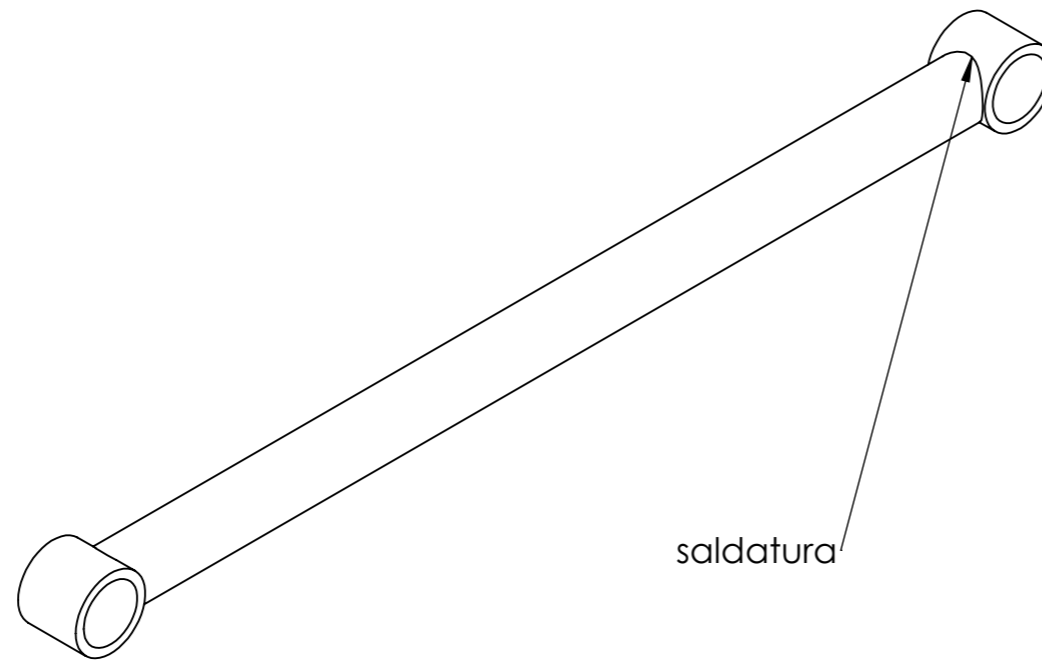
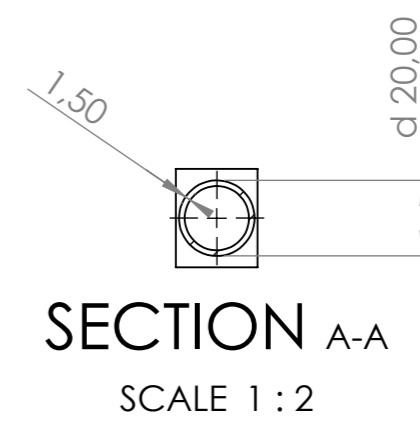
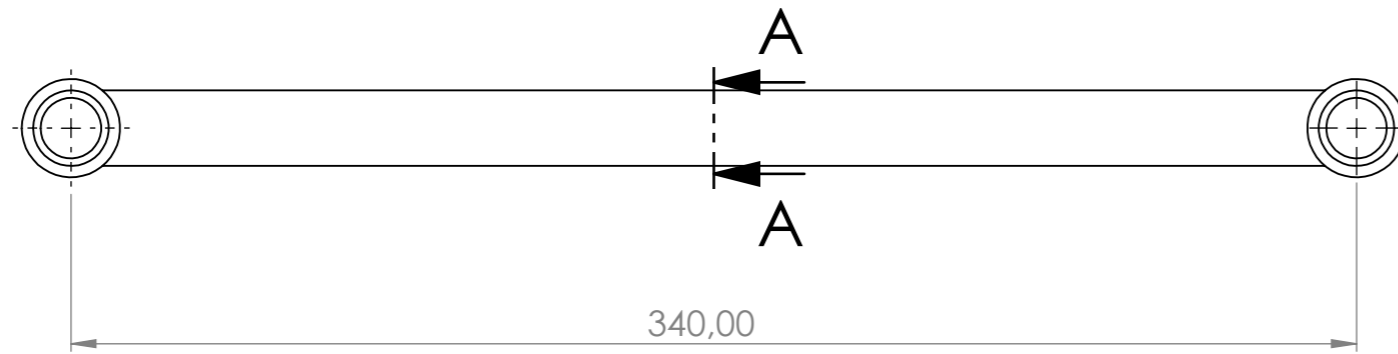
CORDONE DI  
SALDATURA




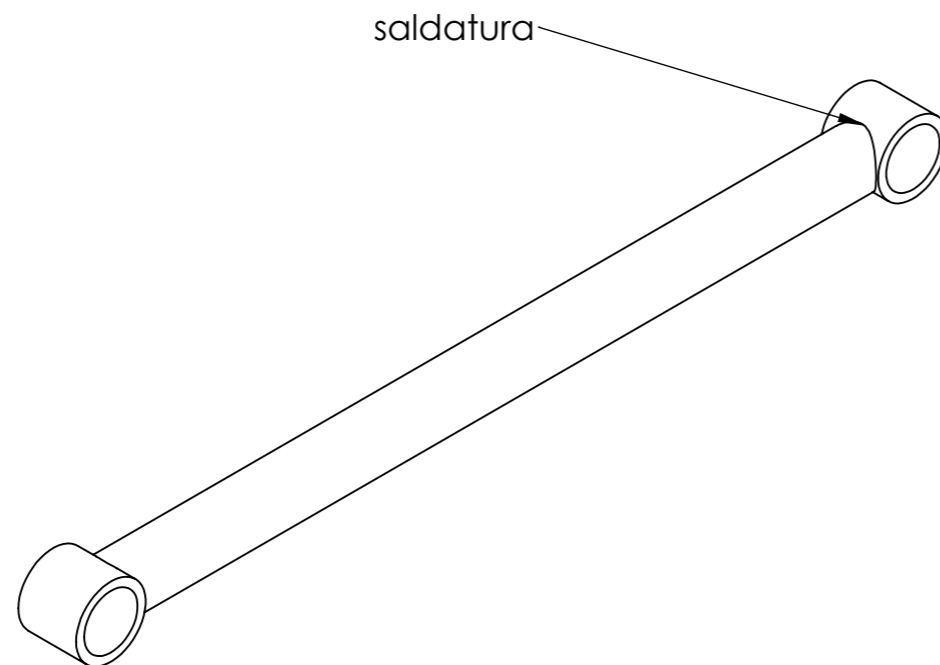
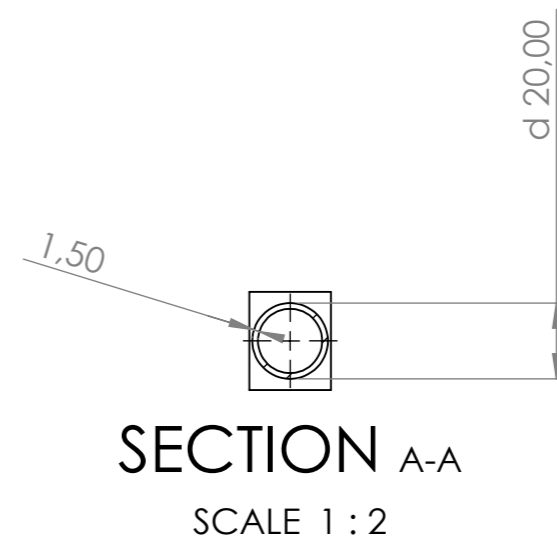
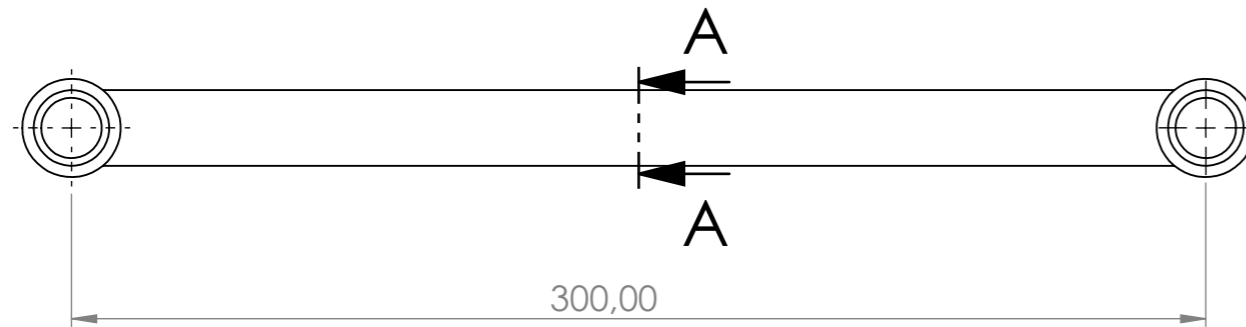
PROJECT  
Monoski Unipd


TITLE:  
Side Plate

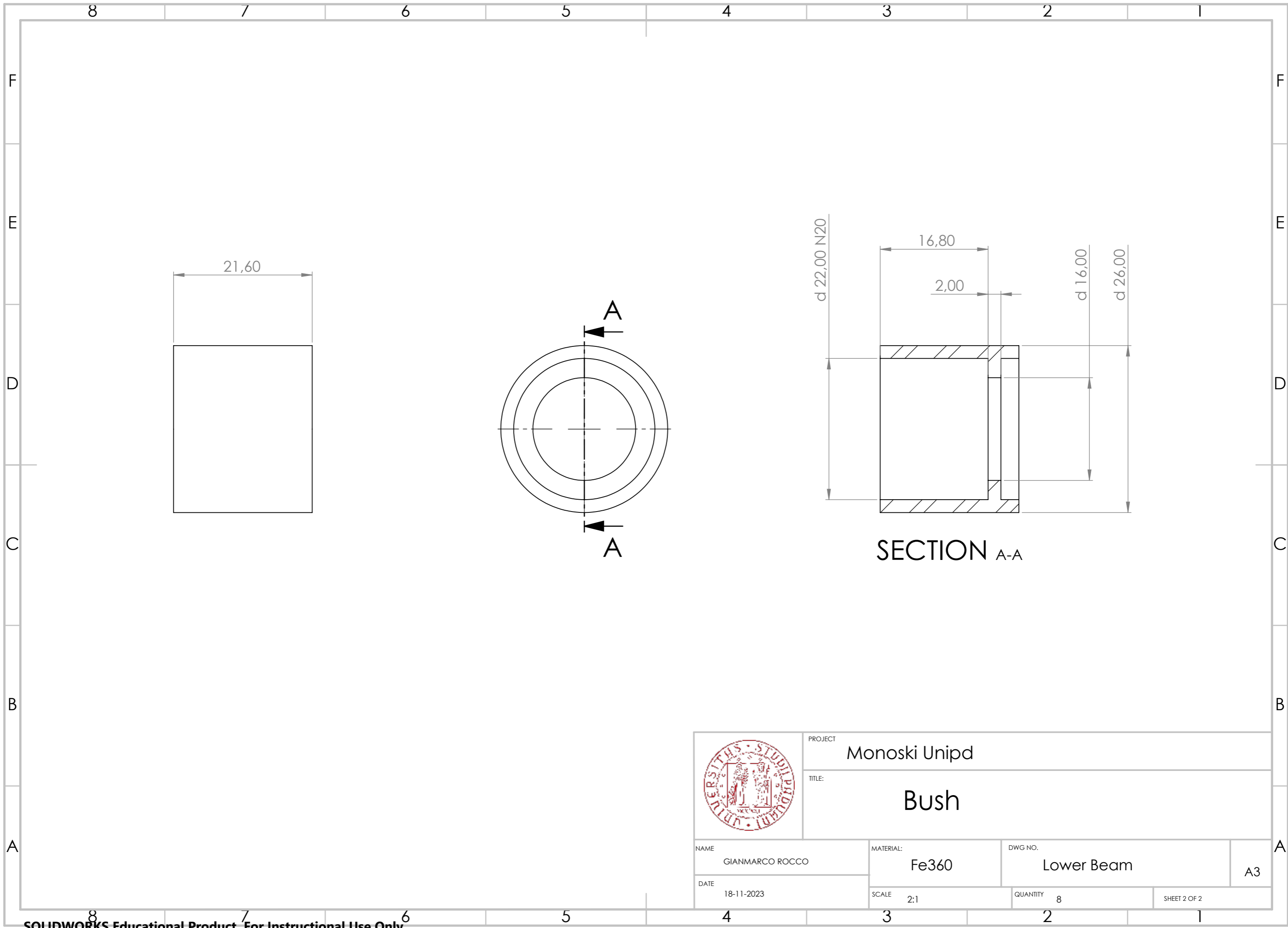
NAME GIANMARCO ROCCO	MATERIAL: Alluminium	DWG NO. Upper Triangle	A3
DATE 29-11-2023	SCALE 1:2	QUANTITY 1	SHEET 4 OF 1



	PROJECT Monoski Unipd		
	TITLE: Upper Beam		
NAME GIANMARCO ROCCO	MATERIAL: 25CrMo4	DWG NO. Upper Beam	A3
DATE 18-11-2023	SCALE 1:2	QUANTITY 2	SHEET 1 OF 2



	PROJECT Monoski Unipd		
	TITLE: Lower Beam		
NAME GIANMARCO ROCCO	MATERIAL: 25CrMo4	DWG NO. Lower Beam	A3
DATE 18-11-2023	SCALE 1:2	QUANTITY 2	SHEET 1 OF 2



PROJECT: Monoski Unipd

TITLE: Bush

NAME: GIANMARCO ROCCO

MATERIAL: Fe360

DWG NO.: Lower Beam

A3

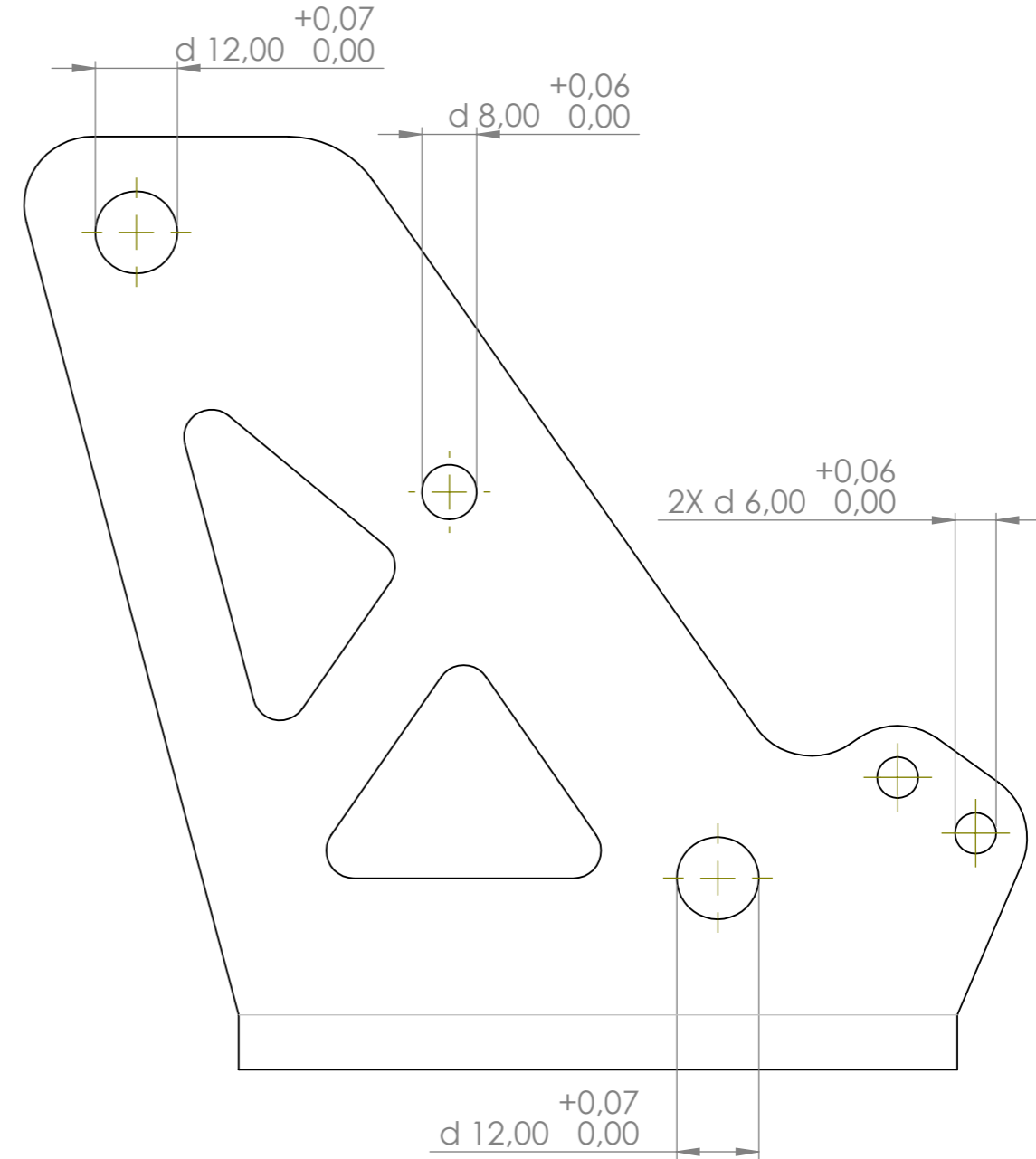
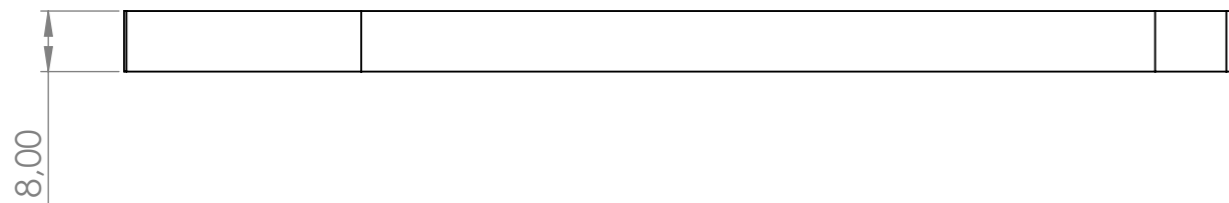
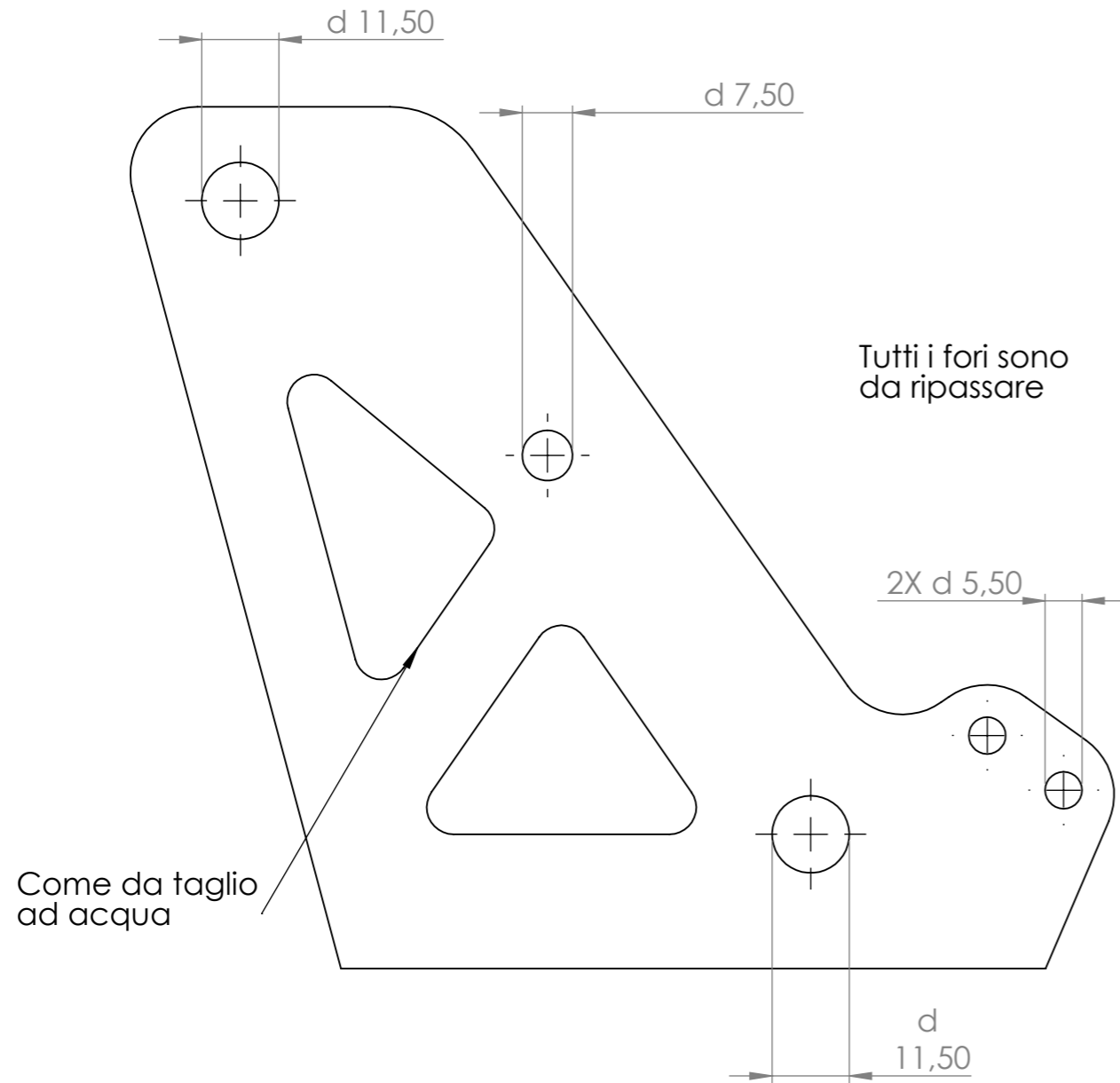
DATE: 18-11-2023

SCALE: 2:1

QUANTITY: 8

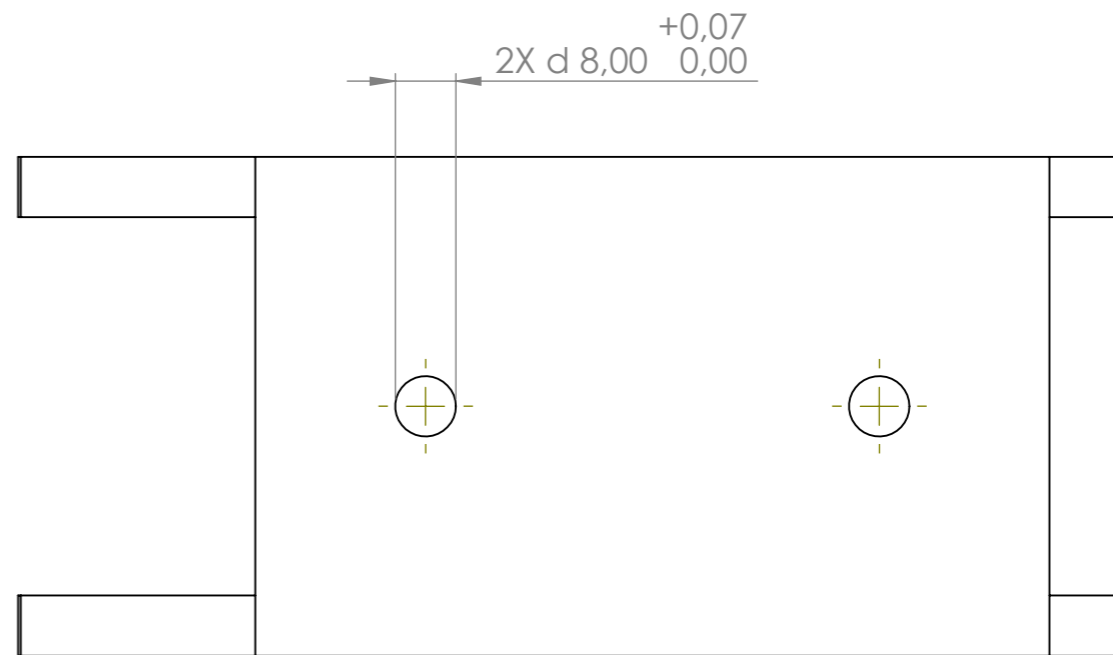
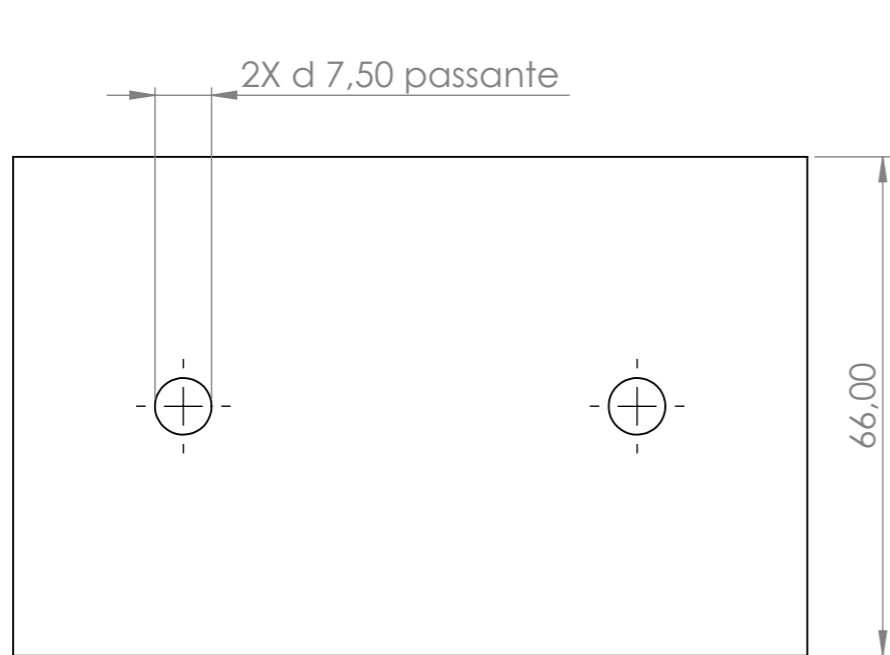
SHEET 2 OF 2

VERSIONE TAGLIO AD ACQUA



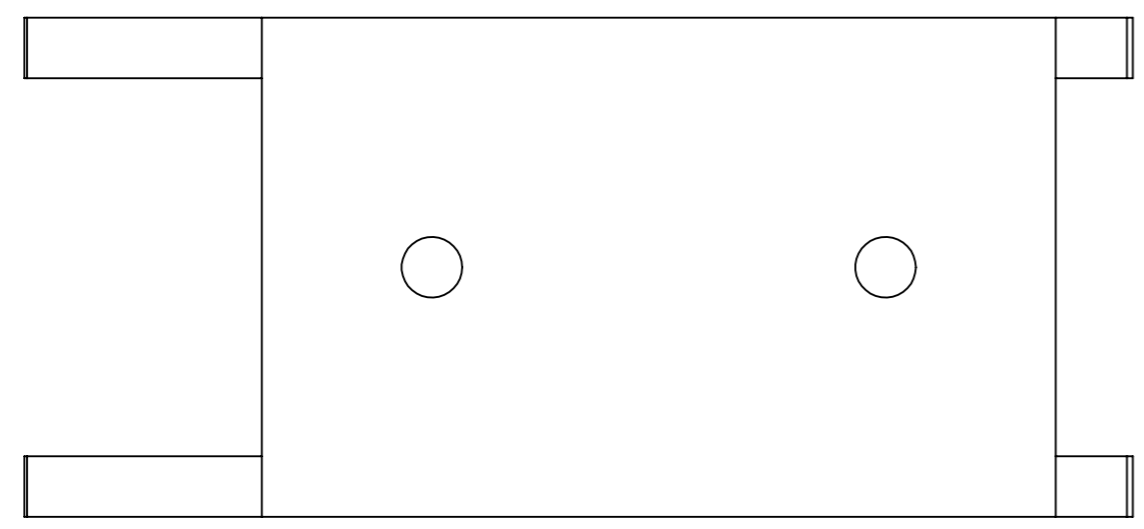
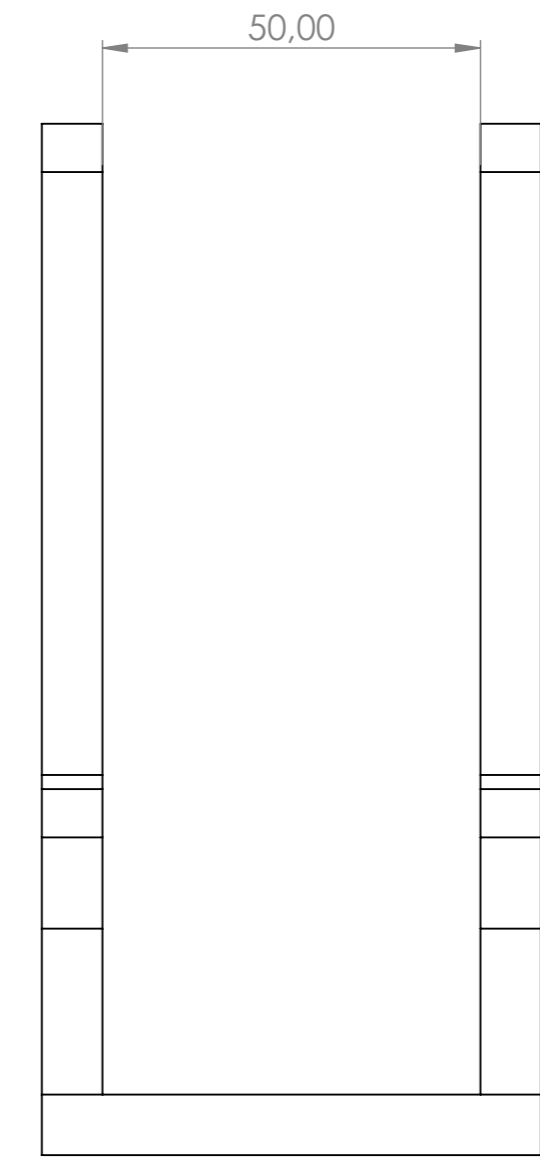
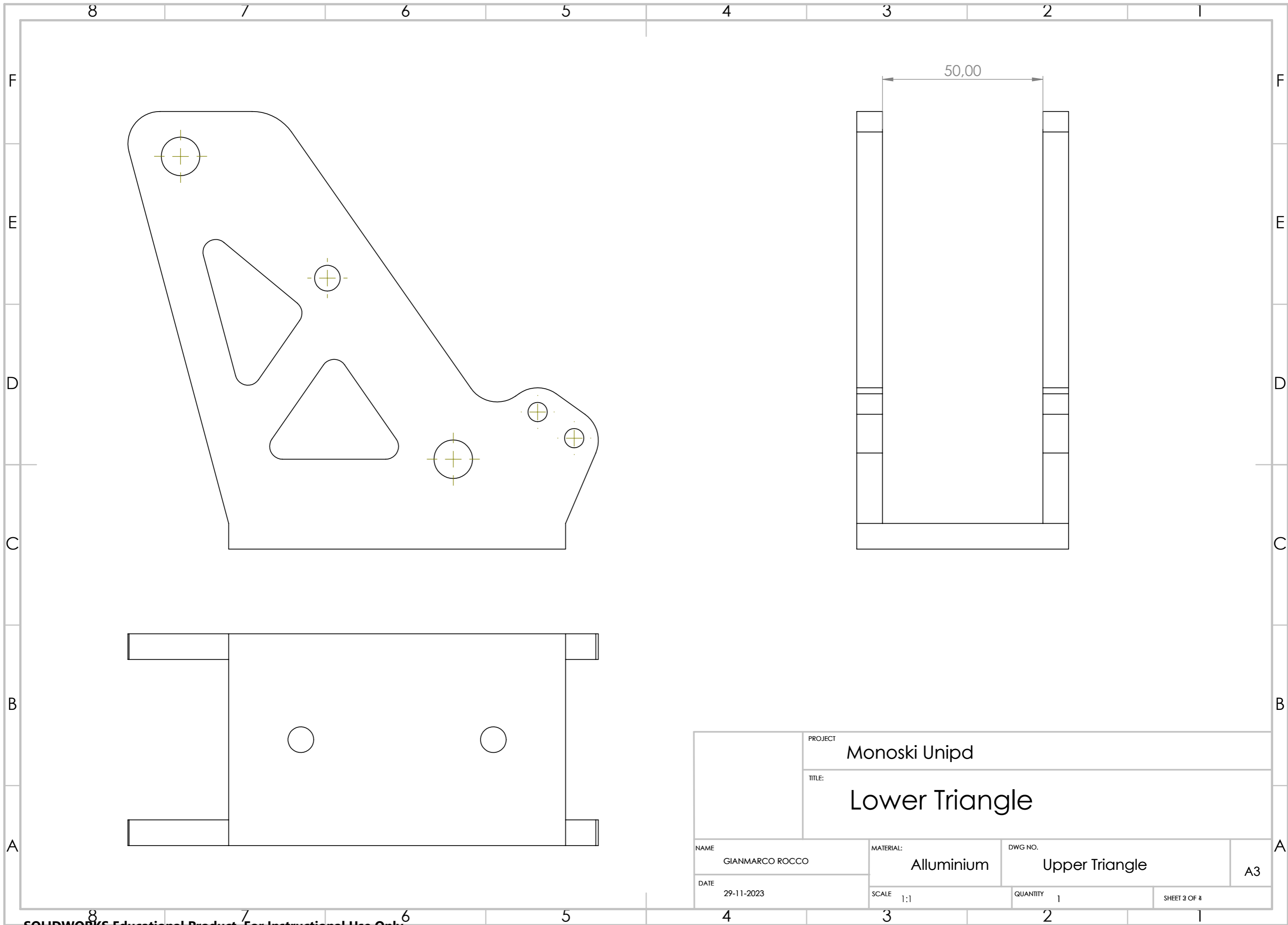
PROJECT		Monoski Unipd	
TITLE:		Backing Plate	
NAME	GIANMARCO ROCCO	MATERIAL:	Alluminium
DATE	29-11-2023	DWG NO.	Lower Triangle
SCALE		1:1	QUANTITY
			1
		SHEET 1 OF 4	
		A3	

VERSIONE TAGLIO AD ACQUA

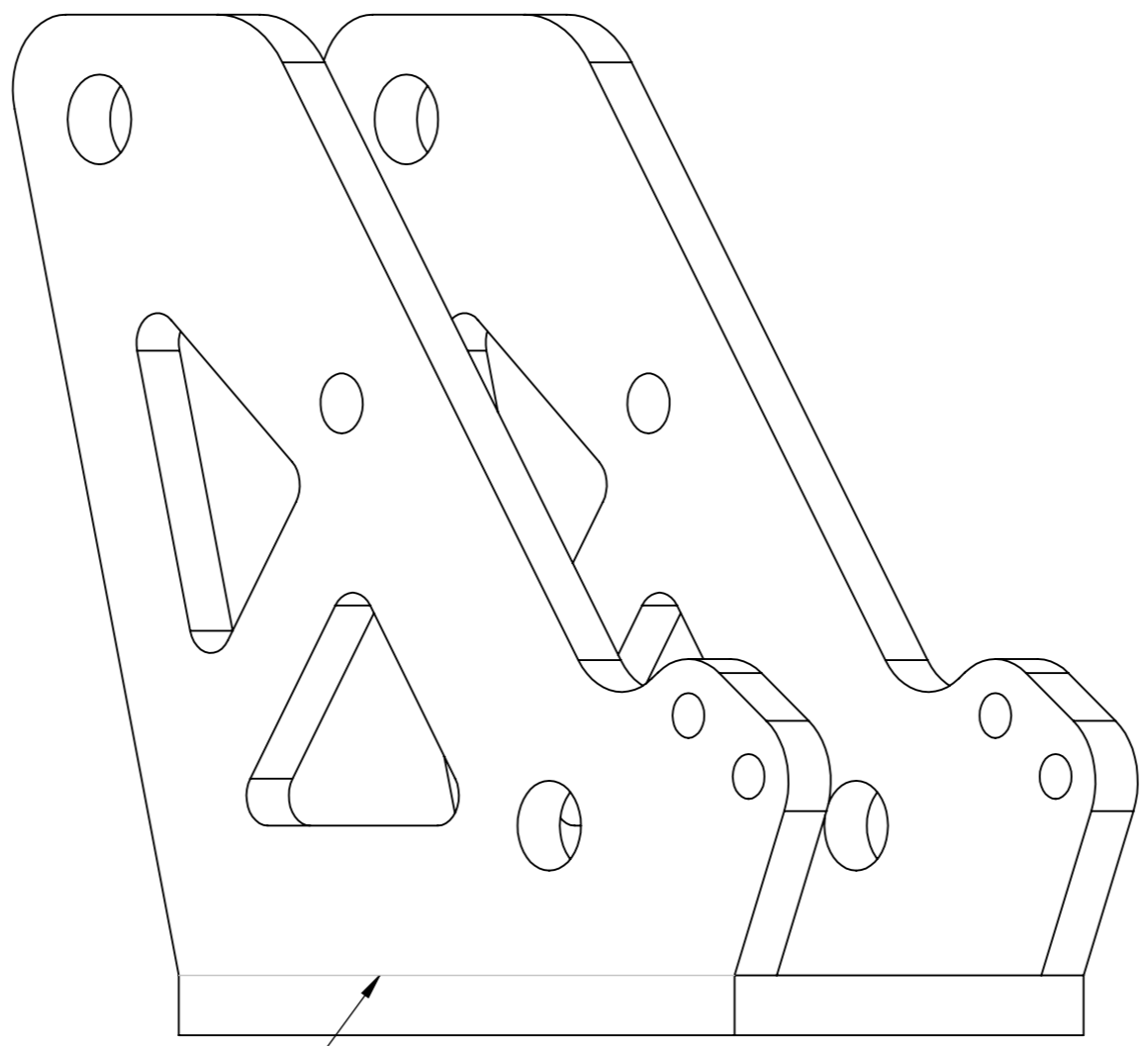


PROJECT		Monoski Unipd				
TITLE:		Backing Plate				
NAME	GIANMARCO ROCCO	MATERIAL:	Alluminium	DWG NO.	Upper Triangle	A3
DATE	29-11-2023	SCALE	1:1	QUANTITY	1	SHEET 2 OF 4





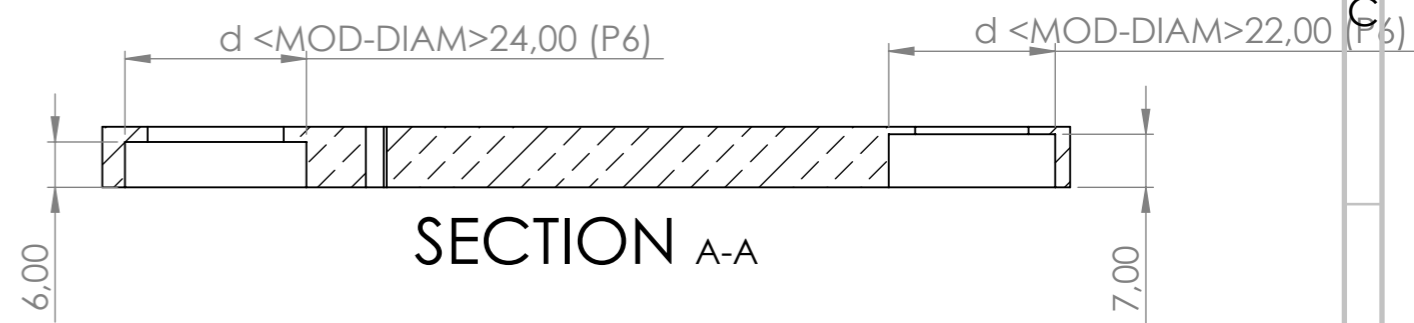
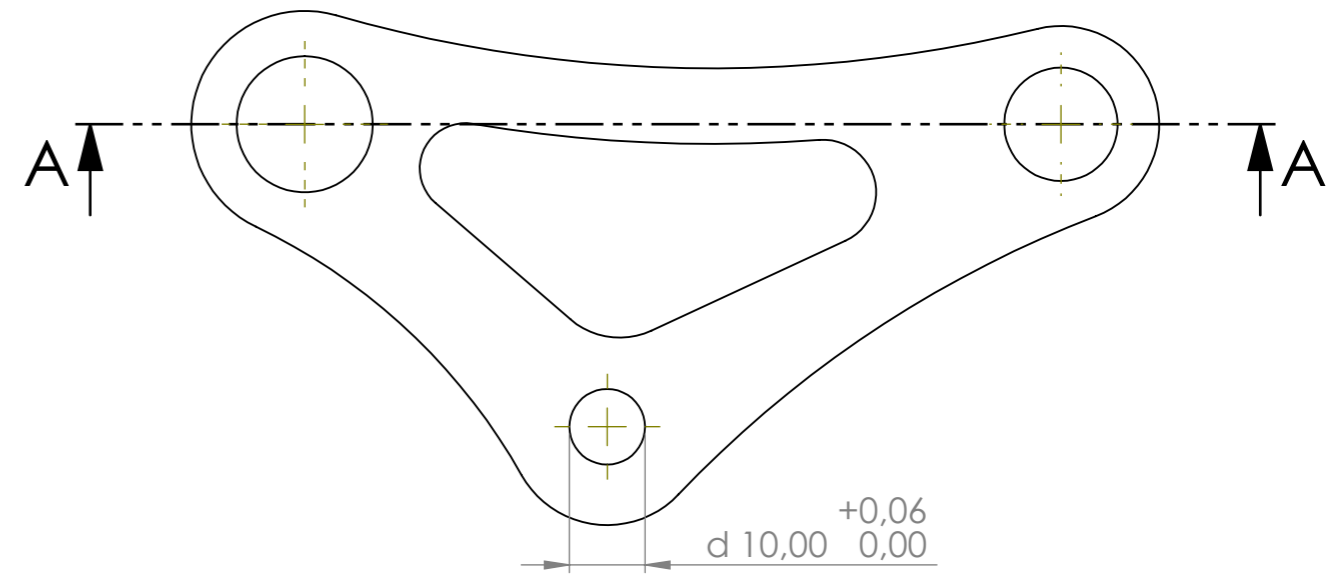
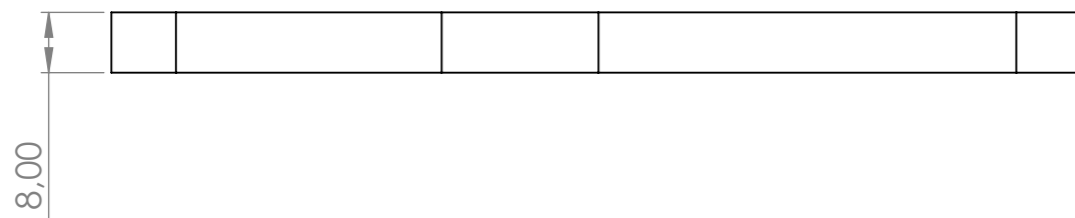
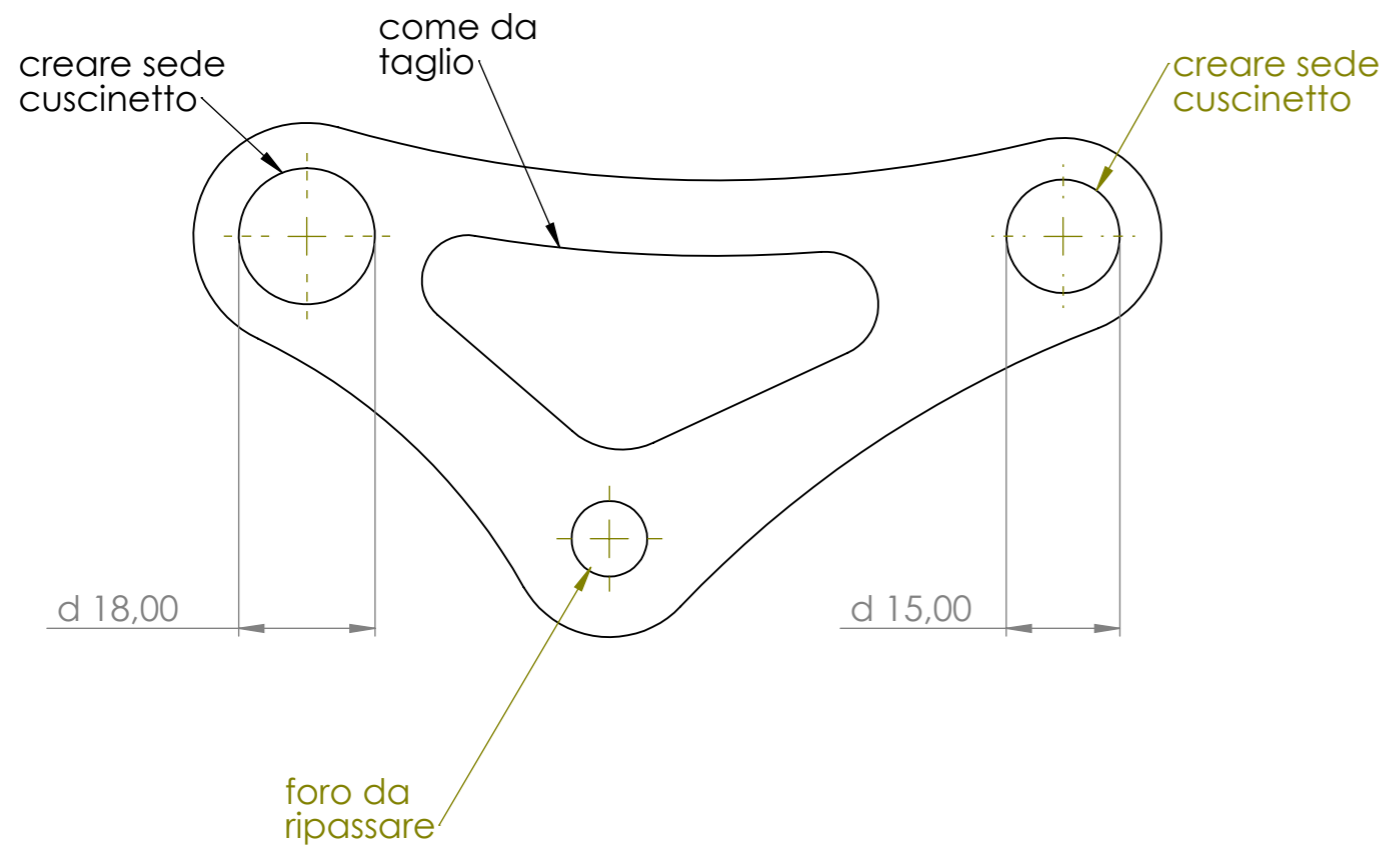
PROJECT		Monoski Unipd			
TITLE:		Lower Triangle			
NAME	GIANMARCO ROCCO	MATERIAL:	Alluminium	DWG NO.	Upper Triangle
DATE	29-11-2023	SCALE	1:1	QUANTITY	1
				SHEET 3 OF 4	A3




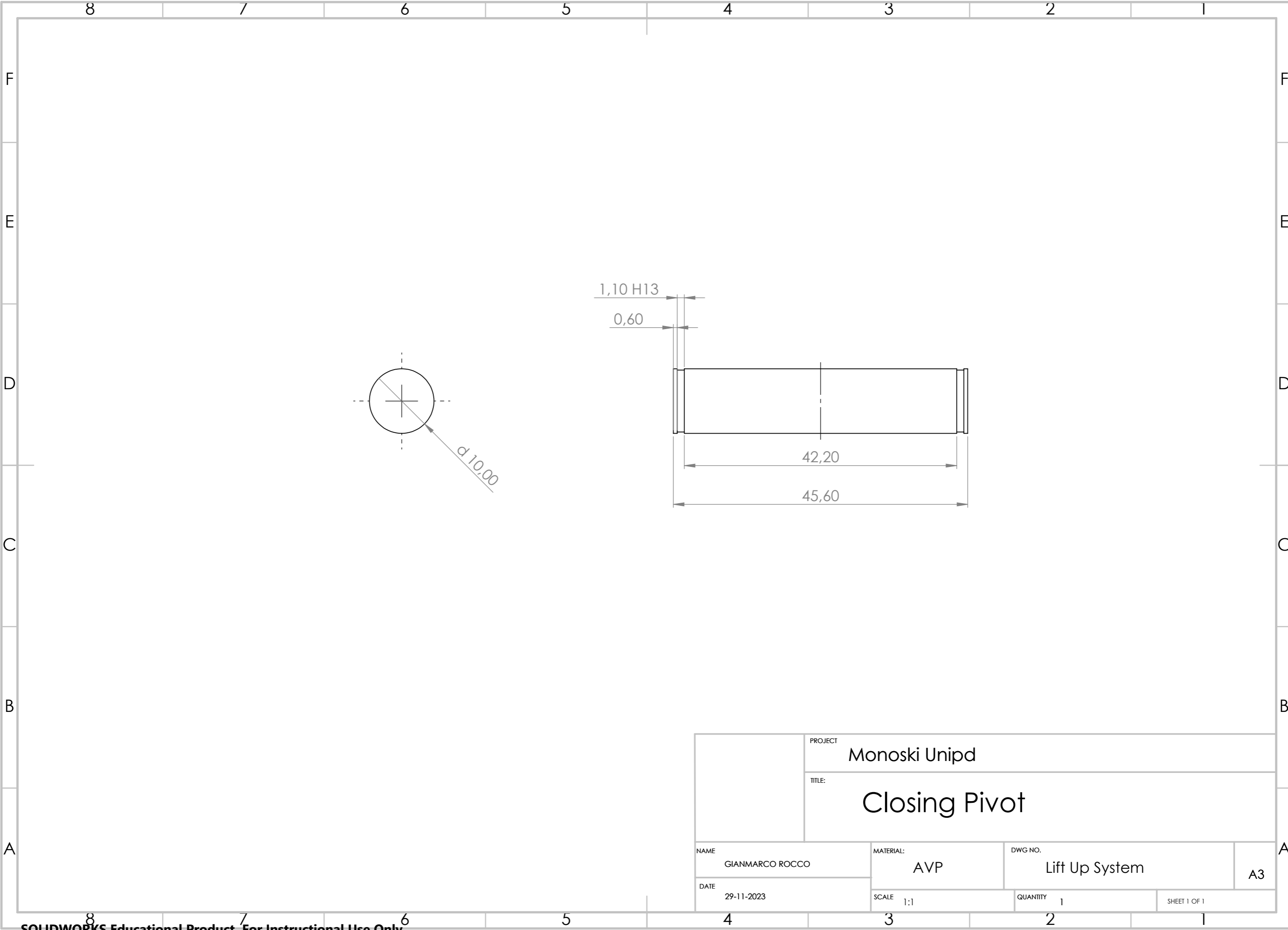
Cordone di saldatura

		PROJECT Monoski Unipd		
		TITLE: Backing Plate		
NAME GIANMARCO ROCCO	MATERIAL: Alluminium	DWG NO. Upper Triangle		A3
DATE 29-11-2023	SCALE 1:1	QUANTITY 1	SHEET # OF # 1	

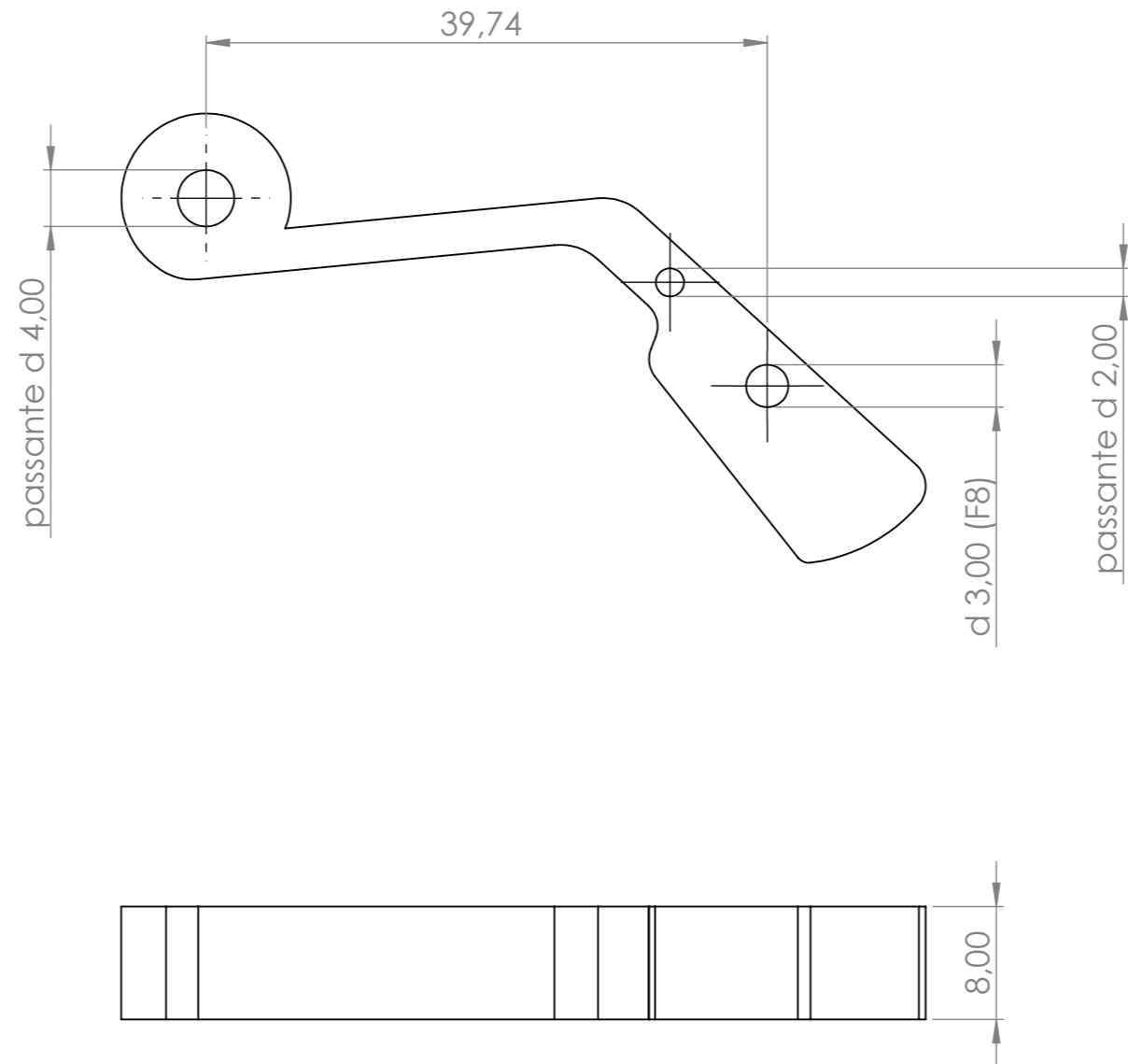
# VERSIONE TAGLIO AD ACQUA



	PROJECT Monoski Unipd		
	TITLE: Right Side Plate		
NAME GIANMARCO ROCCO	MATERIAL: Aluminium	DWG NO. Lift Up triangle	A3
DATE 29-11-2023	SCALE 1:1	QUANTITY 1	SHEET 1 OF 2

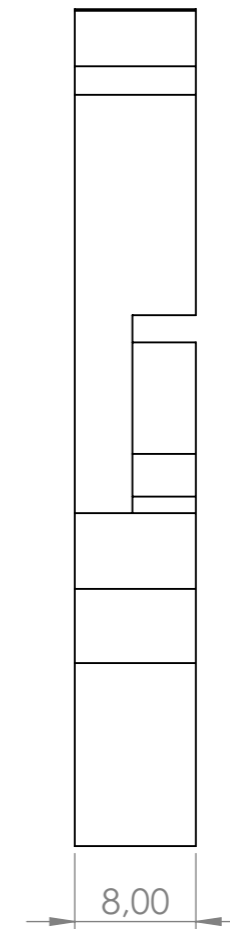
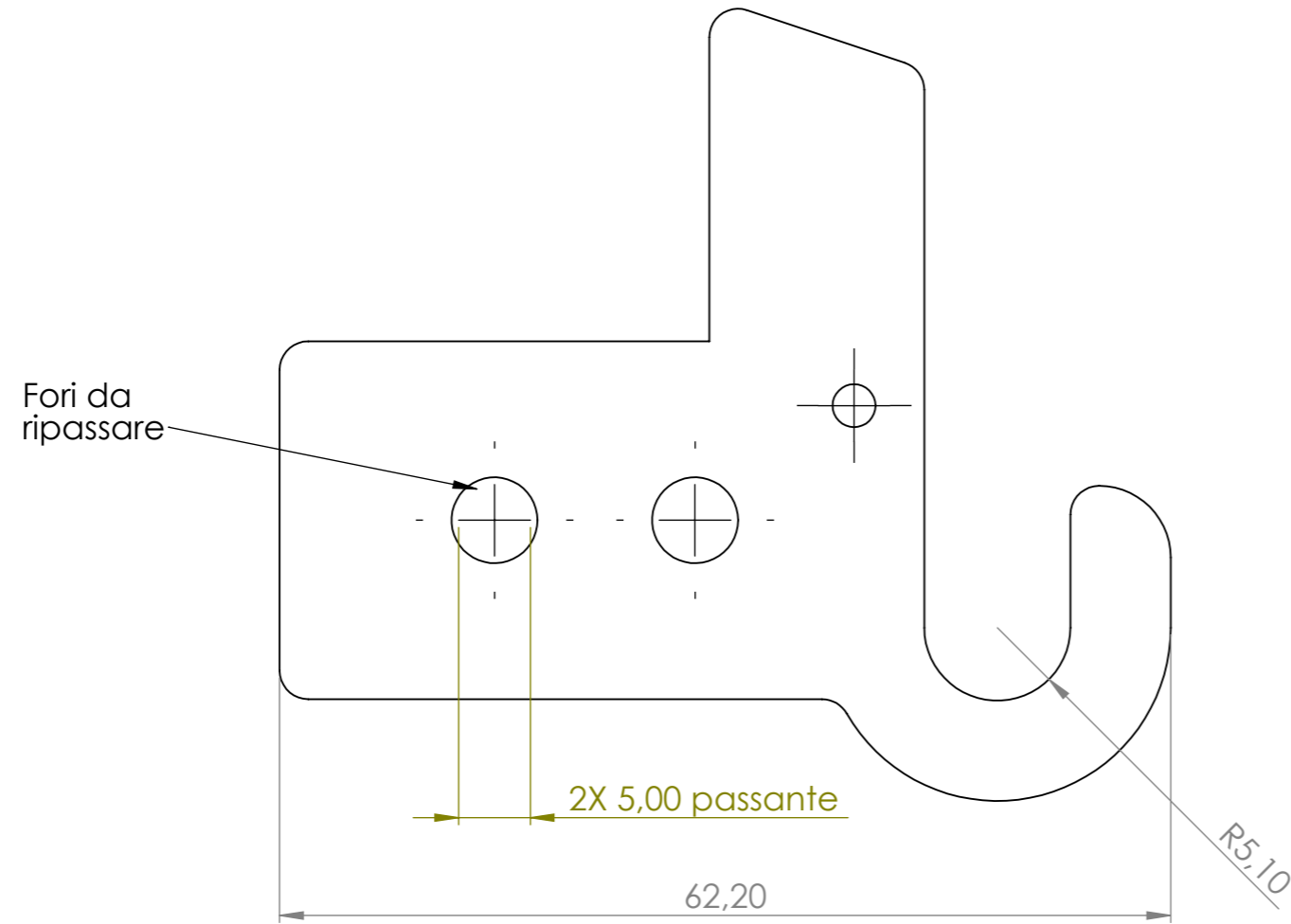



	PROJECT Monoski Unipd		
	TITLE: Closing Pivot		
NAME GIANMARCO ROCCO	MATERIAL: AVP	DWG NO. Lift Up System	A3
DATE 29-11-2023	SCALE 1:1	QUANTITY 1	SHEET 1 OF 1

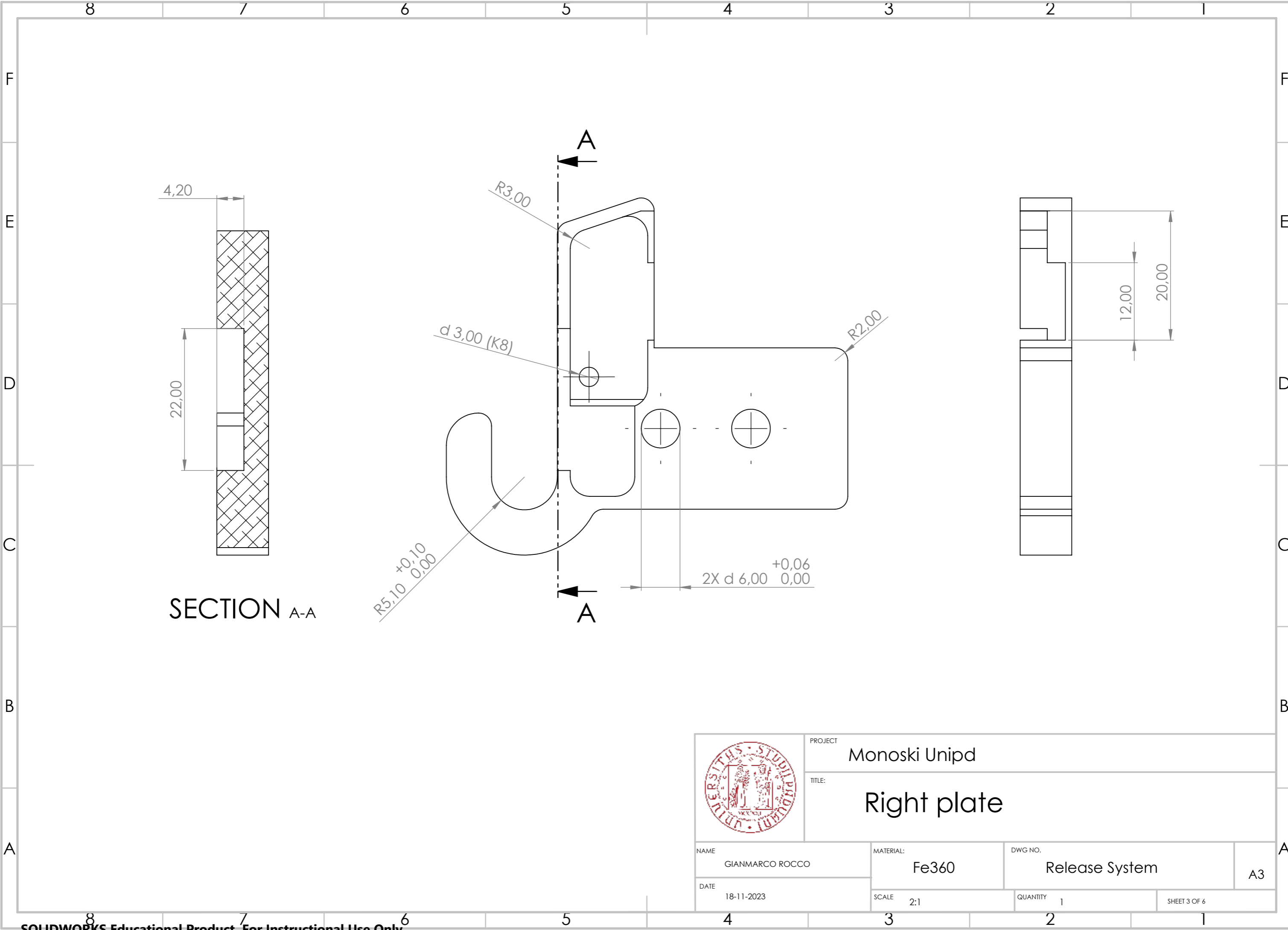


	PROJECT Monoski Unipd		
	TITLE: Latch Handle		
NAME GIANMARCO ROCCO	MATERIAL: Fe360	DWG NO. Release System	A3
DATE 18-11-2023	SCALE 2:1	QUANTITY 1	SHEET 1 OF 6

VERSIONE TAGLIO AD ACQUA

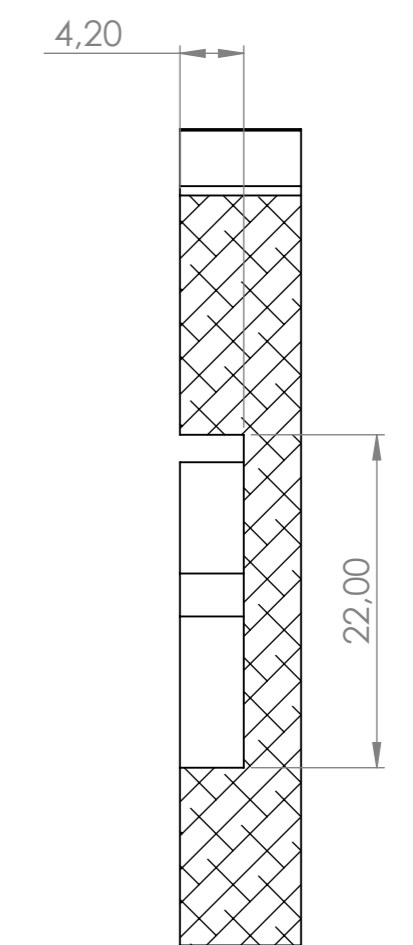
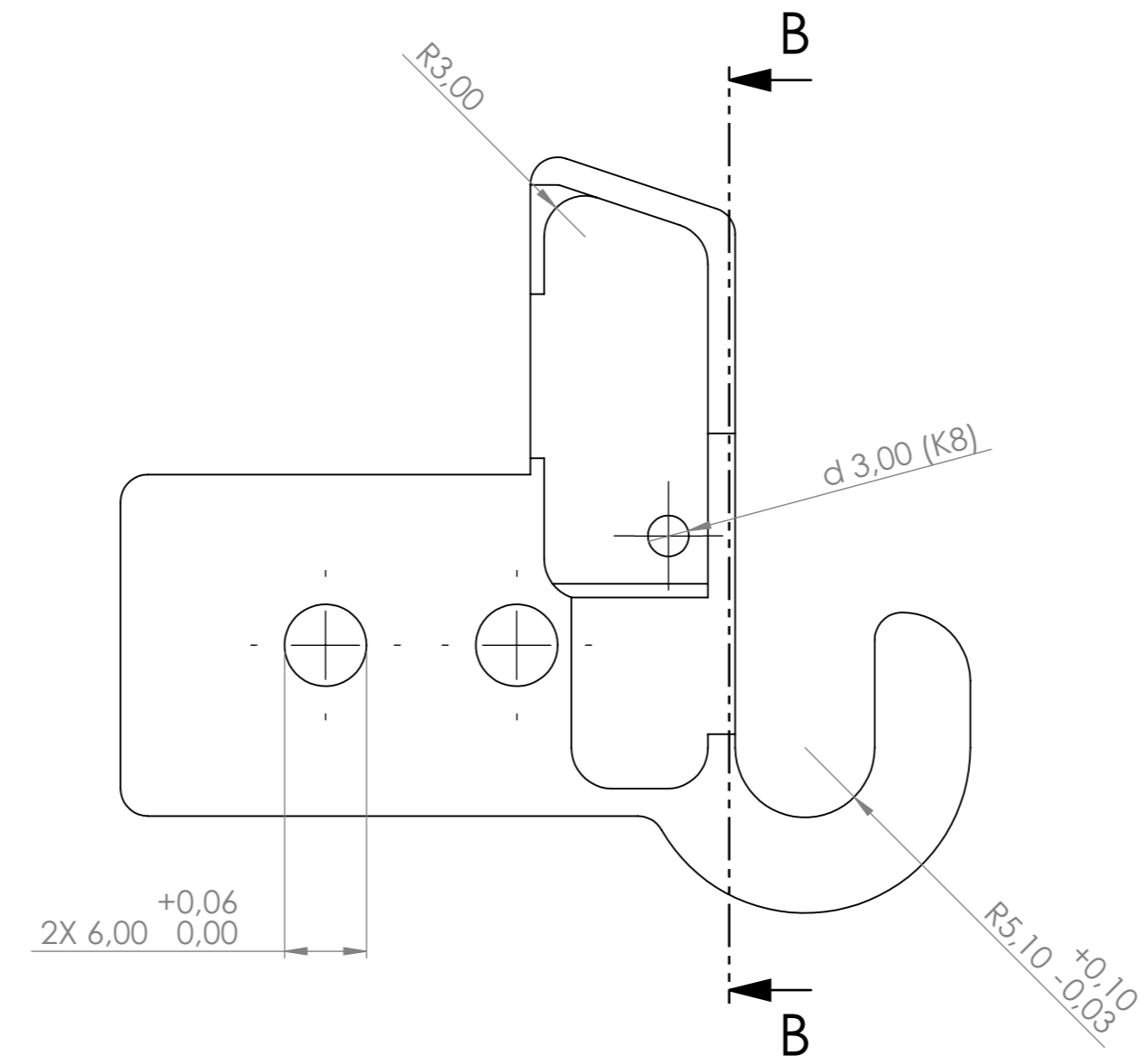
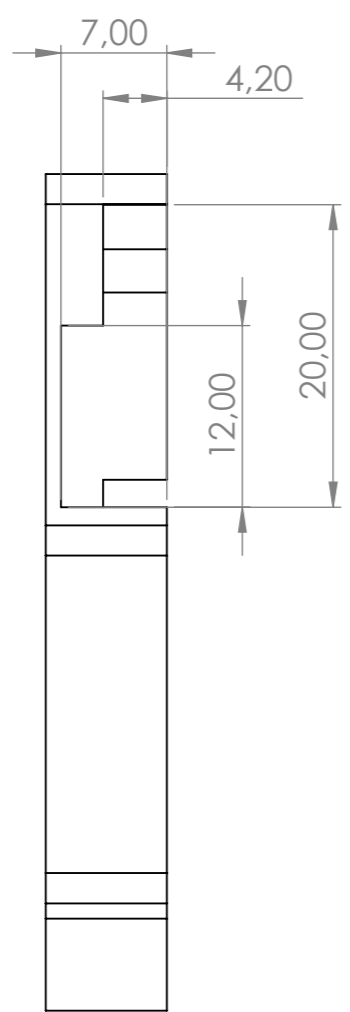


	PROJECT Monoski Unipd		
	TITLE: Plate		
NAME GIANMARCO ROCCO	MATERIAL: Fe360	DWG NO. Release System	A3
DATE 18-11-2023	SCALE 2:1	QUANTITY 2	SHEET 2 OF 6




SECTION A-A

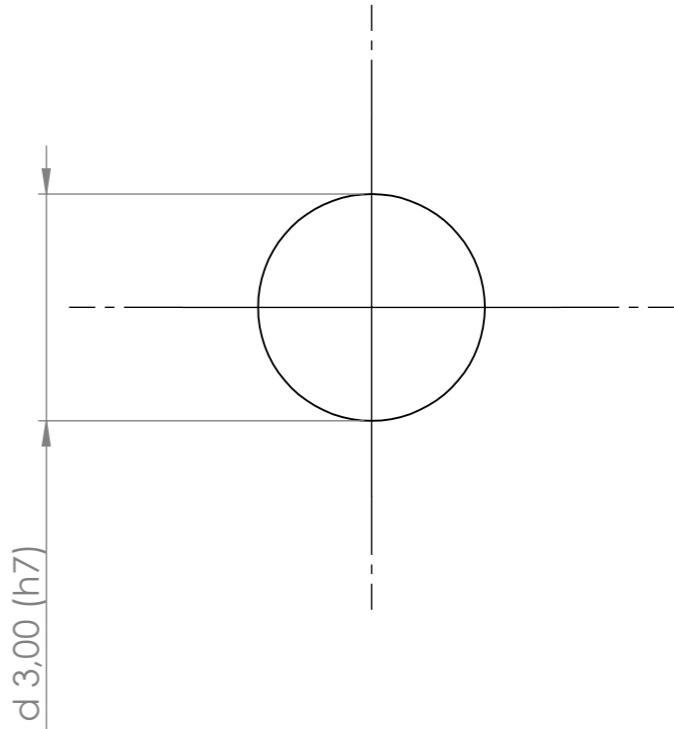
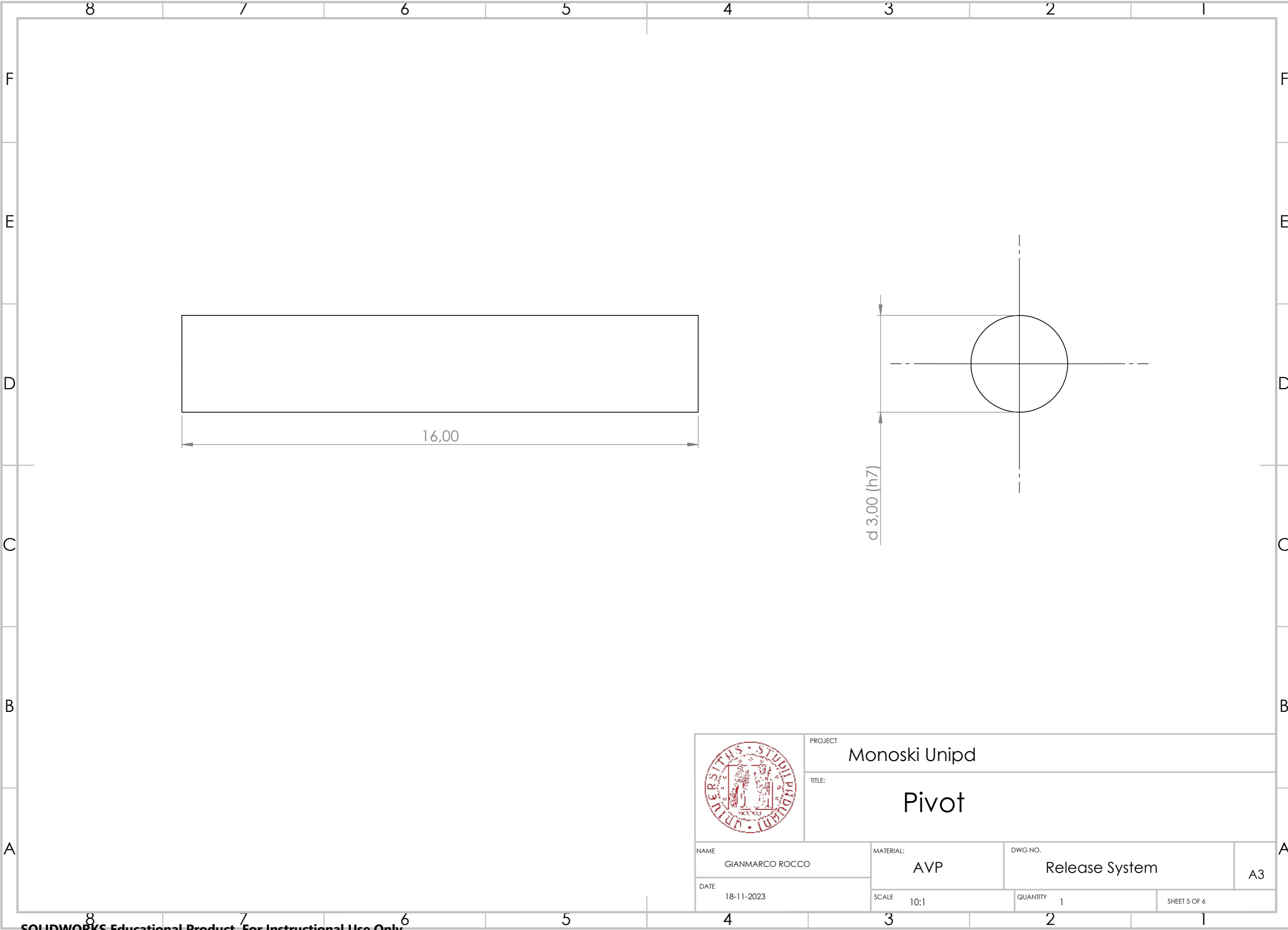
	PROJECT Monoski Unipd		
	TITLE: Right plate		
NAME GIANMARCO ROCCO	MATERIAL: Fe360	DWG NO. Release System	A3
DATE 18-11-2023	SCALE 2:1	QUANTITY 1	SHEET 3 OF 6



SECTION B-B

	PROJECT Monoski Unipd		
	TITLE: Left System		
NAME GIANMARCO ROCCO	MATERIAL: Fe360	DWG NO. Release System	A3
DATE 18-11-2023	SCALE 2:1	QUANTITY 1	SHEET 4 OF 6





PROJECT: Monoski Unipd

TITLE: Pivot

NAME: GIANMARCO ROCCO

MATERIAL: AVP

DWG NO.: Release System

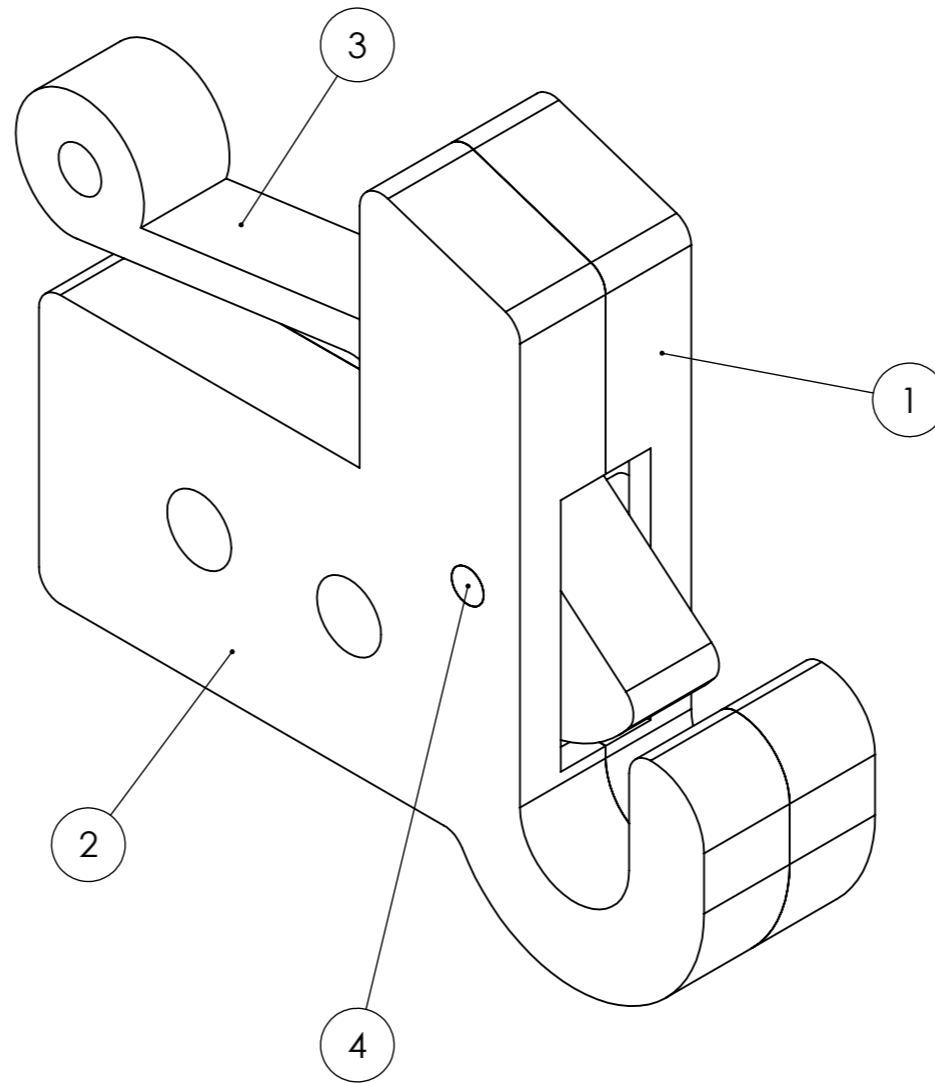
A3

DATE: 18-11-2023


SCALE: 10:1

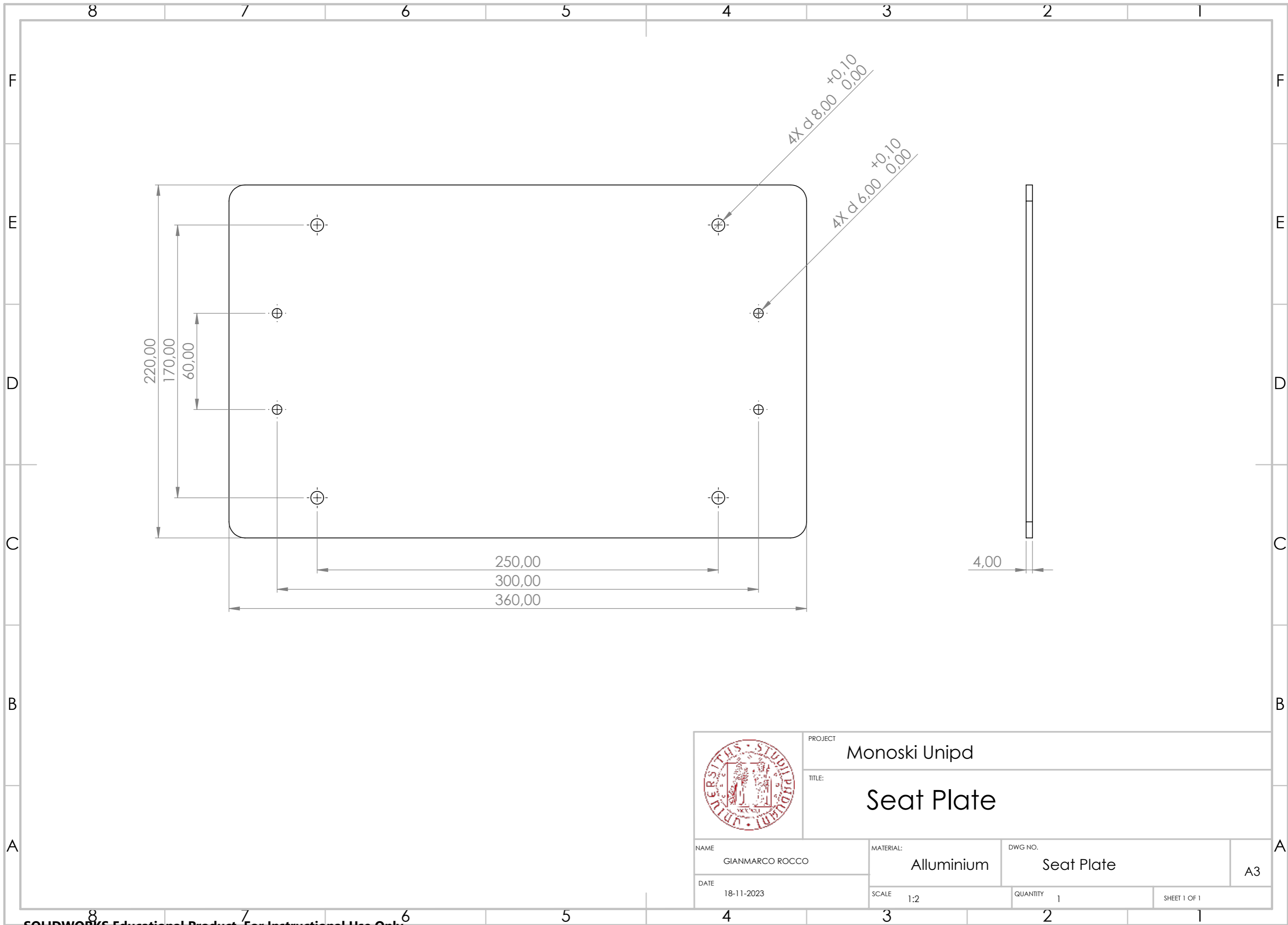
QUANTITY: 1

SHEET 5 OF 6



ITEM NO.	DESCRIPTION	QTY.
1	Left PLate	1
2	Right PLate	1
3	Latch Handle	1
4	Pivot	1

	PROJECT Monoski Unipd		
	TITLE: Release System		
NAME GIANMARCO ROCCO	MATERIAL: Fe360	DWG NO. Release System	
DATE 18-11-2023	SCALE 2:1	QUANTITY 1	A3
		SHEET 6 OF 6	



PROJECT  
Monoski Unipd

TITLE:  
Seat Plate

NAME  
GIANMARCO ROCCO

MATERIAL:  
Alluminium

DWG NO.  
Seat Plate

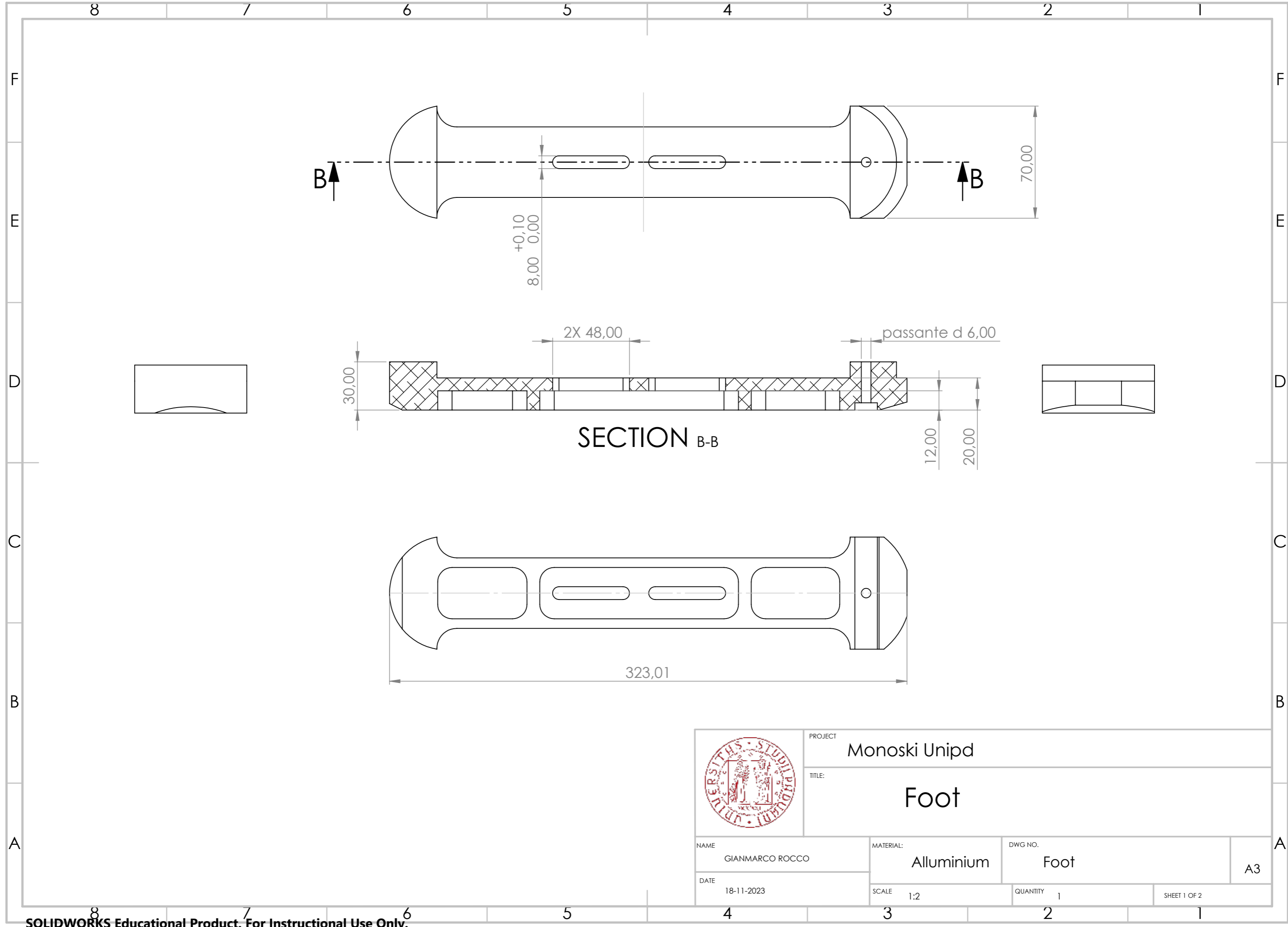
A3

DATE  
18-11-2023

SCALE  
1:2

QUANTITY  
1

SHEET 1 OF 1



PROJECT: Monoski Unipd

TITLE: Foot

NAME: GIANMARCO ROCCO

MATERIAL: Alluminium

DWG NO.: Foot

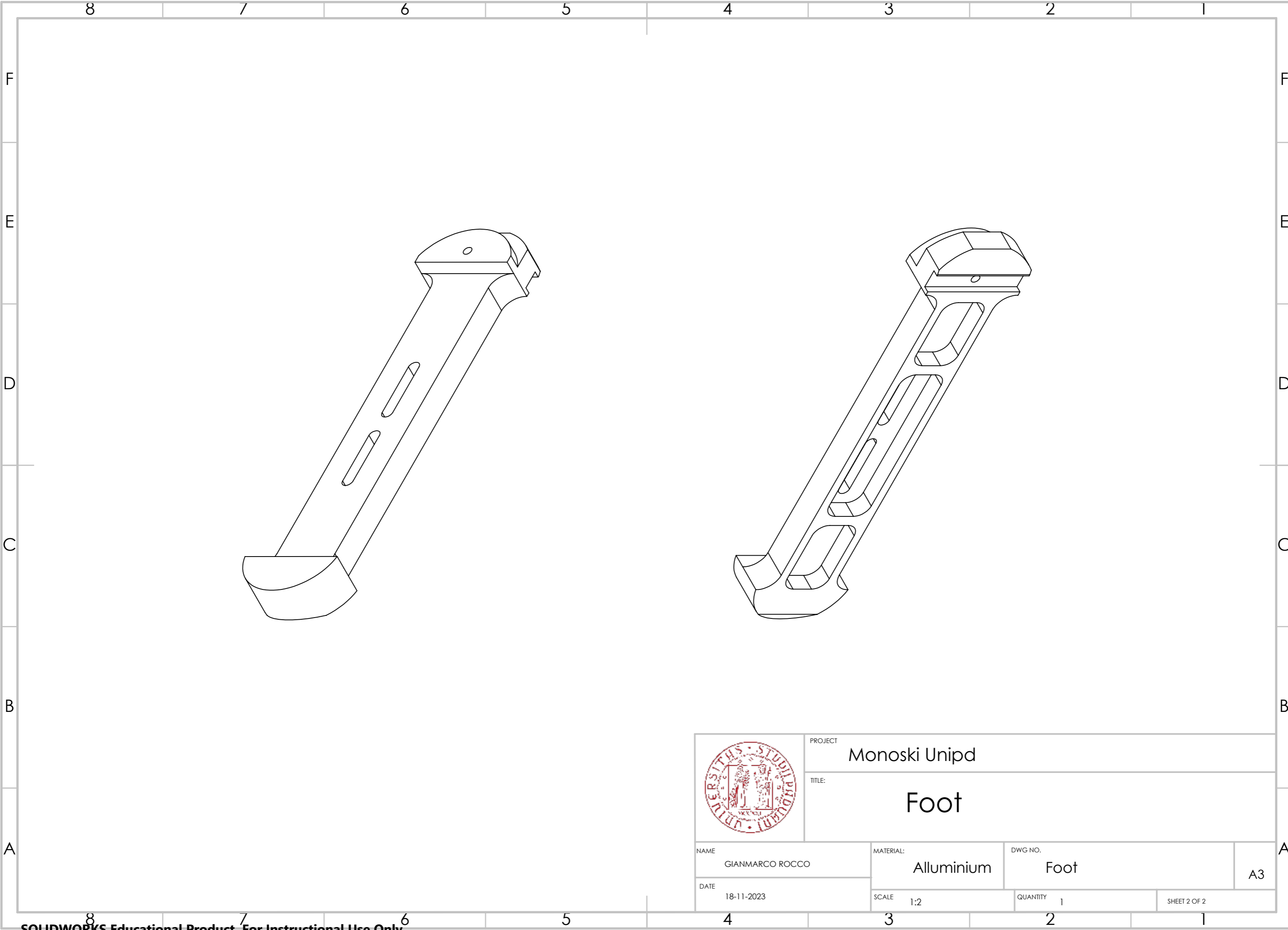
A3

DATE: 18-11-2023

SCALE: 1:2

QUANTITY: 1

SHEET 1 OF 2



	PROJECT Monoski Unipd		
	TITLE: Foot		
NAME GIANMARCO ROCCO	MATERIAL: Alluminium	DWG NO. Foot	
DATE 18-11-2023	SCALE 1:2	QUANTITY 1	A3
		SHEET 2 OF 2	